ASSESSING THE UTILITY OF BAROMETRIC RESPONSE FUNCTIONS IN ESTIMATING HYDROGEOLOGICAL PARAMETERS OF THE HIGH PLAINS AQUIFER

By

Brooks John Bailey

Submitted to the graduate degree program in Geology and the Graduate Faculty of the University of Kansas in partial fulfillment of the requirements for the degree of Master of Science.

_____

Chairperson Dr. Randy L. Stotler

_____

Dr. James J. Butler, Jr.

_____

Dr. George Tsoflias

Date Defended: 11/16/2016

The Thesis Committee for Brooks John Bailey

certifies that this is the approved version of the following thesis:

ASSESSING THE UTILITY OF BAROMETRIC RESPONSE FUNCTIONS IN ESTIMATING HYDROGEOLOGICAL PARAMETERS OF THE HIGH PLAINS AQUIFER

_____

Chairperson Dr. Randy L. Stotler

Date approved: 5/9/2017

Abstract

Accurate estimates of hydrogeological parameters, such as hydraulic conductivity, are important for effective groundwater management strategies and contaminant transport studies in aquifers worldwide, including the High Plains aquifer (HPA) of the central United States. Traditional methods of estimating hydraulic conductivity such as pumping tests, are time consuming and resource intensive, while slug tests are primarily designed to estimate the horizontal component (K_x), rather than the vertical component (K_z). Over the last few decades, researchers have utilized the inverse relationship between water level changes in wells induced by step changes in barometric pressure, or barometric response, as an alternative methodology for estimating these parameters. The purpose of this study is twofold: 1. Assess the utility of time and frequency domain barometric response functions (BRFs) for estimating hydrogeological parameters including barometric efficiency (BE) and K_x; and 2. Estimate K_z within predominately unconfined portions of the HPA characterized by thick vadose zones. To assess the utility of BRFs for estimating hydraulic parameters, values of BE, K_x, and K_z were estimated with time and frequency domain BRF analyses near two Kansas Geological Survey Index Wells in Scott and Thomas County, Kansas. Values of K_x derived from time domain and frequency domain BRF analyses were compared to those estimated from slug tests. BE values estimated through both the time and frequency domain BRFs were similar, while K_x values estimated with BRFs were one to two orders of magnitude lower than those estimated through slug tests. Based on these results, both time and frequency domain BRFs are effective methods of estimating the BE of an aquifer, while K_x values estimated with these methods are only suitable as lower boundary estimates due to the influence of skin effects or an additional hydrogeological process not accounted for in the BRF analytical models, such as a vertical component of flow above the

screened interval of a well in an aquifer. Although K_z values calculated through the estimation of vertical hydraulic diffusivity in the HPA were within an order of magnitude of those in other aquifers with similar hydrogeological settings, these estimates are likely inaccurate given the implausibly low estimates of α values, low K_x values, and apparent systematic deviations in the fitting curves of the frequency domain BRF. Improved results may be possible through modifying the frequency domain analytical solution to account for water table fluctuation and partial penetration within an unconfined setting as well as incorporating wellbore storage and skin effects. The form of the time domain BRF changed from 2013 to 2015, resulting in decreased estimates of K and α values. This provides further evidence of the transient nature of BRFs and suggests that they can potentially indicate changes in local hydrogeological conditions.

Acknowledgements

I would like to thank the following entities for their support over the course of the completion of my M.S. thesis:

- University of Kansas Geology Department
- Kansas Geological Survey
- University of Kansas Graduate School

Special thanks to Jim Butler, Randy Stotler, Ed Reboulet, and Steve Knobbe for help conducting fieldwork and lab tests. Additional thanks to George Tsoflias for serving on my committee. Further thanks to Geoffrey Bohling for consultations regarding KGS Barometric Response Function Software.

Table of Contents

1. Introduction 1
2. Background 2
2.1 Barometric Efficiency 3
2.2 Barometric Response Functions – Time Domain 9
2.2a Confined Response 9
2.2b Unconfined Response 10
2.2c Borehole and Well Screen Effects 14
2.2d BRF Calculation – Time Domain 15
2.3 Application of BRFs 16
2.4 Barometric Response Functions – Frequency Domain 18
2.4.1 BRF General Form – Frequency Domain 20
2.4.2 BRF Calculation – Frequency Domain 24
2.4.3 BRF Analytical Model – Frequency Domain 27
2.5 Study Area 33
2.5a Scott County (SC) Site 35
2.5b Thomas County (TH) Site 35
3. Methods 38
3.1 Barometric Response Functions (BRFs) – Time Domain 40
3.2 Analytical BRF Model – Time Domain 40
3.3 Analytical BRF Model – Frequency Domain 42
3.4 Slug Tests 44
4. Results 45
4.1 BRFs – Time Domain 45
4.2 Analytical BRF Model – Time Domain 46
4.3 Slug Tests 48
4.4 BRFs – Frequency Domain 51
5. Discussion 51
5.1 BRFs – Time Domain 51
5.2 Analytical BRF Model – Time domain 52
5.3 Slug Tests 53

5.4 BRFs – Frequency Domain 54
5.5 Sources of Error 63
6. Conclusions 65
7. Future Work 66
References 68
Appendix A: Analytical Time Domain BRF Model - Excel Spreadsheet Code 71
Appendix B: Analytical Frequency Domain BRF Model – MATLAB code 76
Appendix C: Slug Test Model Fitting Curves 104
Appendix D: Sensor Testing and Sampling Interval Analyses 122

List of Figures

Figure 1: Illustration of the stress equilibrium within an idealized confined aquifer. Total downward stress within the aquifer at (α_T), a product of the pressure of the overlying solid material and barometric pressure, is balanced by the effective stress (σ_e) of the aquifer grains and the pore pressure (p) of the water between the grains (adapted from Harrington and Cook, 2011). 5

Figure 2: Three types of generalized barometric response functions (BRFs): unconfined, confined, and skin effects and wellbore storage. Unconfined responses feature a response delay due to the transmission of air pressure through the vadose zone. Confined aquifers have a constant (static) BE value due to instantaneous transmission of barometric pressure load to the water level within the aquifer. Skin effects and borehole storage produces a time-lag due to the finite travel time associated with water movement between the borehole and the surrounding aquifer formation (adapted from Rasmussen and Crawford, 1997). 11

Figure 3: Illustration of barometric pressure propagation within an unsaturated zone overlying an unconfined aquifer. For a given step change in barometric pressure, the propagation of the barometric pressure wave is controlled by the pneumatic diffusivity (α) of the vadose zone. Since the barometric pressure wave must pass through tortuous pathways before reaching the water table, there is often a finite time lag associated with a water level change produced by a given step change in barometric pressure. This is especially true for wells within deep, unconfined aquifers with thick vadose zones (adapted from Weeks, 1979)..... 12

Figure 4: Cross sectional diagram of an idealized, semiconfined aquifer, featuring hydrostratigraphic units on the left and frequency domain barometric response function (BRF) parameters on the right. Estimated parameters for the relevant processes include vertical air flow within the vadose zone (D_{unsat}), vertical groundwater flow within the semiconfining unit (D_{con}), aquifer transmissivity (T_{aqu}), and vadose zone length (L_{unsat}) (adapted from Odling et al., 2015). 22

Figure 5: Generic frequency domain barometric response function (BRF) gain plot. Barometric efficiency (BE) increases with increasing frequency, plateaus at the static (confined) barometric efficiency, and then decreases with increasing frequency. 23

Figure 6: Generic phase plot. Phase advance occurs at phase angles greater than -180°, while phase lag occurs at values less than -180°. This occurs in three phases according to the periodic fluctuations in atmospheric pressure (adapted from Hussein et al., 2013). 24

Figure 7: Study area featuring two Kansas Geological Survey Index Wells within the High Plains Aquifer of western Kansas. The two long term monitoring wells are located in Scott and Thomas counties, within Kansas Groundwater Management Districts 4 and 1, respectively. Data source: State of Kansas GIS Data Access & Support Center (DASC)..... 34

Figure 8: Cross sectional lithology for both SC (a) and TH (b) wells (identified as "*I"*). Adapted from Young et al. (2007). 37

Figure 9: Water level and barometric pressure data at Scott County Index Well. Data were collected at 10 second intervals over a period of 17 days..... 39

Figure 10: Water level and barometric pressure data at Thomas County Index Well. Data were collected at 10 second intervals over a period of 25 days..... 39

Figure 11: Barometric response function (BRF) for the Thomas County Index Well and time domain analytical model. BRF calculated during the recovery period of 2013. Analytical model superposites the Hovrslev (1951) (A) and Weeks (1979) (B) models..... 41

Figure 12: Time domain barometric response function (BRF, data points) and associated time domain fitted analytical solution (solid lines) for the SC and TH sites for 2013 (a) and 2015 (b). The analytical BRF solution is the supoerposition of the Hvorslev (1951) slug test solution and Weeks' (1979) pneumatic transmission model, visually fitted to calcualted BRFs. Time series water level and barometric pressure data were selected from the recovery limb (Jan. – March, 2013 and Nov. – Dec., 2015). Data from 2015 were obtained at a higher acquisition interval (10 sec) than from 2013 (1 hr). Data are plotted every 1 hour and every 10 mintues for 2013 and 2015, respectively.. 49

Figure 13: Normalized head plot of ten slug tests at Scott County Index Well (SC). 49

Figure 14: Normalized head plot of ten slug tests at Thomas County Index Well (TH). 49

Figure 15: Selected slug tests from SC and TH. Tests were initiated sequentially with 2 ft. (0.6 m) and 4 ft. (1.2 m) solid PVC slugs. Recording intervals were set at 0.5 and 1.0 seconds for TH and SC, respectively..... 50

Figure 16: Coherence and water level amplitude spectrum for Scott County Index Well. Low coherence at values less than 0.2 CPD and greater than 12 CPD are attributable to the effects of recharge and low barometric pressure signal amplitude at higher frequencies. 59

Figure 17: Estimated BRF (phase and gain) and best fit curves for Scott County Index Well. Larger margin of error at ~0.01 CPD may be due to recharge effects..... 60

Figure 18: Coherence and water level amplitude spectrum for Thomas County Index Well. Low coherence at values less than 0.2 CPD and greater than 12 CPD are attributable to the effects of recharge and low barometric pressure signal amplitude at higher frequencies. 61

Figure 19: Estimated BRF (phase and gain) and best fit curves for Thomas County Index Well 62

Figure A1: Weeks (1979) Pneumatic Transmission Model..... 72

Figure A2: Hvorslev (1951) Slug Test Model…….....73

Figure A3: Analytical BRF with Well-Formation Effects……73

Figure A4: Empirical BRF…….....74

Figure A5: Parameter estimation through visual curve matching of the time domain BRF analytical model to empirical time domain BRF…….....75

Figure C1: Cooper et al. (1967) slug test model fitting curve for Scott County Index Well…...104

Figure C2: KGS (1994) slug test model fitting curve for Scott County Index Well……...105

Figure C3: Hvorslev (1951) slug test model fitting curve for Scott County Index Well…….106

Figure C4: Cooper et al. (1967) slug test model fitting curve for Thomas County Index Well..107

Figure C5: KGS (1994) slug test model fitting curve for Thomas County Index Well……...108

Figure C6: Hvorslev (1951) slug test model fitting curve for Thomas County Index Well……109

Figure D1: Sampling intervals of ten seconds, one minute, ten minutes, and one hour at Thomas County Index Well. Qualitative analyses indicate that the ten-minute sampling interval best optimizes signal to data storage ratio…….....125

List of Tables

Table 1: Well data for Scott and Thomas County Index Wells……34

Table 2: Estimated parameters for Scott (SC) and Thomas (TH) County Index Wells. These parameters are barometric efficiency (BE), pneumatic diffusivity (α), horizontal hydraulic conductivity (K_x), specific storage (S_s), aquifer transmissivity (T_{aqu}), hydraulic diffusivity (D_{con}), and vertical hydraulic conductivity (K_z). Estimation methods are time and frequency domain barometric response functions (BRF-T and BRF-F, respectively) and slug tests. Frequency domain estimates of K_x were calculated from estimates of T_{aqu} by subtracting an estimated confining layer thickness of 5 m from the saturated thicknesses of SC (36.34 m) and TH (17.92 m) (Table 1).……..45

Table 3: Estimated hydraulic conductivity (K), storativity (S), Specific storage (S_s), and y-intercept (y_0) from three slug test methods. Note: saturated thickness (b) values of 24.85 m and 18.60 m used for Scott County Index Well (SC) and Thomas County Index Well (TH), respectively……50

Table C1: Scott County Index Well slug test data……...110

Table C2: Thomas County Index Well slug test data……..120

1. Introduction

Estimating aquifer hydraulic properties is a critical component of effective groundwater resource management and contaminant transport studies. In many cases, the most important and commonly estimated hydraulic property of an aquifer is the horizontal component of hydraulic conductivity (K_x), which is a function of both the water flowing within the aquifer, as well as the properties of the media composing the aquifer (Freeze and Cherry, 1979). Accurate estimates of aquifer hydraulic properties, including K_x, enable groundwater managers and scientists to make informed decisions regarding sustainable use of existing groundwater resources, as well as responsible development of new sources of groundwater supply (Healy and Cook, 2002).

The problem with obtaining accurate estimates of aquifer hydraulic properties is that aquifers are complex systems of heterogeneous composition. The High Plains aquifer (HPA) of the central United States, which is predominately composed of a mix of unconsolidated sediments, is a prime example of a complex aquifer system. This aquifer is one of the largest and most important aquifers in the country, spanning portions of eight states and providing approximately 23% of the nation's groundwater (Maupin and Barber, 2005). Additionally, traditional methods of estimating aquifer hydraulic properties, such as slug tests and pumping tests, are often limited to assessing the horizontal component of hydraulic conductivity (K_x) within an aquifer. Although the vertical component of hydraulic conductivity (K_z) can be estimated through pumping tests in partially penetrating wells and pumping tests that incorporate leakage from overlying confining units, these tests are time-consuming and can last several days (e.g., Odling et al., 2015).

Over the last few decades, several researchers started pursuing alternative methodologies to address the problem of estimating K values, including quantifying the relationship between

well water levels and barometric pressure as they relate to aquifer properties (e.g., Weeks, 1979; Rojstaczer et al. 1988; Rojstaczer and Riley, 1990; Evans et al., 1991; Rasmussen and Crawford, 1997; Hussein et al., 2013; and Odling et al., 2015). The relationship between water levels and barometric pressure can be quantified through Barometric Response Functions (BRFs), which can be calculated in both the time and frequency domain using continuous water level and barometric pressure data records acquired from any given well or borehole. The purpose of this paper is to assess the utility of BRFs in both the time and frequency domain for estimating hydraulic properties of the HPA, particularly, the vertical component of hydraulic conductivity (K_z). Since barometric pressure and water levels can be measured unattended, this methodology could potentially function as a time and cost effective alternative or supplement to conventional methods for estimating aquifer hydraulic properties. Additionally, better estimates of hydraulic properties, particularly K_z, will improve our collective knowledge of numerous hydrogeological processes including groundwater recharge, contaminant transport, and the anisotropy of groundwater flow in the HPA as well as other similar aquifers worldwide.

2. Background

The impact of barometric pressure on water levels in wells was first observed and quantified by the French mathematician Blaise Pascal in the 17th century (Pascal, 1973). Since that time, scientists have established an inverse relationship between changes in barometric pressure and changes in water level, with an increase in barometric pressure resulting in a decrease in water level within a well (e.g., Jacob, 1940). More recently, researchers explored the mechanisms governing this phenomenon further and utilized barometric pressure and water level data to glean valuable insights into aquifer properties (e.g., Weeks, 1979; Rasmussen and Crawford, 1997; Batu, 1998). The two main quantitative tools used to assess the relationship

between barometric pressure changes and water level response are: 1. Barometric Efficiency (BE) and 2. Barometric Response Functions (BRFs). BRFs can be developed in both the time domain and the frequency domain, depending on the quantitative needs of a project. The development and implementation of both of these tools in the time and frequency domains is described in the following sections.

2.1 Barometric Efficiency

In his seminal paper on the flow of water in an elastic confined aquifer, Jacob (1940) derived from first principles the parameter that would later be formalized as Barometric Efficiency (BE). BE is formally defined as the ratio of the change in hydraulic head (*h*) in a well caused by a step change in barometric pressure to the step change in barometric pressure head itself (p_a/γ) (Gonthier, 2007):

$$BE = \frac{\Delta h}{\Delta(\frac{p_a}{\gamma})} \quad (1)$$

where γ is the specific gravity of water, the product of the density of water and gravitational acceleration (ρg). BE is a dimensionless value ranging from 0-1. BE values near zero indicate the barometric pressure load is borne primarily by the aquifer pore water, while BE values near one indicate the barometric pressure load is borne primarily by the aquifer framework. Practically, BE is the ability of aquifer material to retard the transmission of land surface barometric pressure changes to the pore water within the aquifer (Price, 2009). BE values near zero are often associated with shallow, unconfined aquifers featuring thin vadose zones. In these aquifers, increases in barometric pressure rapidly propagate through the vadose zone, increasing

the total head within the aquifer. Conversely, BE values near one are associated with confined aquifers featuring rigid aquifer material or unconfined aquifers featuring thick vadose zones. Low permeability units and thick vadose zones both act to delay and/or inhibit the transfer of barometric pressure changes at the land surface to the aquifer pore water. To derive this relationship, Jacob (1940) used the concept of an elastic aquifer volume. This concept was first proposed by Meinzer (1928), who was one of the first to suggest that aquifers were compressible, rather than incompressible, as was commonly thought at the time. The governing equation for the derivation of BE is the stress equilibrium equation for an aquifer (Terzaghi, 1925). The stress equilibrium equation expresses the total downward stress on an arbitrary plane within an aquifer (σ_T) as the sum of the weights of the overlying soil, water, and the barometric pressure load at the ground surface, balanced by the pressure of water (p) within the pores of the aquifer, combined with the effective stress of the solid grains composing the rigid aquifer skeleton (σ_e) (Figure 1). This is expressed as:

$$\sigma_T = \sigma_e + p \qquad 2)$$

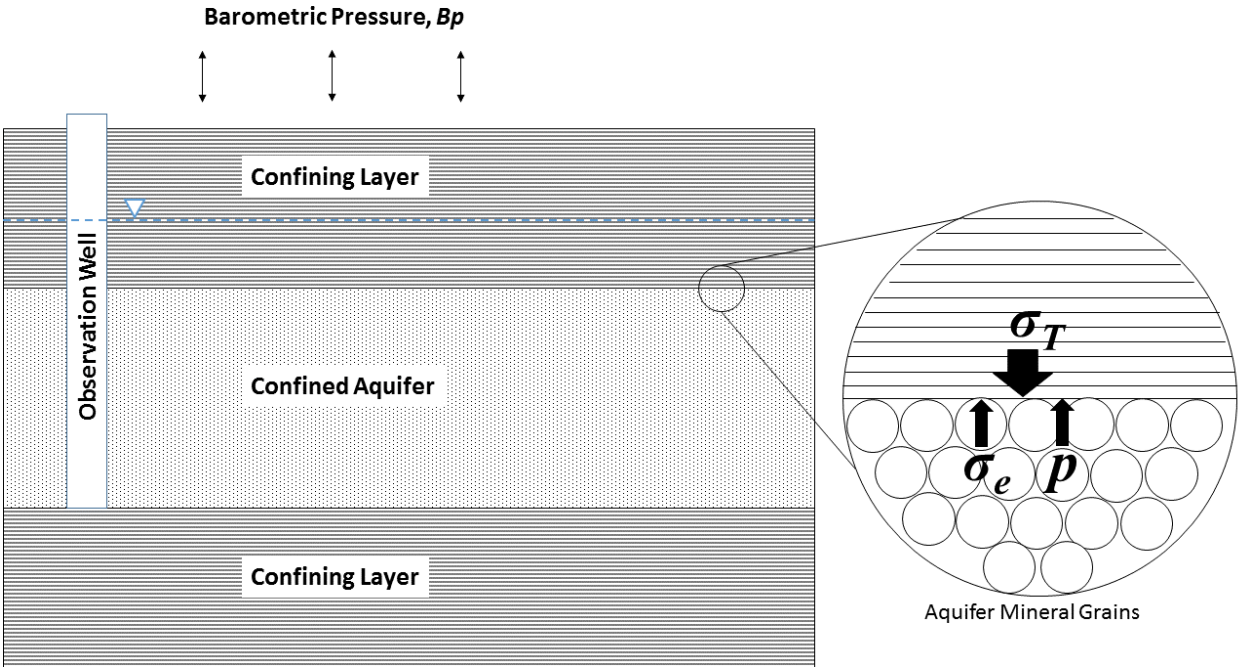

Figure 1: Illustration of the stress equilibrium within an idealized confined aquifer. Total downward stress within the aquifer at (α_T), a product of the pressure of the overlying solid material and barometric pressure, is balanced by the effective stress (σ_e) of the aquifer grains and the pore pressure (p) of the water between the grains (adapted from Harrington and Cook, 2011).

Following Jacob's (1940) derivation, barometric efficiency is derived from the stress equilibrium equation (Eq. 2) by assuming that the total downward stress within the aquifer (σ_T) is constant, with the exception of a change in barometric pressure (p_a). Eq. (2) then becomes (Batu, 1998):

$$\sigma_e + p = \sigma_T = p_a + constant \quad (3)$$

which, after differentiating and rearranging, becomes:

$$dp - dp_a = -d\sigma_e \tag{4}$$

In a well, the water pressure within the aquifer (p) is balanced by the sum of the weight of barometric pressure (p_a) and the weight of the water in the well above the measuring point (γh). Thus, the change in water pressure within the aquifer can be expressed as

$$dp = dp_a + \gamma dh \tag{5}$$

where h is the water surface elevation in the well. Rearranging equations (4) and (5) to solve for the components expressed in the BE Eq. (1) results in:

$$\frac{dp_a}{\gamma} = \frac{dp}{\gamma} + \frac{d\sigma_e}{\gamma} \tag{6}$$

$$dh = \frac{dp}{\gamma} - \frac{dp_a}{\gamma} \tag{7}$$

Dividing Eq. (7) by Eq. (6) and substituting with Eq. (4) leads to:

$$\frac{dh}{\frac{dp_a}{\gamma}} = -\frac{1}{\frac{dp}{d\sigma_e} + 1} \tag{8}$$

where the negative sign reflects that an increase in barometric pressure results in a decrease in water level within a well. Since the terms in Eq. (8) are identical to those in the formal definition of Eq. (1), it is apparent that:

$$BE = \frac{dh}{\frac{dp_a}{\gamma}} = -\frac{1}{\frac{dp}{d\sigma_e} + 1} \tag{9}$$

Given the terms in the fully-derived BE equation (Eq. 9), it follows that rigid, less compressible aquifers (smaller values of $\frac{dp}{d\sigma_e}$) have larger BE values (up to 1) while less rigid, more compressible aquifers (larger values of $\frac{dp}{d\sigma_e}$) have lower BE values (as low as 0) (Price, 2009). Although these two BE endmembers do exist, BE values between 0.2 and 0.7 are most common (Acworth and Brain, 2008).

BE is estimated using several methods including the average-of-ratios method, median-of-ratios method, Clark method, and slope method (Davis and Rasmussen, 1993; Gonthier, 2007). The slope method is commonly used due its simplicity and ease in assessing BE estimate reliability. This method uses ordinary least squares regression of changes in barometric pressure head on the x-axis, with changes in well water level on the y-axis, to estimate BE (Batu, 1998). The slope of the best-fit line through the data is the BE estimate and the r-squared value from the linear regression fit functions as an indicator of the reliability of the estimates. Thus, the equation for the slope method of estimating BE is a direct application of Eq. (1):

$$BE = \frac{\Delta(\sum \Delta h)}{\Delta\left[\sum \Delta\left({}^{dp_a}/_{\gamma}\right)\right]} \tag{10}$$

Typically, estimates of BE are made using discrete barometric pressure and water level data over short time intervals (often hourly) (Gonthier, 2007). BE is a useful parameter for correcting well water levels for fluctuations in barometric pressure (Gonthier, 2007). Batu (1998) expresses the water level correction equation accounting for the impact of barometric pressure on water levels as:

$$h_c = h - \Delta h = h - BE\Delta\left(\frac{p_a}{\gamma}\right) \tag{11}$$

where h_c is the corrected hydraulic head value, h is the measured hydraulic head value, and Δh represents the change in hydraulic head expressed as the product of the barometric efficiency (BE) associated with a step change in barometric pressure head $\Delta\left(\frac{p_a}{\gamma}\right)$. Thus, water level data are corrected for the influence of barometric pressure on hydraulic head over a time series by multiplying the BE obtained from each paired water level and barometric pressure measurement by the step change in barometric pressure head for that time value within the time series. This value is then added to the measured water level. Negative Δh values indicate a decrease in water level (increase in barometric pressure), while positive Δh values indicate an increase in water level (decrease in barometric pressure) (Batu, 1998). BE can also be used to estimate aquifer storage properties within confined aquifers (Jacob, 1940).

2.2 Barometric Response Functions – Time Domain

Although barometric efficiency is a useful parameter for quantifying the relationship between barometric pressure changes and corresponding water level changes within a well, its utility is limited to short-term responses, on the order of several hours to a single day (Butler et al., 2011). The Barometric Response Function (BRF), which is essentially BE over a longer time (i.e. the response in time to a step change in barometric pressure), is more useful in assessing the relationship between barometric pressure and water levels over longer time intervals (several days to weeks) (Rasmussen and Crawford, 1997; Spane, 2002; Butler et al., 2011). Rasmussen and Crawford (1997) and Spane (2002) identified three type curves indicative of confined aquifer response, unconfined aquifer response, and responses influenced by well screen or skin effects (Figure 2). The mechanisms governing these three responses are discussed in the following sections.

2.2a Confined Response

In confined aquifers, barometric pressure is transmitted directly downward and nearly instantaneously to the aquifer through grain to grain transmission (Weeks, 1979) (Figure 1). Within the aquifer, the pressure load is shared between the aquifer skeleton and the pore water within the formation, while the same pressure load is experienced in full by the water column within the open well. This disparity in how the barometric pressure load is shared between the well and the surrounding aquifer creates a pressure imbalance, which can result in water flow from the well into the aquifer (in the case of an increase in barometric pressure), or flow from the aquifer into the well (in the case of a decrease in barometric pressure) (Ferris et al., 1962; Weeks, 1979; Hussein et al., 2013). Since the pressure load for a step change in barometric pressure is applied nearly instantaneously to the well and aquifer, the barometric response for a confined

aquifer is nearly constant in time. As a result, the diagnostic BRF for a confined aquifer is a horizontal, or near-horizontal line on a plot of BE vs. time (Rasmussen and Crawford, 1997) (Figure 2).

2.2b Unconfined Response

In unconfined aquifers, a slightly different mechanism governs the barometric response of the aquifer (Figure 3). For unconfined aquifers with thin, permeable vadose zones, a barometric pressure change is readily transmitted through the shallow vadose zone and transferred rapidly to the pore water within the aquifer (Price, 2009). Unlike the grain to grain mechanism of the confined response, where the barometric pressure change is shared between the aquifer skeleton and the pore water within the formation, the pressure change is borne primarily by the pore water. As a result, the barometric pressure change is distributed more evenly between the pore water within the formation and the water column within the open well, leading to less of a pressure imbalance between the two. Thus, for unconfined aquifers with thin, permeable vadose zones, BE and the corresponding BRF are zero (Rasmussen and Crawford, 1997). In order for an unconfined aquifer to exhibit a barometric response, there must be a time delay for the transmission of the barometric pressure change as it travels through the vadose zone to the water table.

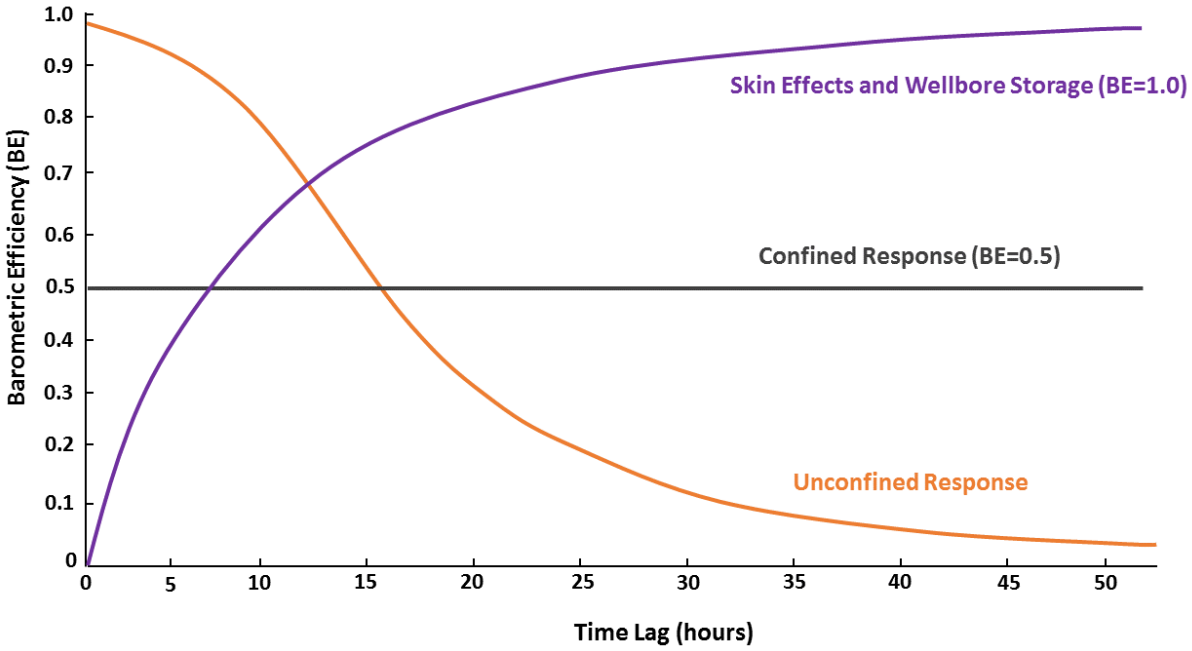

Figure 2: Three types of generalized barometric response functions (BRFs): unconfined, confined, and skin effects and wellbore storage. Unconfined responses feature a response delay due to the transmission of air pressure through the vadose zone. Confined aquifers have a constant (static) BE value due to instantaneous transmission of barometric pressure load to the water level within the aquifer. Skin effects and borehole storage produce a time-lag due to the finite travel time associated with water movement between the borehole and the surrounding aquifer formation (adapted from Rasmussen and Crawford, 1997).

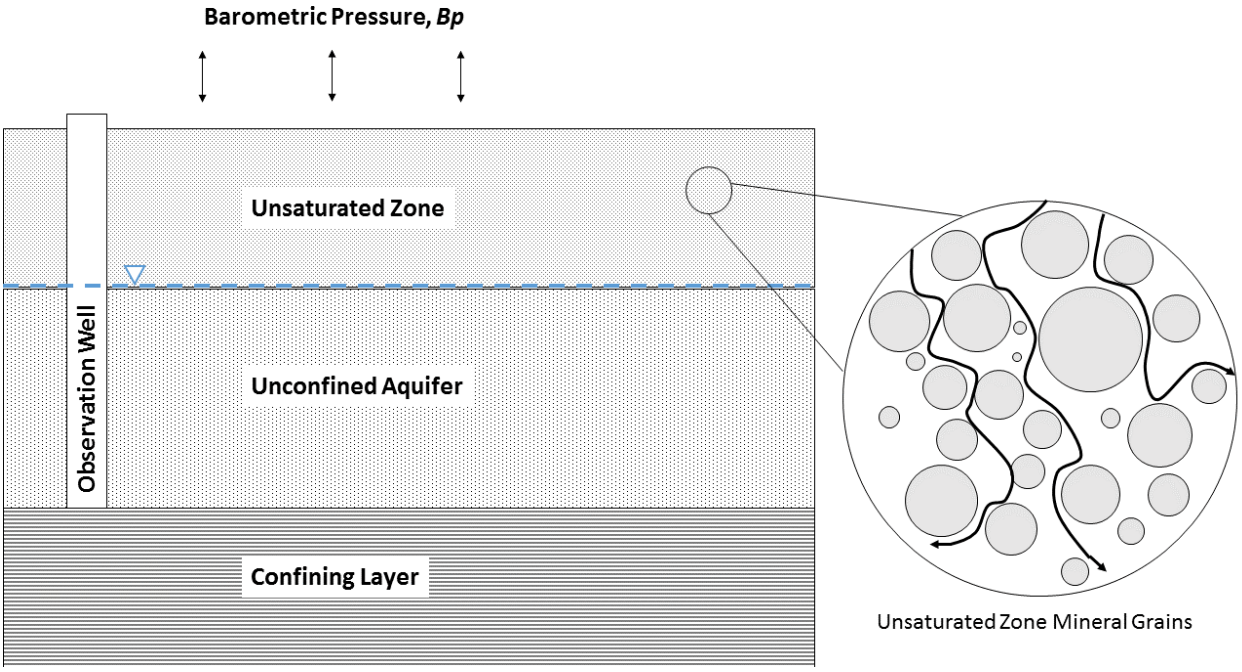

Figure 3: Illustration of barometric pressure propagation within an unsaturated zone overlying an unconfined aquifer. For a given step change in barometric pressure, the propagation of the barometric pressure wave is controlled by the pneumatic diffusivity (α) of the vadose zone. Since the barometric pressure wave must pass through tortuous pathways before reaching the water table, there is often a finite time lag associated with a water level change produced by a given step change in barometric pressure. This is especially true for wells within deep, unconfined aquifers with thick vadose zones (adapted from Weeks, 1979).

In the case of a deep, unconfined aquifer with a thick vadose zone like the one examined by Weeks (1979) in Lubbock, Texas, there is a finite time delay for the propagation of the barometric pressure wave through the vadose zone before it reaches and acts on the water table (Weeks, 1979). This time delay of barometric pressure through the vadose zone is quantified with a parameter known as pneumatic diffusivity (α). This is a lumped parameter that incorporates both the properties of the vadose zone media as well as the gas within the soil (Weeks 1979). Pneumatic diffusivity has the dimensions of (L^2/T) and is included in the 1-D differential equation for pneumatic head (potential):

$$\alpha \frac{\partial^2 h}{\partial z^2} = \frac{\partial h}{\partial t} \tag{12}$$

where *h* is the pneumatic potential (L) and z is the depth within the vadose zone (L) (Rasmussen and Crawford, 1997). Based on the similarities between Eq. (12) and the differential equation for diffusion, it is evident that α has much the same function as the diffusion coefficient (Hussein et al., 2013).

Pneumatic diffusivity commonly ranges from 0.02 to 0.07 m^2/s, and directly influences the time it takes for barometric pressure changes to impact the water table (Weeks, 1979). Larger values of α are associated with smaller time lags, while smaller values of α are associated with larger time lags (Rasmussen and Crawford, 1997). Thus, the time it takes for a barometric pressure change to propagate through the vadose zone is influenced by the pneumatic diffusivity of the sediments within the vadose zone, and leads to a delay in the transmission of the barometric pressure change at the land surface to the water in the aquifer. As a result, the diagnostic BRF for an unconfined aquifer with a thick vadose zone starts at a high value and

decreases exponentially on a plot of BE vs. time. This is because the water table within the unconfined aquifer is "shielded" by thick sediments, which cause the barometric pressure change to navigate the tortuous paths between the void spaces between the sediment grains. Initially, the BE of the aquifer is high since the water table has not yet experienced the barometric pressure change, but as the barometric pressure wave propagates through the vadose zone, the BE begins to decrease with time and ultimately reaches a value near zero when the barometric pressure wave finally reaches the water table and the load is borne primarily by the pore water within the aquifer (Spane, 2002) (Figure 2).

2.2c Borehole and Well Screen Effects

In the two previous sections describing the driving mechanisms of barometric response in confined and unconfined aquifers, an instantaneous equalization of pressure between the aquifer and the well is assumed (Spane, 2002). However, there is commonly a finite time delay associated with moving a finite volume of water between the aquifer and the well to equilibrate the pressure imbalance generated by the initial step change in barometric pressure (Rasmussen and Crawford, 1997). This time lag varies as a function of aquifer properties, such as storativity and transmissivity, in addition to the quality of the connection between the aquifer and the well, known as "skin effects" (Spane, 2002). Aquifers with lower transmissivity and storage values have delayed barometric responses associated with borehole effects, while wells with partially clogged screens or shortened screen lengths may also experience delayed barometric responses due to the inhibited connection between the aquifer and the well (Ramsussen and Crawford, 1997; Fileccia, 2011). The effects of borehole storage and skin effects may be observed in wells installed in both confined and unconfined aquifers. This appears on a BRF as an initial delay in water level response (Spane, 2002) (Figure 2).

2.2d BRF Calculation – Time Domain

As mentioned above, BRFs are simply BE as a function of time. BRFs are calculated via regression deconvolution of paired water level and barometric pressure changes (Furbish, 1991; Olsthoorn, 2008). Regression deconvolution involves estimating how a quantity (water level in a well) changes in response to a stimulus (step change in barometric pressure) when the response (change in water level) is irregular and not instantaneous (Toll and Rasmussen, 2007). Rasmussen and Crawford (1997) applied regression deconvolution to water level and barometric pressure data to develop BRFs to estimate the time lag response between step changes in barometric pressure and the corresponding change in water level. This was accomplished through the use of a linear set of regression equations between barometric pressure and water levels:

$$\Delta W(t) = \alpha(0)\Delta B(t) + \alpha(1)\Delta B(t-1) + \alpha(2)\Delta B(t-2) + \cdots + \alpha(m)\Delta B(t-m) \quad (13)$$

which is more simply expressed in summation notation as:

$$\Delta W(t) = \sum_{i=0}^{m} \alpha(i)\Delta B(t-i) \quad (14)$$

where $\Delta W(t)$ is the change in water level at time *t*, $\Delta B(t-i)$ is the change in barometric pressure at *i* timesteps before time *t*, $\alpha(i)$is the unit response function (BE) at lag *i*, and *m* is the maximum number of time lags (Toll and Rasmussen, 2007). As discussed in the section on BE, the unit response function $\alpha(i)$ is estimated via ordinary least squares linear regression between water level changes and barometric pressure changes. After estimating the BE for each time step,

the BRF at the lag of interest *j*, A_j, is calculated as the sum of the unit response functions at their respective time lags, up to the time lag of interest *j*:

$$BRF = A_j = \sum_{i=0}^{j} \alpha(i) \tag{15}$$

2.3 Application of BRFs

Since their development in the late ‘70s and early ‘80s, BRFs have been used in several hydrogeological applications. Researchers over the last few decades have developed time domain (Weeks, 1979; Furbish, 1991; Rasmussen and Crawford, 1997) and frequency domain (Van der Kamp and Gale, 1983; Rojstaczer, 1988; Quilty and Roeloffs, 1991) methods for calculating BRFs. The relationship between barometric pressure and water levels within nearly perfectly confined aquifers, which tend to have constant BE, can often be assessed with the BE methods discussed in the section above. However, the relationship between barometric pressure and water levels for semiconfined aquifers and unconfined aquifers with thick vadose zones are more accurately assessed with both time and frequency domain BRFs, since BE changes transiently for these types of aquifers (Hussein et al., 2013).

One of the most widely used applications of BRFs is correcting piezometric water level data for the effect of changes in barometric pressure. Failure to account for changes in head induced by barometric pressure, which can be as large as 30 cm, can in some cases lead to a misinterpretation of water availability, groundwater flow gradient, and parameter estimation from conventional hydraulic aquifer tests (Rasmussen and Crawford, 1997; Toll and Rasmussen, 2007; Butler et al., 2013). Several researchers (Rasmussen and Crawford, 1997; Batu, 1998; Toll and Rasmussen, 2007; Gonthier, 2007) used the residual (i.e. difference between observed and

predicted hydraulic head) from the regression deconvolution of paired barometric pressure and water level measurements (Section 2.1) as a correction factor for well water levels for both static water level as well as drawdown data from pumping tests.

Another application of BRFs is determining whether an aquifer is confined or unconfined. Rasmussen and Crawford (1997) were among the first researchers to demonstrate that BRFs can be used for this purpose with their analysis of eleven wells at the Savannah River Site within the Atlantic Coastal Plain of South Carolina. These wells were chosen based on site stratigraphy such that seven were within an unconfined aquifer, while the other four were within a confined portion of an adjacent aquifer. The differing shapes of the BRFs from these wells resulted in a set of "type curves" for identifying whether an aquifer is confined or unconfined.

Hare and Morse (1997) confirmed the utility of BRFs to identify zones of retarded vertical transmission of barometric pressure changes through the vadose zone within a sandy, unconfined aquifer. In this study, BRFs were used to assess the performance of a containment system consisting of a bentonite cap and impermeable cutoff wall within a Superfund site located in upstate New York. Wells screened within the containment system displayed BE values near 0.94 (94%), while wells screened outside of the containment zone had near-zero BE values. This result demonstrated that the bentonite cap within the containment system retarded vertical transmission of barometric pressure changes to the water table through the otherwise thin vadose zone of a sandy, unconfined aquifer.

Natural extensions of the capability of BRFs to determine whether an aquifer is confined or unconfined are verifying hydrostratigraphic continuity and determining the degree of aquifer confinement. For proximal wells within a confined aquifer, Rasmussen and Crawford (1997)

suggested that wells with similar confined responses are located within similar hydrostratigraphic intervals. Thus, the BRF is also indicative of the lateral extent of the confining unit overlying the aquifer. Butler et al. (2011) also utilized this application of BRFs to determine the lateral extent of a confining layer within the High Plains Aquifer of south-central Kansas. Additionally, they demonstrated that the form of the BRF indicates the degree of confinement in semi-confined aquifers.

2.4 Barometric Response Functions – Frequency Domain

BRFs have also been used to determine a variety of aquifer properties within a wide range of hydrogeological settings. Geldon et al. (1997) used calculated BE values and a previously determined specific storage value to calculate the effective porosity of tuffaceous rock within uncased sections of boreholes in the elastic confined aquifer near Yucca Mountain in Nevada. Anochikwa et al. (2012) used superimposed soil moisture loading and pore pressure barometric response data to estimate the stress and strain properties of a near-surface aquitard in Saskatchewan, Canada. Rojstaczer (1988) fit an analytical solution to a frequency domain BRF to estimate vertical pneumatic diffusivity, lateral aquifer permeability and vertical hydraulic diffusivity within an unconfined aquifer near Mammoth Lakes, California. Evans et al. (1991) built on the frequency domain BRF analytical model of Rojstaczer (1988) by assuming a compressible saturated zone near the phreatic surface as well as the amount of skin effects induced by low permeability zones near the well screen, which retards horizontal water flow. Evans et al. (1991) used their modified frequency domain analytical model to estimate vertical and horizontal hydraulic diffusivity through the saturated zone, as well as vertical pneumatic diffusivity through the vadose zone, for several wells screened in an unconfined portion of the Nubian Formation near Aswan, Egypt. Recent research utilized BRFs to characterize aquifer

vulnerability to vertical flow of contaminants through zones of higher hydraulic conductivity in aquitards (Hussein et al., 2013; Odling et al., 2015). Finally, Hussein et al. (2013) used a frequency domain method approach to generate and estimate aquifer properties from BRFs for three wells screened in the semiconfined Chalk Aquifer of East Yorkshire, UK.

According to Furbish (1991), the time domain approach is most useful for directly filtering water level changes due to barometric pressure changes, while the frequency domain method is more useful for determining aquifer properties since it solves the differential equations for flow of both air and water within the subsurface. It should be noted that the time domain can also be used to solve for flow through the use of partial differential equations (Butler et al., 2011). The frequency domain BRF capitalizes on diurnal and semidiurnal barometric pressure variations resulting from daily increases in ground temperature relative to the atmosphere and ozone heating within the atmosphere (Hussein et al. 2013). Solar daily variations of barometric pressure (S(p)) can be mathematically represented as a series of sinusoidal functions with amplitudes (S_n), phases (σ_n), and harmonic coefficients (A_n and B_n) (Chapman and Lindzen, 1970):

$$S(p) = \sum_n S_n \tag{16}$$

where

$$S_n = s_n sin(nt + \sigma_n) = A_n \cos(nt) + B_n \sin(nt) \tag{17}$$

Consequently, the frequency domain form of the BRF utilizes units of cycles/day (CPD) and incorporates signal gain and phase angle. Signal gain (BE) refers to the amplitude of the barometric pressure signal, while phase angle is expressed with respect to the mean solar day of 360° (Chapman and Lindzen, 1970). By the convention established by Rojstaczer et al. (1988), a phase of -180° corresponds to the response of a perfectly confined aquifer, while a phase angle greater than and less than -180° represent phase advance and phase lag, respectively. The diurnal (S_1) and semidiurnal (S_2) components of barometric pressure variations periodically occur at frequencies of ~1 CPD and ~2 CPD, respectively, while aperiodic barometric pressure signal fluctuations typically occur below 1 CPD (Quilty and Roeloffs, 1991; Hussein et al., 2013).

2.4.1 BRF General Form – Frequency Domain

The frequency domain form of the BRF was first developed and implemented nearly a decade after Weeks' (1979) pneumatic-transmission time domain BRF by Rojstaczer (1988), within an semiconfined aquifer near Mammoth Lakes, California. Rojstaczer (1988) noted that a stepchange in barometric pressure leads to three head imbalances within a given aquifer that can lead to fluid flow: 1. Pneumatic diffusivity (vertical airflow) through the vadose zone due to the pressure imbalance between the surface of the earth and the water table; 2. Vertical groundwater flow through the confining layer to the aquifer due to the head imbalance between the water table and the aquifer; and 3. Horizontal groundwater flow between the borehole and the aquifer due to the pressure imbalance between the open borehole and the aquifer (Figure 4). The governing equations and flow solutions for all three of these flow mechanisms are discussed in Section 2.4.3. Based on these three imbalances, Rojstaczer et al. (1988) defined three distinct stages for a generic frequency domain BRF at low, intermediate, and high frequencies. The qualitative shape of a generic frequency domain curve is that of a modified bell curve and is a function of the

hydrogeological properties of the aquifer, as well as the dimensions of the borehole (Hussein et al., 2013) (Figures 5 and 6). The first stage, which occurs at the lowest frequencies, gain (BE) exponentially increases with increasing frequency from an initial near-zero value, while phase decreases with increasing frequency. According to Odling et al. (2015) the primary control on the frequency response during the first stage of the BRF is attributable to the properties of the confining layer of the semiconfined aquifer. At the low frequencies of stage 1, the well is in equilibrium with the pore pressure of the aquifer and the aquifer exhibits a gain (BE) of zero and phase approaching zero, which is consistent with the gain and phase values of an unconfined aquifer (Rojstaczer, 1988; Odling et al., 2015). The second stage of the generic BRF, which occurs at intermediate frequencies, characterized by a plateau of both gain and phase. At these intermediate frequencies, the water level response is lagged -180° from the barometric pressure signal and the BRF is indicative a fully confined aquifer with a static BE (Hussein et al. 2013). The response at intermediate frequencies is largely independent of fluid properties and is primarily a function of the elastic properties of the porous media comprising the aquifer skeleton (Rojstaczer, 1988). The width of the third and final stage of the BRF at the highest frequencies features decreasing gain and decreasing phase with increasing frequency. This is because at higher frequencies, the water level within the borehole cannot keep up with the rapid changes in barometric pressure. As a result, the form of the BRF once again approaches that of an unconfined aquifer, with both gain and phase approaching zero (Odling et al., 2015).

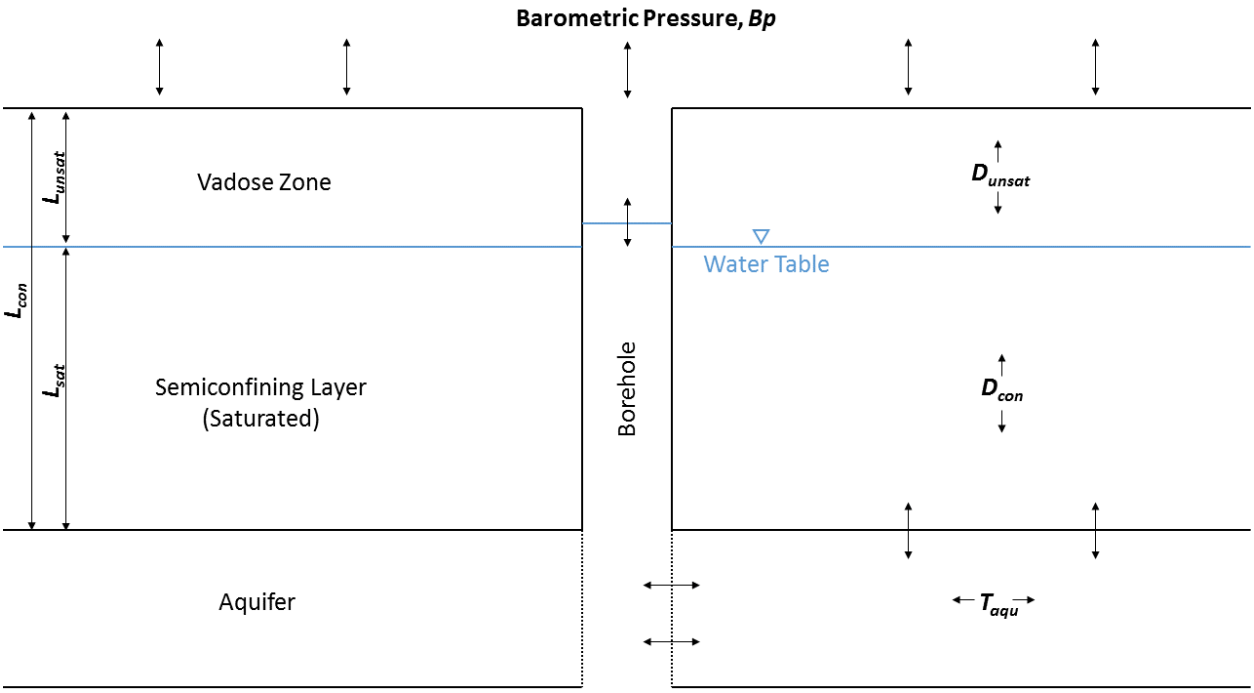

Figure 4: Cross sectional diagram of an idealized, semiconfined aquifer, featuring hydrostratigraphic units on the left and frequency domain barometric response function (BRF) parameters on the right. Estimated parameters for the relevant processes include vertical air flow within the vadose zone (D_{unsat}), vertical groundwater flow within the semiconfining unit (D_{con}), aquifer transmissivity (T_{aqu}), and vadose zone length (L_{unsat}) (adapted from Odling et al., 2015).

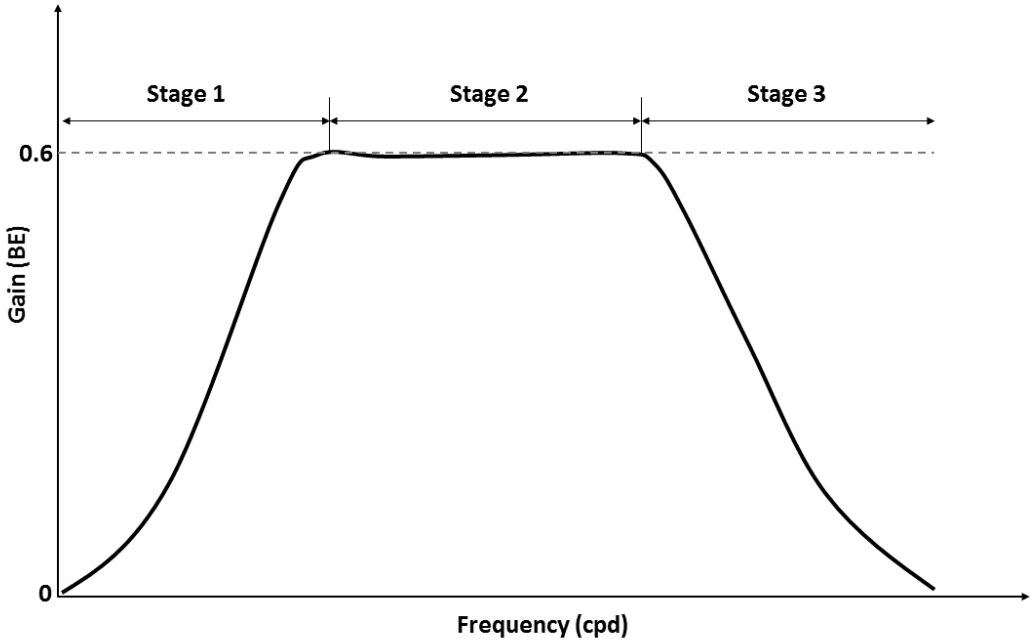

Figure 5: Generic frequency domain barometric response function (BRF) gain plot. Barometric efficiency (BE) increases with increasing frequency, plateaus at the static (confined) barometric efficiency, and then decreases with increasing frequency.

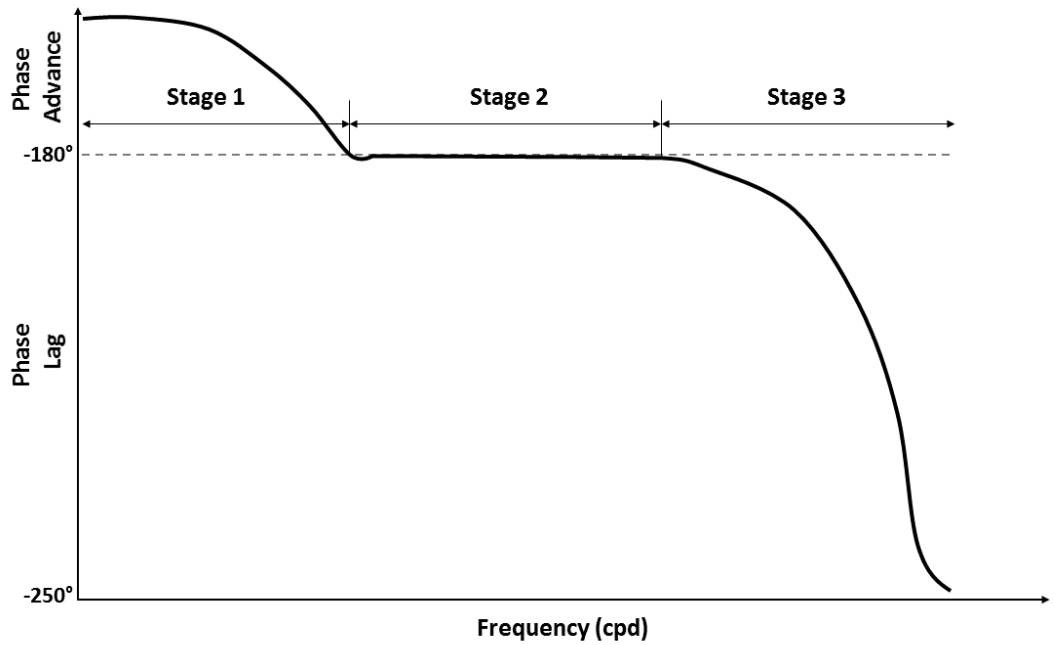

Figure 6: Generic phase plot. Phase advance occurs at phase angles greater than -180°, while phase lag occurs at values less than -180°. This occurs in three phases according to the periodic fluctuations in atmospheric pressure (adapted from Hussein et al., 2013).

2.4.2 BRF Calculation – Frequency Domain

The frequency domain form of the BRF is calculated in a similar way to the time domain form of the BRF. Both forms involve the deconvolution of the borehole water level record by the barometric pressure record to assess the effect of the system input (barometric pressure) on the system output (changes in water level) (Bendat and Piersol, 2000; Hussein et al., 2013). Unlike the time domain, which uses linear regression to estimate the time-lagged response of water levels to changes in barometric pressure (Rasmussen et al., 1997), the frequency domain form of the BRF is calculated entirely in the frequency domain itself using signal processing techniques. The primary technique used by other researchers *(*Rojstaczer, 1988; Rojstaczer and Riley, 1990; and Quilty and Roeloffs, 1991) is cross spectral deconvolution by ensemble averaging (Welch, 1967). In this technique, the time domain water level and barometric pressure records are divided into several equally-spaced and partially overlapping segments. Once the time series is equally

divided, each time domain segment is converted into the frequency domain through a Fourier transform. Fourier transforms provide a continuous spectral representation of a time domain signal by representing that signal as a product of sinusoidal functions (Bendat and Piersol, 2000). The general form of a Fourier transform *X(f)* is commonly expressed as:

$$X(f) = \int_0^\infty h(t) e^{-j2\pi f t} dt \tag{18}$$

where *h(t)* is the time domain series and *j* is the imaginary component of the transform ($\sqrt{-1}$). Thus, the output of a Fourier transform is a complex number, featuring both real and imaginary components. Once all of the overlapping, equally-spaced time series data have been transformed into the frequency domain, a frequency response function is calculated for each pair of overlapping time series segments. A frequency response function is the ratio of the cross spectra of the water level and barometric pressure frequency domain signals to the auto spectra of barometric pressure (Quilty and Roeloffs, 1991). Frequency response functions, also known as transfer functions, are linear, time-invariant functions commonly utilized to quantitatively assess the relationship between a single system input and its corresponding system output (Bendat and Piersol, 2000). An example of a frequency response function (BRF) used to represent the impact of barometric pressure input on the water level output is (Hussein et al., 2013):

$$BRF(f) = \frac{X_{WB}}{X_{BB}} \tag{19}$$

where X_{WB} is the cross spectra of water level and barometric pressure signals and X_{BB} is the auto spectra of the barometric pressure signal. Spectral density functions, including cross spectra and auto spectra, are simply the Fourier transformed individual time domain records. Cross (power) spectral density represents the distribution of signal power per unit frequency, while auto spectral density represents the Fourier transformed estimate of the autocorrelation (cross-correlation of a signal with itself) sequence of the signal (Bendat and Piersol, 2000). Gain (A) and phase (θ) are calculated with the frequency response function by taking the modulus (absolute value) and argument (complex inverse tangent) as follows (Hussein et al., 2013):

$$A^{BRF} = |BRF(f)| \tag{20}$$

$$\theta^{BRF} = arctan\left[\frac{imag\big(BRF(f)\big)}{real(BRF)}\right] \tag{21}$$

Since the frequency response function generates a complex function, the argument of this value is the angle between the complex plane and the positive real axis (Bendat and Piersol, 2000). The final steps of the cross spectral deconvolution by ensemble averaging technique is to then use the frequency response BRF for each segment of the time domain signal so that several overlapping BRFs are created from the original signal (Quilty and Roeloffs, 1991). A final, smoothed BRF is then calculated by averaging all of the partially independent BRF segments (Odling et al., 2015). Hussein et al. (2013) noted that the final step of ensemble averaging of the partially independent BRFs optimizes and improves the accuracy of the final BRF, which would otherwise have less accuracy with fewer, longer segments at lower frequencies and greater accuracy at higher

frequencies with more, shorter segments. The final BRF is calculated with error bars of one standard deviation across all frequencies.

2.4.3 BRF Analytical Model – Frequency Domain

Rojstaczer's (1988) frequency domain, analytical BRF model for the hypothetical water level response for a well in a semiconfined aquifer is presented in the following sections. As mentioned in Section 2.4.1, the three main components of flow induced by a step change in barometric pressure are vertical airflow, vertical groundwater flow to the aquifer through the confining layer, and horizontal groundwater flow between the borehole and aquifer. The governing equations of flow for all three of these flow mechanisms are discussed in the following sections.

2.4.3.1 Vertical air flow

Earlier time domain BRF work (Weeks, 1979) introduced the concept of pneumatic diffusivity. In this process, air flows through the vadose zone due to the pressure gradient between the surface of the earth and the water table. The governing equation for this process is expressed as:

$$\alpha \frac{\partial^2 p_a}{\partial z^2} = \frac{\partial p_a}{\partial t} \tag{22}$$

which is constrained by boundary conditions of:

$$p_a(-L, t) = A\cos(\omega t) \tag{23}$$

$$p_a(L,t) = A\cos(\omega t) \tag{24}$$

where α is the pneumatic diffusivity, p_a is barometric pressure, and A and ω represent the respective amplitude and frequency of a given barometric pressure wave. By convention, the boundary condition of $-L$ represents the surface of the earth, the water table is assigned a depth of zero, and L represents the lower extent of the model domain. Rojstaczer (1988) developed the solution to the above governing equation with the given boundary conditions, which is expressed as:

$$p_a = (M - iN)A\exp(i\omega t) \tag{25}$$

where M and N represent

$$M = \frac{2\cosh(\sqrt{R})\ \cos(\sqrt{R})}{\cosh(2\sqrt{R}) + \cos(2\sqrt{R})} \tag{26}$$

$$N = \frac{2\sinh(\sqrt{R})\sin(\sqrt{R})}{cosh(2\sqrt{R}) + cos(2\sqrt{R})} \tag{27}$$

and R is a dimensionless frequency of:

$$R = \frac{L^2\omega}{2\alpha} \tag{28}$$

and is thus dependent on the pneumatic diffusivity of the vadose zone and the depth of the water table. A key assumption in Rojstaczer's (1988) analytical, frequency domain BRF is that airflow

induced by a step change in barometric pressure at the earth's surface is predominately vertical. If non-vertical flow paths are taken by gas passing through the vadose zone, then the relatively simple, one-dimensional governing equation may need to be adjusted to account for the non-vertical portion of gas flow.

2.4.3.2 Vertical groundwater flow

The second component of vertical flow induced by a step change in barometric pressure is that of groundwater moving vertically from the water table, through the confining unit (if present), to the aquifer. Assuming groundwater flow between the water table and the aquifer is strictly vertical, the governing equation for changes in pore pressure as a result of periodic atmospheric pressure fluctuations can be expressed as (Rojstaczer, 1988):

$$D_{con}\frac{\partial^2 p}{\partial z^2} = \frac{\partial p}{\partial t} + \omega\gamma\, A\, \sin(\omega t) \tag{29}$$

where D_{con} is the vertical hydraulic diffusivity from the water table to the aquifer, through the confining unit, p is the change in pore pressure of water within the formation, and γ is the loading efficiency, or the ratio of change in pore pressure to change in surface load. It can be noted that (29) is structurally similar to (22), which are both equations for vertical, one-dimensional flow. The key difference for the vertical flow of groundwater from the water table to the aquifer is that the sinusoidal component of periodic atmospheric pressure fluctuations is accounted for with the frequency term. Assuming the standard convention of downward, compressive stress as positive, the boundary conditions for the governing equation of vertical groundwater flow are:

$$p(0,t) = MA\cos(\omega t) + NA\sin(\omega t) \tag{30}$$

$$p(\infty,t) = A\gamma\cos(\omega t) \tag{31}$$

and z=0 represents the depth of the water table. Based on these boundary conditions, Rojstaczer (1988) derived the solution to the governing equation for vertical groundwater flow (29):

$$p = (M + iN - \gamma)A\exp\left(-(i+1)(0.5qS')^{\frac{1}{2}}\right)(\exp(i\omega t) + A\gamma\exp(i\omega t)) \tag{32}$$

where S' is the confining layer storage coefficient and q is a dimensionless frequency composed of the confining layer vertical hydraulic conductivity *K'* and the confining layer thickness *b'*.

$$q = \frac{b'\omega}{K'} \tag{33}$$

For the sake of simplicity in fitting the analytical solution to empirically calculated BRFs, this equation can be expressed as the dimensionless frequency of *Q*, a product of vertical hydraulic diffusivity D_{con}:

$$Q = \frac{qS'}{2} = \frac{b'^2\omega}{2D_{con}} \tag{34}$$

It is important to note, once again, the key assumption of strictly vertical groundwater flow induced by fluctuations in atmospheric pressure. If a non-vertical component of flow existed,

then the governing equation and boundary conditions would need to be adjusted by incorporating additional flow directions to account for the additional non-vertical component of groundwater flow from the water table to the aquifer.

2.4.3.3 Horizontal groundwater flow

The third and final component of flow induced by a step change in atmospheric pressure is horizontal groundwater flow between the borehole and the aquifer. The governing equation for this scenario was proposed by Rojstaczer (1988) by assuming that groundwater flow within the aquifer is strictly horizontal:

$$\frac{\partial^2 s}{\partial r^2} + \frac{1\partial s}{r\partial r} - \frac{K's}{Kbb'} = \frac{S_s \partial s}{K\partial t} \tag{35}$$

where *s* represents the head change in the aquifer associated with the finite volume of water flowing between the well and the aquifer due to barometric pressure fluctuations, S_s is aquifer specific storage, *K* is the horizontal hydraulic conductivity of the aquifer, *K'* is the vertical hydraulic conductivity of the semi confining layer, and *b* and *b'* are the thickness of the aquifer and semi confining layer, respectively. The boundary conditions for this flow domain were derived by Cooper et al. (1965) for seismically induced water level variations and are as follows:

$$s(\infty, t) = 0 \tag{36}$$

$$\lim_{r \to 0} \frac{r\partial s}{\partial r} = \frac{\omega r_w^2 x_0}{2Kb} \sin(\omega t) \tag{37}$$

where K represents the horizontal component of aquifer hydraulic conductivity, r_w is the well radius, and x_0 represents the amplitude of the water level fluctuation that is produced from a step change in barometric pressure and the associated flow of water between the borehole and the aquifer. Given these boundary conditions, the solution to equation (35) for the water level change at a point proximal to the well screen s_w is:

$$s_w = i0.5x_0K_0\left[W^2\left(S^2 + {}^1\!/_{q^2}\right)\right]^{0.25}\exp[i0.5\{tan^{-1}(qs)\}]\exp(i\omega t) \tag{38}$$

where K_0 is a zero-order, modified Bessel function of the second kind, S is the aquifer storage coefficient (Ssb), and W is the dimensionless frequency:

$$W = \frac{\omega r_w^2}{Kb} \tag{39}$$

of the aquifer.

Thus, the three responses to potential imbalances that arise due to periodic fluctuations in barometric pressure (vertical air flow, vertical groundwater flow, and horizontal groundwater flow) can be expressed and solved with appropriate governing equations and boundary conditions. The final solutions to these three flow problems, assuming that all assumptions of flow direction are maintained, can thus be expressed in terms of three dimensionless frequencies: R, Q, and W, which are each a function of pneumatic diffusivity (α), hydraulic diffusivity (D_{con}), and horizontal hydraulic conductivity or transmissivity, respectively (Rojstaczer et al., 1988).

The purpose of this paper is to assess the utility of both time and frequency domain BRFs for estimating hydraulic properties of the HPA. Of particular interest is the vertical component of of hydraulic conductivity (Kz), since estimations of this parameter improve our understanding of hydrogeological processes including anisotropy of groundwater flow and groundwater recharge. A better understanding of these processes will improve groundwater management strategies in the HPA and other similar aquifers throughout the world.

2.5 Study Area

The study area is located within the High Plains aquifer (HPA) of western Kansas, at two of the Kansas Geological Survey (KGS) Index Wells (monitoring wells) in Scott and Thomas counties, within Kansas Groundwater Management Districts (GMD) 1 and 4, respectively (Figure 7). These wells were constructed as part of the High Plains Aquifer Calibration Monitoring Well Program, which was launched in 2007 with the goal of improving understanding of hydrologic responses at the local level within the HPA and improving long-term groundwater management strategies (Young et al., 2007). Both wells are constructed with Sch. 40 6.35 cm ID (2.5 in) PVC with mill slot screens 3.05 meters long (Table 1). Each well is equipped with a barometric pressure transducer (INW, PT2X) and a vented water level pressure transducer (INW, PT2X), all of which record pressure every hour. Each well is also equipped with a telemetry system that transmits water-level and barometric-pressure data to the KGS servers every 2 hours (Young et al., 2007). Additional well construction information is provided in Table 1.

Table 1: Well data for Scott and Thomas County Index Wells.

Parameter (units)	Scott IW	Thomas IW
TOC Elevation (m ASL)	904.39	971.53
Total depth (m)*	68.65	85.89
Depth to Water (m)*	42.31	67.97
Saturated Thickness (m)	26.34	17.92
Screened Length (m)	3.05	3.05
Screened Interval (m)	65.53 – 68.58	83.52 – 86.56
Casing radius (cm)	3.2	3.2

*Total depth and depth to water measured at TH and SC on November 13 and December 9, 2015, respectively.

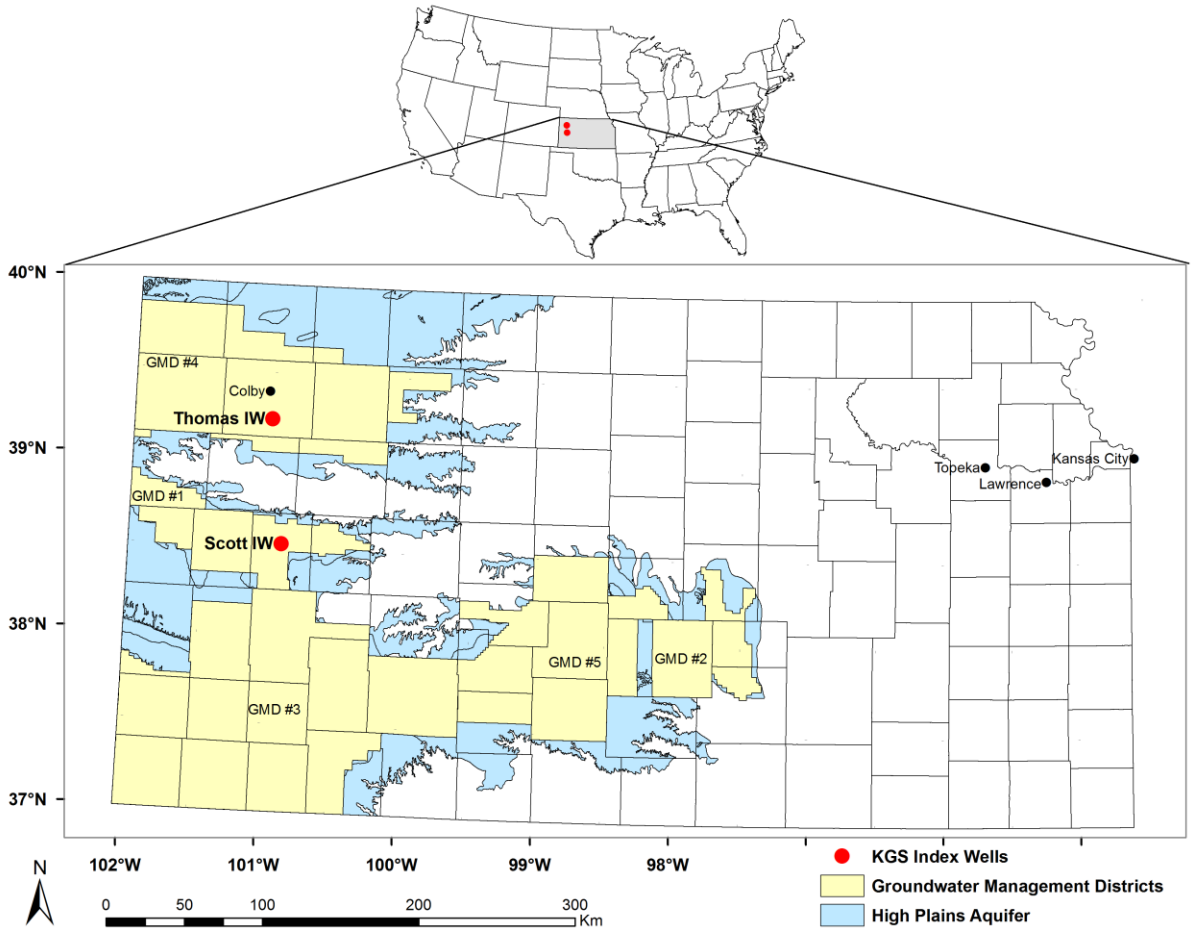

Figure 7: Study area featuring two Kansas Geological Survey Index Wells within the High Plains aquifer of western Kansas. The two long term monitoring wells are located in Scott and Thomas counties, within Kansas Groundwater Management Districts 4 and 1, respectively. Data source: State of Kansas GIS Data Access & Support Center (DASC).

2.5a Scott County (SC) Site

The SC site is located at NE 1/4 NE 1/4 NE 1/4 Sec. 1, T.18S R.33W, along the north edge of a depression in the bedrock known as the "Scott-Finney depression" (Young et al., 2007). This is the only area in the eastern region of GMD1 with significant groundwater reserves remaining (Meyer et al., 1970; Young et al., 2007). The surficial geology of SC consists of unconsolidated Quaternary alluvium, dune sand, and loess deposits, which rest unconformably on upper Cretaceous Niobrara Formation chalk (Waite, 1946). Unconsolidated surficial deposits extend up to 90 m below land surface in SC (Gutentag and Stullken, 1976). The principal aquifer is in the Tertiary Ogallala formation, which consists of unconsolidated sand, gravel, silt, and clay and ranges in thickness from 0-65 m (Waite, 1946; Gutentag and Stullken, 1976). According to Young et al. (2007), this aquifer is predominately unconfined with a consistent lateral thickness. Young et al. (2007) interpreted the lithology at the SC site as vertically heterogeneous, consisting of mostly fine-grained sediments, such as sandy and silty clay, with thicknesses up to 50 m, overlying more permeable coarse-to-fine sand and gravel. The index well at the SC site is completed to a depth of 69.19 m (227 ft) below land surface and is screened from 65.53-68.58 m (215-225 ft) within coarse sand and gravel (Young et al., 2007) (Figure 8a).

2.5b Thomas County (TH) Site

The HPA stratigraphy at the TH site, located at NW 1/4 NW 1/4 NW 1/4 Sec. 33, T.09S R.33W, is more laterally heterogeneous than that of the SC site, featuring coarse sand and gravel interspersed with thin clay and silt lenses (Young et al., 2007). The Ogallala formation near TH ranges from 18.3-83.8 m (60-275 ft) in thickness and unconformably overlies the Pierre Formation shale bedrock (Butler et al. 2013a; Frye 1945). Butler et al. (2013a) observed from water-level changes associated with annual pumping that the saturated unconsolidated interval of

the TH site is characteristic of an unconfined aquifer. Butler et al. (2013a) also noted a yearly increase in water-level from 2009 to 2010, which they interpreted as indicative of a potential source of recharge to the HPA at the TH site. The index well at the TH site is completed to a depth of 87.17 m (286 ft) below land surface and is screened from 83.5-86.6 m (274-284 ft), within fine sand and gravel (Young et al., 2007) (Figure 8b). Based on the "closed system response" of hydrographs of the TH site, Butler et al. (2013) suggested that the screened interval at the TH site is laterally surrounded by relatively low permeability sediments.

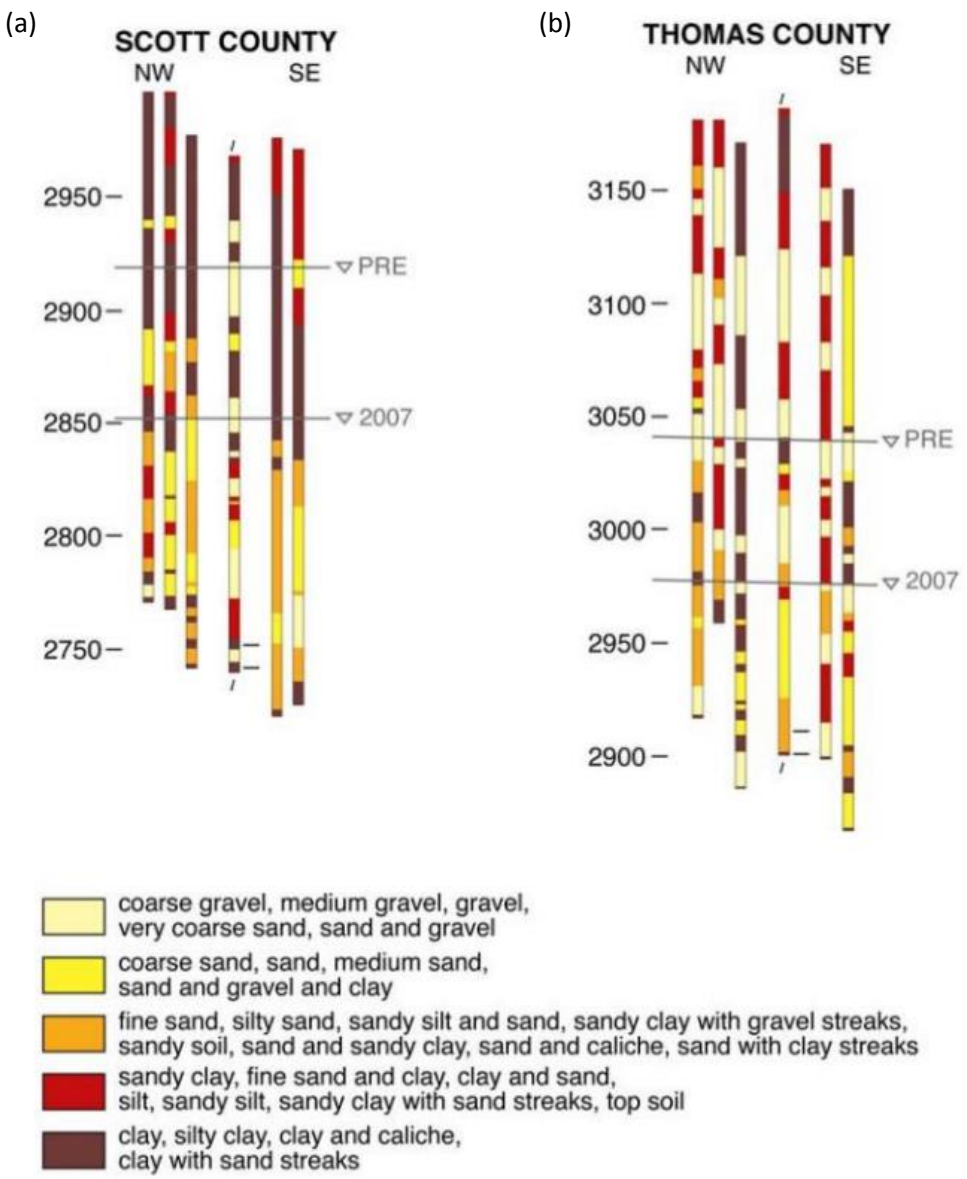

Figure 8: Cross sectional lithology for both SC (a) and TH (b) wells (identified as "*I"*). Adapted from Young et al. (2007).

3. Methods

In order to improve water level and barometric pressure signal resolution, a Campbell Scientific CR1000 datalogger was used to log recordings from two SDI-12 INW PT2X Submersible Pressure/Temperature Smart Sensors at a sampling interval of 10 seconds, which is nearly 360 times more frequent than the original sampling interval of 1 hour used for the initial time domain BRF analysis. Water pressure was measured using a gauge (vented) sensor, which utilizes a vent tube in the cable to reference atmospheric pressure. To account for fluctuations in water level and ensure that the water level did not fall below the gauge sensor, the sensor was installed at a depth of around six meters below the initial water level. Barometric pressure was simultaneously measured using an absolute (nonvented) pressure sensor, which was installed above the water level within the open borehole a short distance below land surface. This methodology is similar to that of Hussein et al. (2013), who used two absolute (nonvented) pressure sensors to measure water pressure and barometric pressure. The main difference is that the simultaneous use of a gauge (vented) sensor for water level and an absolute (nonvented) sensor for barometric pressure eliminates the extra step of determining water level signal by subtracting barometric pressure from the total pressure (water pressure and barometric pressure), reducing error associated with using multiple sensors. Pressure data were obtained in units of PSI and converted directly into equivalent water head (cmH_2O). Prior to analyzing the water level and barometric pressure, the pressure transducer record was detrended by removing any linear trends and subtracting the mean from each data point. This was done to avoid spectral leakage at higher frequencies, which can sometimes occur if there is a trend in the signal (such as recharge during the recovery period for water wells) (Hussein et al., 2013). Barometric pressure and water

level data collected at the TH and SC sites were collected over periods of 17 and 25 days in December 2015 and January 2016, respectively (Figures 9 and 10).

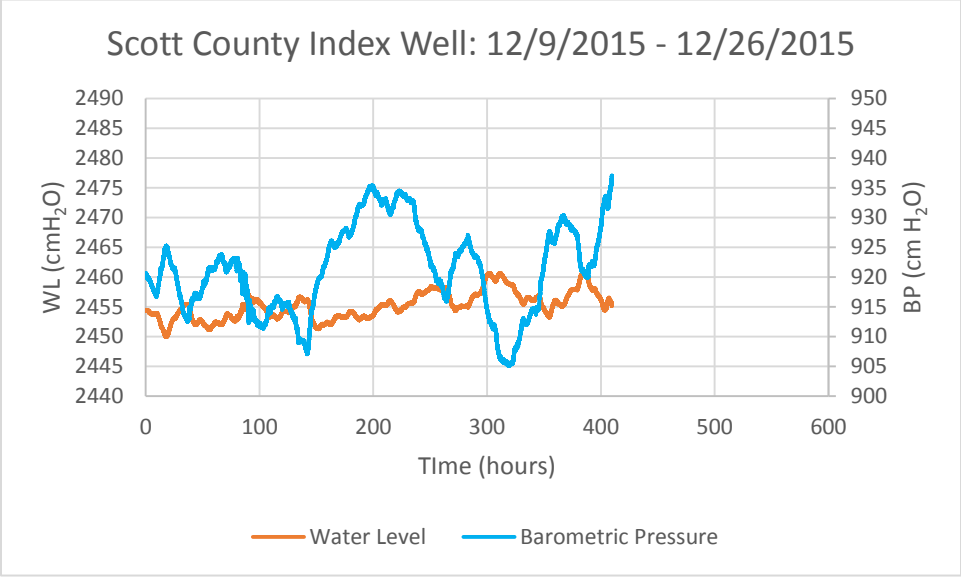

Figure 9: Water level and barometric pressure data at Scott County Index Well. Data were collected at 10 second intervals over a period of 17 days.

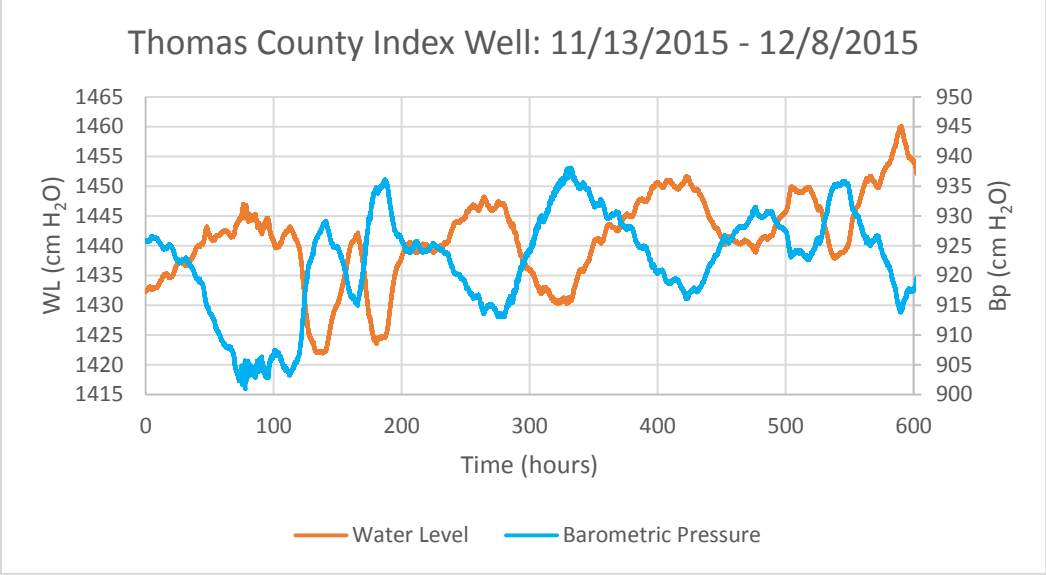

Figure 10: Water level and barometric pressure data at Thomas County Index Well. Data were collected at 10 second intervals over a period of 25 days.

3.1 Barometric Response Functions (BRFs) – Time Domain

Barometric response functions were calculated for both the TH and SC sites using the regression convolution technique of Rasmsussen and Crawford (1997) and Spane (2002), through the spreadsheet-based Visual Basic program developed by the KGS (Bohling et al., 2011). Hourly barometric pressure head (ft) and water level (ft) data obtained from data loggers at both sites were converted to meters and entered into the KGS BRF spreadsheet (Appendix A). In order to minimize the impact of local pumping on water-level response, barometric pressure head and water level data were selected from the recovery period for each well (January 6, 2013 – March 11, 2013), following the methods of Butler et al. (2011) and Bohling et al. (2011). The impact of earth tides on the water level signal was deemed negligible relative to the larger barometric pressure influence on water levels at both sites (Buddemeier et al., 2010). BRFs at both the SC and TH sites were calculated over a time period of around 4 days, which was consistent with the time lag used in previous studies (Butler et al., 2013b; 2013c).

3.2 Analytical BRF Model – Time Domain

Hydraulic conductivity and pneumatic diffusivity were estimated by fitting an analytical model to the calculated time-domain BRFs, following the methods of Butler et al. (2013b) (Figure 9). The time domain analytical BRF model implemented by both Spane (2002) and Butler et al. (2013b) feature a superposition of Hvorslev's (1951) slug-test model and Weeks' (1979) one-dimensional pneumatic transmission model. Since near-well hydraulic conductivity is the primary controlling factor at early time periods and pneumatic diffusivity of the vadose zone is the primary driver of the BRF at later time periods, the Hvorslev (1951) slug-test solution dictates the portion of the BRF up to the peak BE value (A), while Weeks' (1979) pneumatic-transmission model dictates the shape of the curve after the peak BE value (B). The

superimposed analytical BRF model was developed in a spreadsheet-based Visual Basic program, which enabled hydraulic conductivity and pneumatic diffusivity to be adjusted (Butler et al., 2013b). The cell-code version of this spreadsheet is included in Appendix A. The analytical BRF was visually fit to the calculated BRFs by manually adjusting hydraulic conductivity and pneumatic diffusivity, following the methods of Weeks (1979) and Furbish (1991).

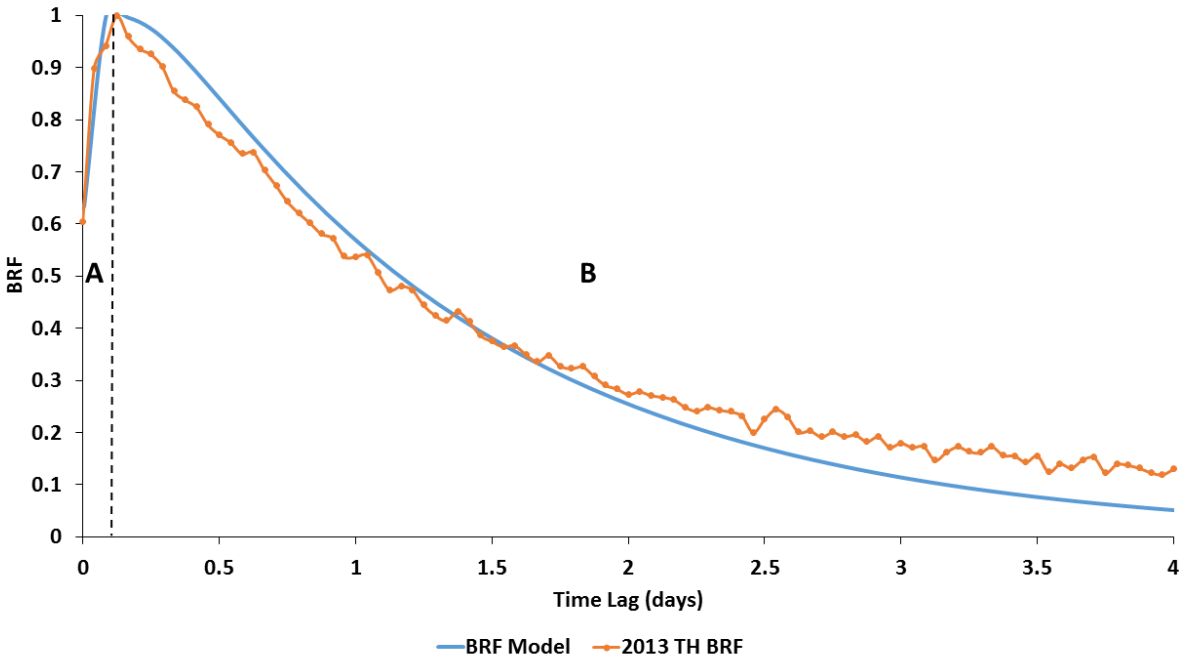

Figure 11: Barometric response function (BRF) for the Thomas County Index Well and time domain analytical model. BRF calculated during the recovery period of 2013. Analytical model superposites the Hvorslev (1951) (A) and Weeks (1979) (B) models.

3.3 Analytical BRF Model – Frequency Domain

The magnitude squared coherence function (C_{WB}) was used to assess the frequency ranges over which the BRF was valid. This function ranges from 0-1 and relates the fractional proportion of a linear system's output signal caused by a given input signal and is expressed as:

$$C_{WB} = \frac{|X_{WB}(f)|^2}{X_{ww}(f)X_{BB}(f)} \tag{40}$$

where $X_{WB}(f)$ is the cross spectrum of the water level and barometric pressure signals, and $X_{WW}(f)$ and $X_{BB}(f)$ are the auto spectra of the water level and barometric pressure signals, respectively (Bendat and Piersol, 2000; Hussein et al., 2013). For a perfectly linear system with a single input and output, a magnitude squared coherence function of one indicates perfect correlation between the system components (Bendat and Piersol, 2000), while values less than one indicate either extraneous noise exists in the signals or other inputs influence the system output (Hussein et al., 2013). Thus, for the purposes of this study, a coherence value near one indicates that there is a strong correlation between the system input (barometric pressure) and the system output (changes in water level). Following the methods of Hussein et al. (2013), a cutoff frequency was established for the frequency at which the coherence dropped to less than 0.5 to ensure that the changes in water level signal were predominately attributable to periodic barometric pressure fluctuations.

This study uses the frequency domain analytical BRF model developed by Rojstaczer et al. (1988) and subsequently modified by Hussein et al. (2013) and Odling et al. (2015) to account for capillary fringe attenuation (Appendix B). The modified form of the analytical model of

Rojstaczer et al. (1988) allows for the saturated zone near the water table to possess finite compressibility and thus the capability of attenuating pressure waves as they pass from the vadose zone to the saturated zone (Evans et al., 1991). This attenuation is attributable to the partial absorption of air pressure waves caused by changes in the volume of encapsulated air near the capillary fringe (Hussein et al., 2013). This BRF model was coded in MATLAB by Hussein et al. (2013) and estimates six hydrogeological parameters for semiconfined aquifers including barometric efficiency (*BE*), vadose zone thickness (L_{unsat}), hydraulic diffusivity of the saturated confining unit (D_{con}), pneumatic diffusivity (D_{unsat}), aquifer transmissivity (T_{aqu}), and an attenuation factor (T_{cf}). Rojstaczer (1988), one of the first researchers to use an analytical BRF model to estimate hydrogeological parameters, developed a method in which the three dimensionless frequencies (R, Q, and W) characteristic of the three flow problems described in the introduction (vertical airflow, vertical groundwater flow, and horizontal groundwater flow) are fit to a calculated BRF. Rojstaczer (1988) likened the process of fitting the analytical BRF model to a calculated BRF to that of pumping test type curve matching, in which water level drawdown data are fit to a dimensionless theoretical response (type curve). The key difference between these two processes is that the BRF analytical model must be simultaneously fit to two different type curves: a gain plot (BE) and a phase plot (Hussein et al., 2013). The fitting is executed within the BRF code developed by Hussein et al. (2013) with the aid of a combined hybrid genetic and pattern search algorithm, which minimizes the sum of square differences between the calculated and modeled BRF within the complex plane. The hybrid algorithm combines the computational efficiency of the pattern search method with the ease of use of the genetic algorithm, which does not require an initial estimate to find the global minimum of the objective function (Alsumait et al., 2010; Liuni et al., 2010).

3.4 Slug Tests

To assess the accuracy of both the time and frequency domain BRFs in estimating near-well hydraulic conductivity of the aquifer, a series of slug tests were performed at both the SC and TH sites. Prior to conducting fieldwork at both sites, AQTESOLV (HydroSOLVE, Inc., Reston, VA) was used to estimate the expected water level recovery time at both sites by simulating forward solution slug tests incorporating the K_x values estimated from the time domain BRF at each site. Based on these preliminary analyses, each slug test at SC and TH was estimated to last around three hours. Following the methods of Butler (1998), a total of 10 slug tests were carried out at each site (20 total) using both rising and falling head initiation and 2-foot (0.6 m) and 4-foot (1.2 m) solid PVC slugs in ascending order of initial displacement. Water level data were collected with absolute (nonvented) In-Situ MiniTroll Pro data loggers at sampling intervals of 0.5 and 1.0 seconds at the TH and SC sites, respectively. Water level data were downloaded from each sensor using Win-Situ 4 software and graphed in a series of overlapping plots of normalized head. The least noisy of each set of 10 slug tests was chosen for analysis within AQTESOLV, adhering to the methods of Butler (1998). Based on the Midwest Geosciences Group Field Guide for Slug Testing and Data Analysis, wells at both the SC and TH sites were identified as partially penetrating, "Category I" wells, featuring screened intervals below the water table within an unconfined aquifer (Midwest Geosciences Group, 2007). As a result, slug test data from both sites were analyzed using the Cooper et al. (1965) and KGS models (Butler 1998). Furthermore, to maintain consistency with the time domain BRF model, the data were also analyzed using the Hvorslev (1951) model for unconfined hydrogeological settings.

4. Results

4.1 BRFs – Time Domain

The BRFs for the SC and TH sites exhibit an exponentially decreasing response, which is characteristic of unconfined aquifer conditions (Figure 2). Although the qualitative shape of the two responses is similar, there are a some key differences between the two sites with respect to magnitude of response and recovery time. The TH site reached a peak BE value of around 0.99 after three hours and decreased to a value of 0.07 after four days (Figure 10, Table 2). Compared to the TH site, the SC site's BE response was nearly half that of the TH site at 0.5, but occurred at approximately the same time lag (three hours). The recovery time was also three days shorter for the SC site, taking around one day to recover to a BE of near 0.1.

Table 2: Estimated parameters for Scott (SC) and Thomas (TH) County Index Wells. These parameters are barometric efficiency (BE), pneumatic diffusivity (α), horizontal hydraulic conductivity (K_x), specific storage (S_s), aquifer transmissivity (T_{aqu}), hydraulic diffusivity (D_{con}), and vertical hydraulic conductivity (K_z). Estimation methods are time and frequency domain barometric response functions (BRF-T and BRF-F, respectively) and slug tests. Frequency domain estimates of K_x were calculated from estimates of T_{aqu} by subtracting a confining layer thickness of 5 m from the saturated thicknesses of SC (36.34 m) and TH (17.92 m) (Table 1).

Index Well	Method	BE (-)	α (m^2/s)	K_x (m/s)	S_s (m^{-1})	T_{aqu} (m^2/s)	D_{con} (m^2/s)	K_z (m/s)
SC	BRF-T	0.01-0.47	0.0390	1.19×10^{-7}	-	-	-	-
	Slug Test	-	-	1.54×10^{-5}	4.79×10^{-6}	-	-	-
	BRF-F	0.52	1.15×10^{-5}	1.22×10^{-7}	-	2.61×10^{-6}	1.07×10^{-3}	3.21×10^{-8}
TH	BRF-T	0.07-0.99	0.0169	4.90×10^{-6}	-	-	-	-
	Slug Test	-	-	1.14×10^{-4}	1.28×10^{-6}	-	-	-
	BRF-F	0.91	9.83×10^{-6}	3.19×10^{-7}	-	4.12×10^{-6}	5.21×10^{-4}	1.56×10^{-8}

4.2 Analytical BRF Model – Time Domain

Visually fitting the time domain analytical BRF solution to the calculated BRFs for both the SC and TH sites provide estimates of near-well hydraulic conductivity (K) and pneumatic diffusivity (α) (Figure 10). The estimated K value at the TH site (4.90 x 10^{-6} m/s) was higher by an order of magnitude and the α value (0.0169 m^2/s) was lower by a factor of two than the values estimated at the SC site (Table 2). From 2013 to 2015, the estimated K value at the TH site decreased by an order of magnitude (4.40 x 10^{-7} m/s), while the α value decreased by around 6% (0.0158 m^2/s). The estimated K value at the SC site decreased by 8% (1.10 x 10^{-7} m/s), while the α value remained the same.

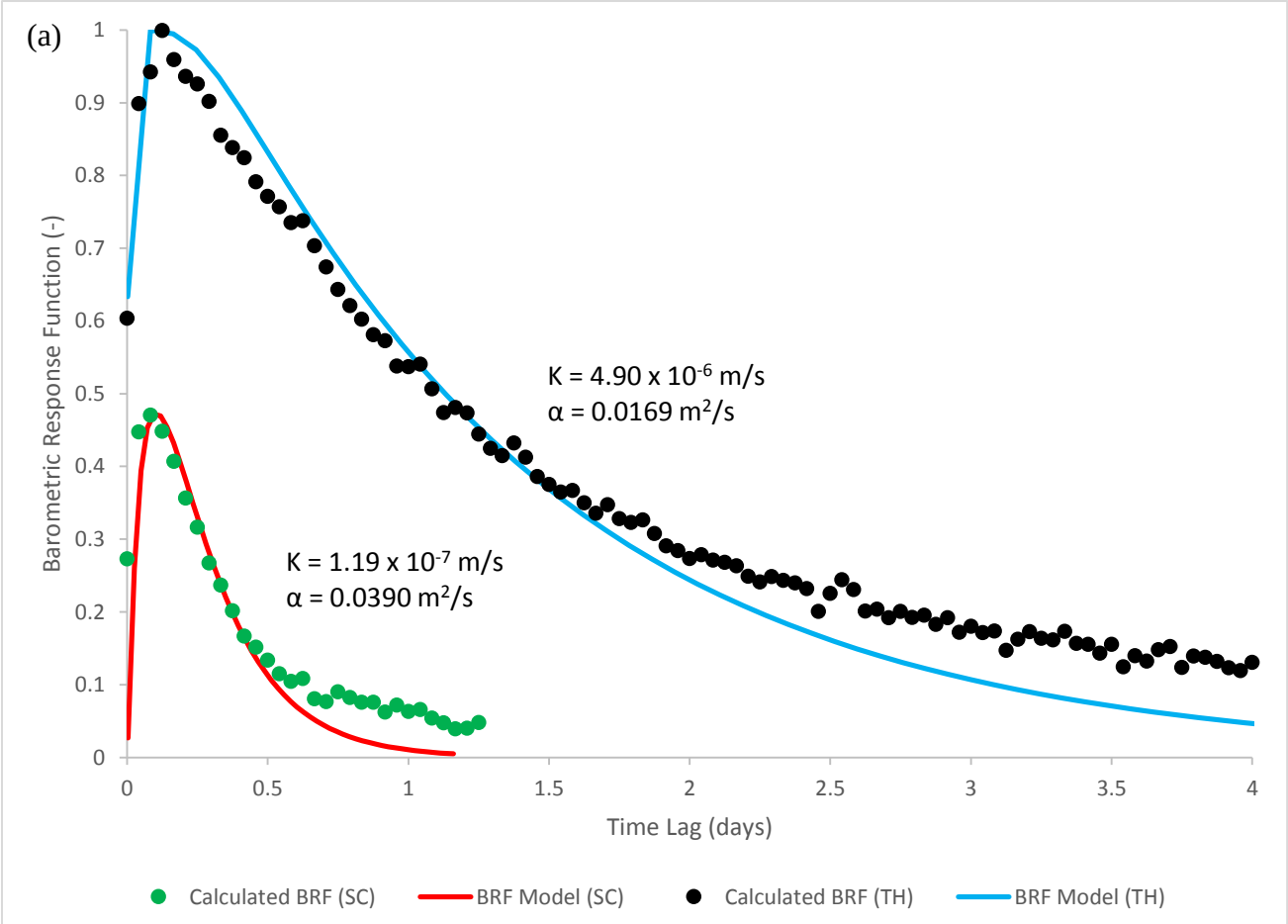

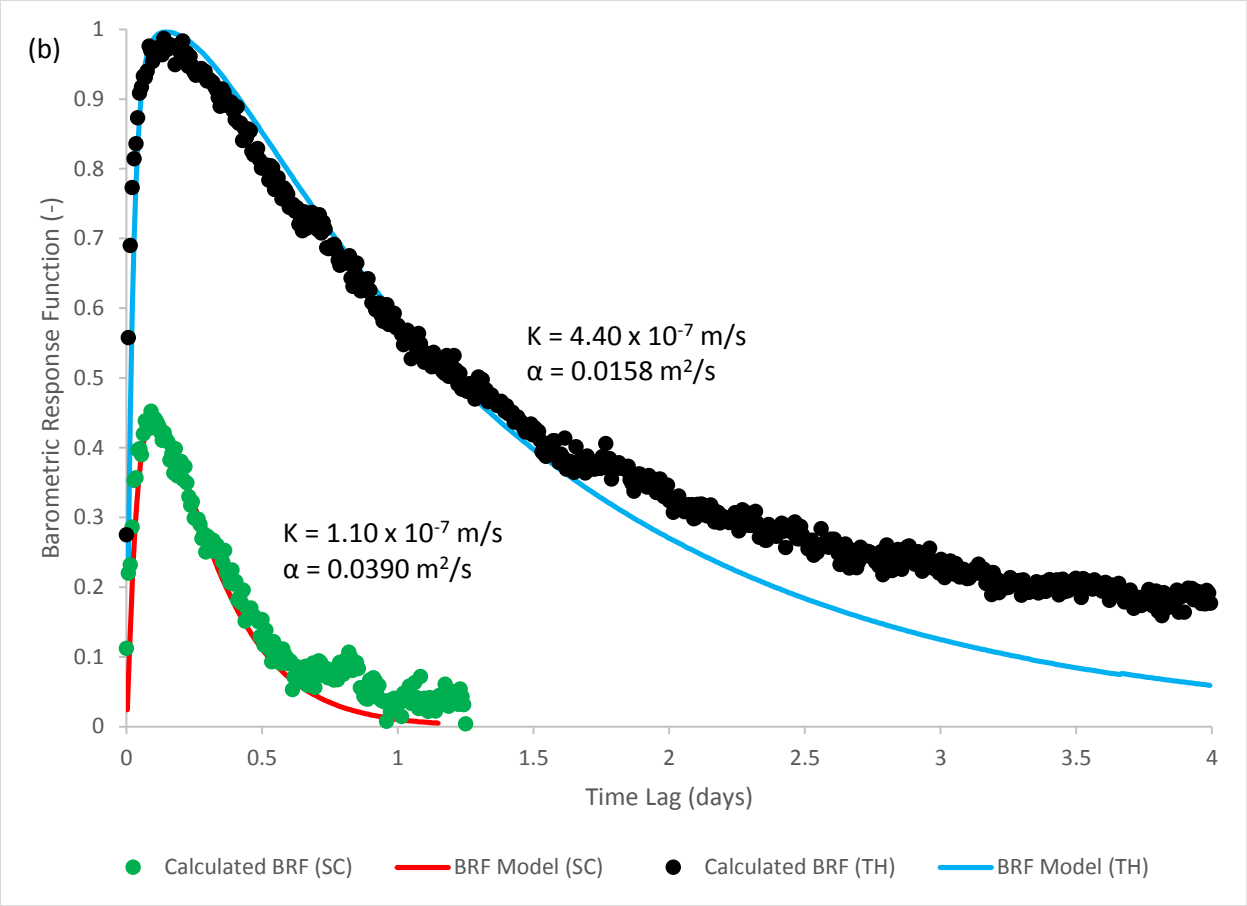

Figure 12: Time domain barometric response function (BRF, data points) and associated time domain fitted analytical solution (solid lines) for the SC and TH sites for 2013 (a) and 2015 (b). The analytical BRF solution is the superposition of the Hvorslev (1951) slug test solution and Weeks' (1979) pneumatic transmission model, visually fitted to calculated BRFs. Time series water level and barometric pressure data were selected from recovery limb hydrograph (Jan. – March, 2013 and Nov. – Dec., 2015). Data from 2015 were obtained at a higher acquisition interval (10 sec) than from 2013 (1 hr). Data are plotted every 1 hour and every 10 minutes for 2013 and 2015, respectively.

4.3 Slug Tests

During the slug tests, measured water levels at both the SC and TH sites recovered to their static values after three minutes and one minute, respectively (Figures 11 and 12). Normalized-head water-level responses reveal good overall agreement based on coinciding plots of all ten slug tests for each respective site (Figures 11 and 12).

The test with the least amount of noise from each site was selected for analysis in AQTESOLV (Figure 13). Following the screening mechanism recommended by Butler (1998), data were initially analyzed using the Cooper et al. (1967) solution for wells screened below the water table within unconfined aquifers. Although hydraulic conductivity values were estimated with the Cooper et al. (1967) solution, the storage values were not physically possible (1.0×10^{-10}), thus nullifying the validity of hydraulic conductivity estimates with that solution (e.g. Midwest Geo., 2007). The KGS model (Butler, 1998) was thus used to estimate near-well hydraulic conductivity and specific storage (Ss). These data indicate that the hydraulic conductivity near the SC well is nearly one order of magnitude lower than the TH well (1.54×10^{-5} m/s and 1.14×10^{-4} m/s, respectively). The estimated K values from slug tests were nearly two orders of magnitude and an order of magnitude larger than those estimated with the time domain BRF for SC and TH, respectively. The SC well has a larger Ss value than the TH well (4.79×10^{-6} and 1.28×10^{-6} m^{-1}, respectively) (Table 2). The Hvorslev (1951) method for unconfined hydrogeological settings was also used to analyze the data. The estimated K values for both the SC and TH sites were nearly two orders of magnitude larger than those estimated with the time domain BRF (1.65×10^{-5} m/s and 1.22×10^{-4} m/s, respectively). Parameter estimates from all three slug test models are presented in Table 3 and fitting curves and data are presented in Appendix C.

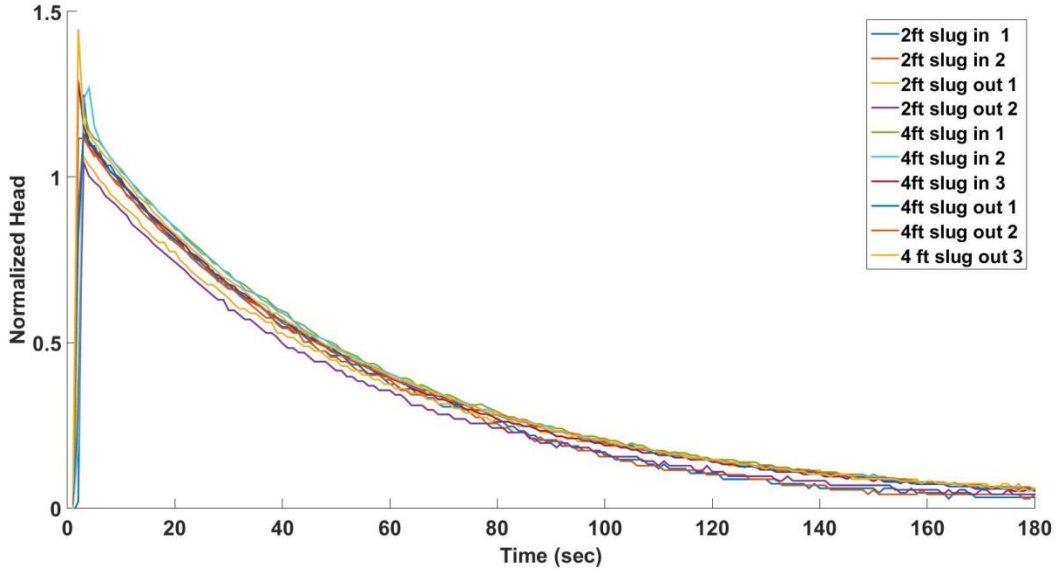

Figure 13: Normalized head plot of ten slug tests at Scott County Index Well (SC).

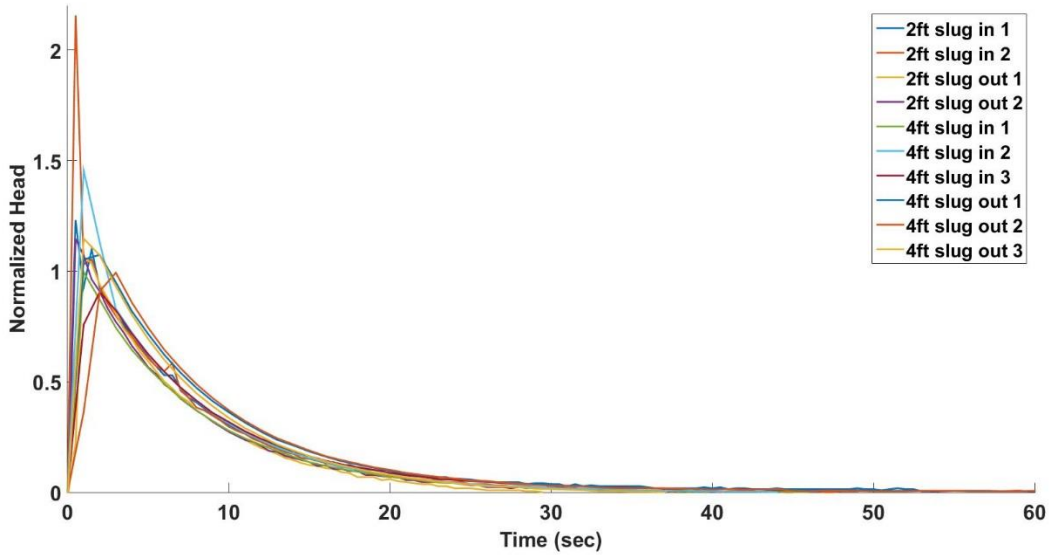

Figure 14: Normalized head plot of ten slug tests at Thomas County Index Well (TH).

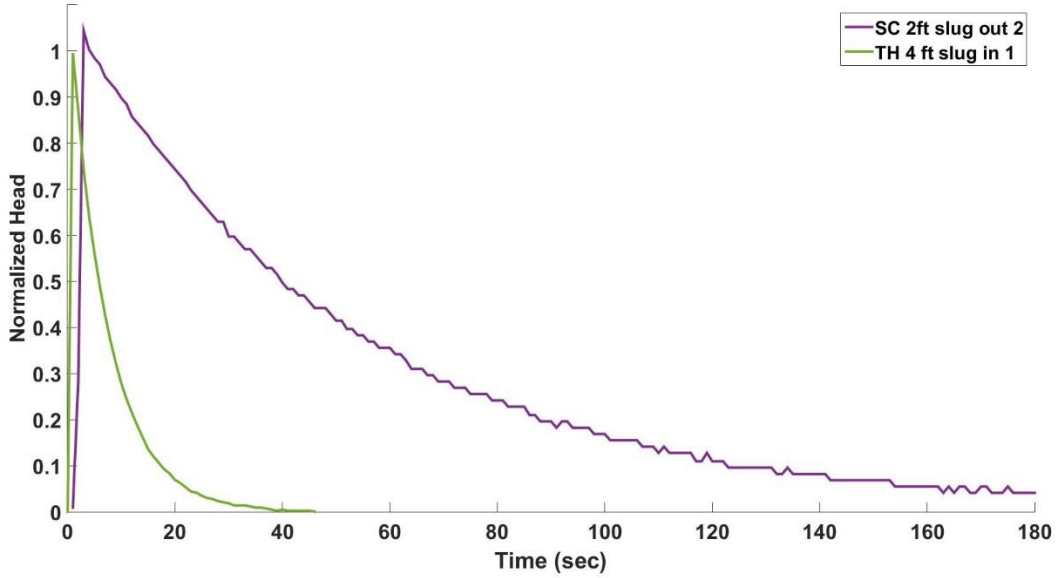

Figure 15: Selected slug tests from SC and TH. Tests were initiated sequentially with 2 ft. (0.6 m) and 4 ft. (1.2 m) solid PVC slugs. Recording intervals were set at 0.5 and 1.0 seconds for TH and SC, respectively.

Table 3: Estimated hydraulic conductivity (K), storativity (S), Specific storage (S_s), and y-intercept (y_0) from three slug test methods. Note: saturated thickness (b) values of 24.85 m and 18.60 m used for Scott County Index Well (SC) and Thomas County Index Well (TH), respectively.

Method	Hvorslev		Cooper et al.		KGS	
Parameter	K (m/s)	y_0 (m)	K (m/s)	S (-)	K (m/s)	S_s (m^{-1})
SC	1.65×10^{-5}	0.16	5.08×10^{-6}	1.0×10^{-10}	1.54×10^{-5}	4.79×10^{-6}
TH	1.22×10^{-4}	0.30	5.00×10^{-5}	1.0×10^{-10}	1.14×10^{-4}	1.28×10^{-6}

4.4 BRFs – Frequency Domain

Hydraulic parameters were estimated for both the SC and TH sites by fitting the analytical frequency domain BRF to the BRF estimated through cross spectral deconvolution of the water level and barometric pressure data records. Parameter estimates are presented in Table 2. The BE value at the SC site (0.52) was nearly half the value estimated at TH (0.91). The transmissivity estimate at SC (2.61 x 10^{-6} m^2/s) was nearly a factor of two less than that of TH (4.12 x 10^{-6} m^2/s). Hydraulic diffusivity and α estimates were larger at SC (1.07 x 10^{-3} m^2/s and 1.15 x 10^{-5} m^2/s) than TH (5.21 x 10^{-4} m^2/s and 9.83 x 10^{-6} m^2/s).

5. Discussion

5.1 BRFs – Time Domain

The exponentially decreasing response curves of the time domain BRFs at both the SC and TH sites indicates that both wells are completed within predominately unconfined portions of the High Plains Aquifer. The lagged barometric response observed at both of these sites is likely attributable to the thick vadose zones present at each site (Rasmussen and Crawford, 1997).

The main difference between the BRFs for the SC and TH sites is the magnitude of the peak BE value and the lag time associated with pressure equilibration within the aquifer. The TH site features both a larger peak BE value and a longer lag time compared to the SC site. This makes sense, given the TH well (87.17 m) was completed nearly 18 m deeper than the SC well (69.19 m) and has a correspondingly thicker (deeper) vadose zone (~68m vs. ~42m, Table 1). This results in a longer time lag for an imposed barometric pressure step change at the surface to diffuse through the vadose zone and reach the water table (Weeks, 1979). The greater degree of

geologic heterogeneity, including the presence of interspersed clay lenses, may also contribute to the retardation of air flow through the vadose zone (e.g., Lu, 1999). The combination of the deeper well construction and the presence of low permeability porous media thus give the TH site a higher peak barometric efficiency value (the pore water within the aquifer is 'shielded' from bearing the load of barometric pressure changes at the land surface) and a larger lagged response time to pressure equilibration (e.g., Price, 2009).

5.2 Analytical BRF Model – Time domain

According to the results of the time domain analytical BRF solution, the TH site has a higher near-well horizontal hydraulic conductivity (K_x) and a lower pneumatic diffusivity (α) than the SC site. The higher estimated K_x value at the TH site is reasonable, since the well is screened within a fine sand unit. Since the screened interval of the SC well features coarse sand and gravel interspersed with less hydraulically conductive clay, the estimated K_x value for this site is plausibly lower than that of the TH site.

The estimated α values at both the SC and TH sites are within the same order of magnitude of α values estimated by Weeks (1979) for a similar mostly unconfined aquifer with a thick vadose zone in Lubbock, Texas (0.018-0.12 m^2/s). The α value at TH site falls just below the lower end of this range (0.0169 m^2/s) and is nearly 2.5 times smaller than that of the SC site. Lower α values indicate the vadose zone is less permeable to air pressure diffusion, and thus likely to have higher BE values due to the shielding effect of the thick vadose zone. This forces barometric pressure disturbance to take a tortuous path en route to the water table (Weeks, 1979; Rasmussen and Crawford, 1997; Butler et al., 2011). The lower estimated α value at the TH site relative to the SC site therefore seems valid given the observed higher BE value and longer BRF lag response time observed at the TH site.

It is interesting to note that the BRFs for both the SC and TH sites changed from 2013 to 2015. Estimated K values decreased at both sites, with an 8% decrease observed at SC and an order of magnitude decrease at TH. It is possible that this decrease may be attributed to clogging within the screened interval of the well due to increased sedimentation (Butler et al., 2014). Additionally, the estimated α value at the TH site decreased by 6%, which could be the result of changes in vadose zone conditions, retarding the propagation of the barometric pressure change. Improved data resolution facilitated visual fitting of the analytical BRF model to the time domain BRF, particularly the ascending limb of the BRF controlled by the Hvorselv (1951) slug test model. The results of this study provide further evidence to the findings of Butler et al. (2011) that BRFs are transient, changing in response to local hydrologic conditions.

5.3 Slug Tests

For both SC and TH, there was a large disparity in the recovery time as estimated with the time domain BRF (around three hours) and as observed during slug tests (less than three minutes). Consequently, the time domain BRF underestimated K_x values at SC and TH (1.19 x 10^{-7} m/s and 4.90 x 10^{-6} m/s, respectively) relative to values calculated from slug tests (1.54 x 10^{-5} m/s and 1.14 x 10^{-4} m/s, respectively) by approximately two orders of magnitude and an order of magnitude, respectively (Table 2). Since the SC and TH wells are partially penetrating and screened over the bottom 3.05 meters of the aquifer, it is likely that the time domain BRF analytical model failed to account for a potential vertical component of flow within the aquifer from the region above the screened interval. Although the specific storage values estimated by the KGS slug test model for SC and TH (4.79 x 10^{-6} m^{-1} and 1.28 x 10^{-6} m^{-1}, respectively), are slightly lower (less than one order of magnitude) than the typically reported Ss range of 4.92 x

10^{-5} to 1.02 x 10^{-4} m^{-1} for dense sandy gravel aquifers, these values are still physically plausible (Batu, 1998).

AQTESOLV was used to determine the well construction parameters necessary to account for the nearly two order of magnitude difference between hydraulic conductivity values estimated with the time domain BRF and slug test methods, presumably due to a potential vertical component of groundwater flow. This was accomplished by adjusting the well casing radius (r_c) and the screen length in AQTESOLV until the estimated K_x value for SC and TH was achieved. This experiment indicated an r_c value of 0.3175 cm (one order of magnitude less than the actual value, 3.175 cm) is needed to produce an output hydraulic conductivity that matched that estimated via the time domain BRF analytical solution. Additionally, a screen length of up to two orders of magnitude larger than the true value (3.05 m) was needed to approach the K_x value estimated by the time domain BRF. These results indicate an inverse relationship between wellbore storage and estimated K_x values from the time domain BRF.

5.4 BRFs – Frequency Domain

Frequency domain BRFs were calculated over a range of 0.1 to 50 cycles/day (CPD) (Figures 16-19), a function of the sampling interval and record lengths at the SC and TH sites. The lower frequency limit is calculated as the product of the number of partially independent segments used to calculate the frequency domain BRF and the proportion of overlap between these segments, divided by the record length (Hussein et al., 2013; Odling et al., 2015). This study followed the methodology of Hussein et al. (2013), which used five water level and barometric pressure segments with 50% overlap. Since the record lengths at the SC and TH sites were 17 and 25 days, respectively, the lower frequency limit for both sites was constrained to ~0.1 CPD. Gubbins (2004) states that the highest hypothetical frequency is 70% of the Nyquist

frequency, which is the inverse of twice the sampling interval. For the data collected in this study, this means that the hypothetical upper frequency boundary is ~3,000 CPD, although this is too high for meaningful analysis of barometric pressure signals. As a result, the actual upper frequency band was limited to lower frequencies sensitive to fluctuations in barometric pressure. This upper frequency limit (50 CPD) is higher than that used by the majority of other researchers (1-2 CPD) (Rojstaczer, 1988; Rojstaczer and Riley, 1990; Quilty and Roeloffs, 1991; Hussein et al., 2013; Odling et al., 2015). In these previous studies, frequency domain analyses of BRFs were constrained to lower frequencies because of a combination of low frequency sampling intervals (15-60 minutes) and the use of lower resolution absolute (nonvented) pressure transducers (Hussein et al., 2013). In this study, higher resolution gauge (vented) pressure transducers and a higher frequency sampling interval (10 seconds) enabled BRF frequencies to be extended to a frequency range similar to that utilized by Evans et al. (1991). The upper frequency limit of 50 CPD was chosen to match the highest frequency range used by Evans et al. (1991) for comparative purposes.

The parameters estimated with frequency domain BRFs at both SC and TH were barometric efficiency (BE), transmissivity (T), pneumatic diffusivity (α), and hydraulic diffusivity (D_{con}). Estimates of BE and D_{con} values were the most physically plausible, while estimates of α and K_x values (calculated from estimates of T) were both significantly lower than those estimated using both time domain BRF analyses and slug tests. The details of these general observations are discussed below.

BE values estimated at SC and TH by both the time and frequency domain BRFs were very similar (Table 2). In both cases, the peak BE value estimated via the time domain BRF was within ~10% of that estimated via the time domain BRF. The similarity in BE estimates at the

two sites indicate that both the time and frequency domain forms of the BRF are capable of producing consistent results with respect to the quantitative relationship between changes in barometric pressure and associated changes in water level in a well.

Transmissivity (T) values, and thus, K_x values (K_x=T/b), estimated from the frequency domain BRF were qualitatively similar to those estimated via both the time domain BRF as well as slug tests, with TH having higher values than SC (Table 2). The estimated T values (2.61×10^{-6} m/s and 4.12×10^{-6} m/s) and saturated thickness values (26.34 m and 17.92 m) correspond to K_x values of 1.02×10^{-7} m/s and 2.30×10^{-7} m/s for SC and TH, respectively (Table 1). Despite the qualitative similarities between K_x values estimated from the time and frequency domain BRFs, both underestimated those determined with slug tests by one to two orders of magnitude.

It is possible that underestimation of K values is attributable to skin effects. Previous researchers noted the finite impact of skin effects on water level response induced by barometric pressure step changes, with incomplete connections between the borehole and surrounding aquifer material associated with delayed water level response within the borehole. The delayed response led to underestimation of groundwater flow between the borehole and the aquifer (Furbish, 1991; Rasmussen and Crawford, 1997; Spane, 2002). Discrepancies as large as two orders of magnitude between K_x values estimated with frequency domain BRFs and those estimated from slug tests were also recently observed (Hussein et al., 2013). These were attributed to the precipitation of calcium carbonate with fractures proximal to the borehole wall within the Chalk Aquifer of East Yorkshire, UK (Hussein et al., 2013). The small (<1 cm) fluctuations in water level induced by barometric pressure within this fractured aquifer were deemed insufficient to overcome the incomplete connection between the borehole and the surrounding aquifer, which lead to lower K_x values than those estimated from slug tests.

However, this interpretation is doubtful and the cause of the discrepancies in estimates of K_x are likely due to additional processes not accounted for in the analytical model, such as a vertical component of groundwater flow above the screened interval of the well in the aquifer.

The results of the present study, despite larger water level response (~30 cm) to barometric pressure change, provide further evidence that skin effects can lead to the underestimation of K_x values by as many as two orders of magnitude. Although water levels in the well change by as much as 30 cm, the amount of time it takes for the changes in water level to occur (~30-40 hrs) is longer than the time scale of the slug tests (<1 hr). Thus, BRF-derived estimates of K_x in wells with skin effects can only provide lower estimates of hydraulic conductivity.

Frequency domain model pneumatic diffusivity (α) estimates were three to four orders of magnitude lower than those estimated from the time domain model (Table 2). The disparity between these estimated values is surprising given that both the time and frequency domain BRFs incorporate the same one dimensional diffusion equation to represent vertical airflow through the vadose zone. Values of α within an order of magnitude of those estimated by Weeks (1979) (0.032-0.064 m^2/s) in a thick, unconfined portion of the HPA near Lubbock, Texas would seem to be more physically plausible for the unconfined, unconsolidated hydrogeological setting featured in the present study. The frequency domain BRF used by Evans et al. (1991) in a predominately consolidated sandstone aquifer in Egypt produced values of α closest to those of Weeks (1979), ranging from $0.5 – 2.0 \times 10^{-3}$ m^2/s. The frequency domain α estimates in this study, however, were more similar to those estimated in previous frequency domain studies featuring different, more consolidated porous media (Rojstaczer and Riley, 1990; Hussein et al., 2013). The discrepancy in estimates of α between the time and frequency domain BRF analyses

may be attributable to the analytical framework of the frequency domain model itself, which was developed within the context of predominately semiconfined aquifers. It is also possible that visually fitting the analytical BRF model to the empirically calculated time domain BRF may lead to discrepancies in parameter estimation. However, this seems unlikely given the close fit and α estimates within the same order of magnitude as those of Weeks (1979) (Appendix A).

Hydraulic diffusivity (D_{con}) values estimated in this study were within one order of magnitude of those estimated by several previous studies (Rojstaczer, 1988; Rojstaczer and Riley, 1990; Evans et al., 1991; Quilty and Roeloffs, 1991; Hussein et al., 2013). This indicates the frequency domain BRF model provides consistent estimates of groundwater flow within the saturated zones of unconfined and semiconfined aquifers. Hydraulic diffusivity is related to the vertical component of hydraulic conductivity (K_z) via the specific storage (S_s) of a given aquifer ($D = K/S_s$). Hydraulic diffusivity estimates derived from the frequency domain BRF correspond to K_z values of 3.21×10^{-8} m/s and 1.56×10^{-8} m/s for SC and TH, respectively, assuming a S_s value of 3.0×10^{-5} m^{-1} utilized by Butler et al. (2011) in a study of a semi confined portion of the HPA.

The hydraulic conductivity anisotropy ratio, which quantifies hydraulic conductivity in two dimensions, is calculated as the quotient of vertical and lateral hydraulic conductivity. Based on the values of K_x and K_z estimated with frequency domain BRFs, the anisotropy ratio is 0.26 and 0.05 for the SC and TH sites, respectively. These anisotropy ratios are qualitatively plausible, since K_z can be one to two orders of magnitude lower than K_x in most aquifers (Batu, 1998). However, it should be noted that the very low α values and low K_x values may be the result of systematic deviations in the frequency domain analytical fitting process, which could skew the results of the calculation of K_z.

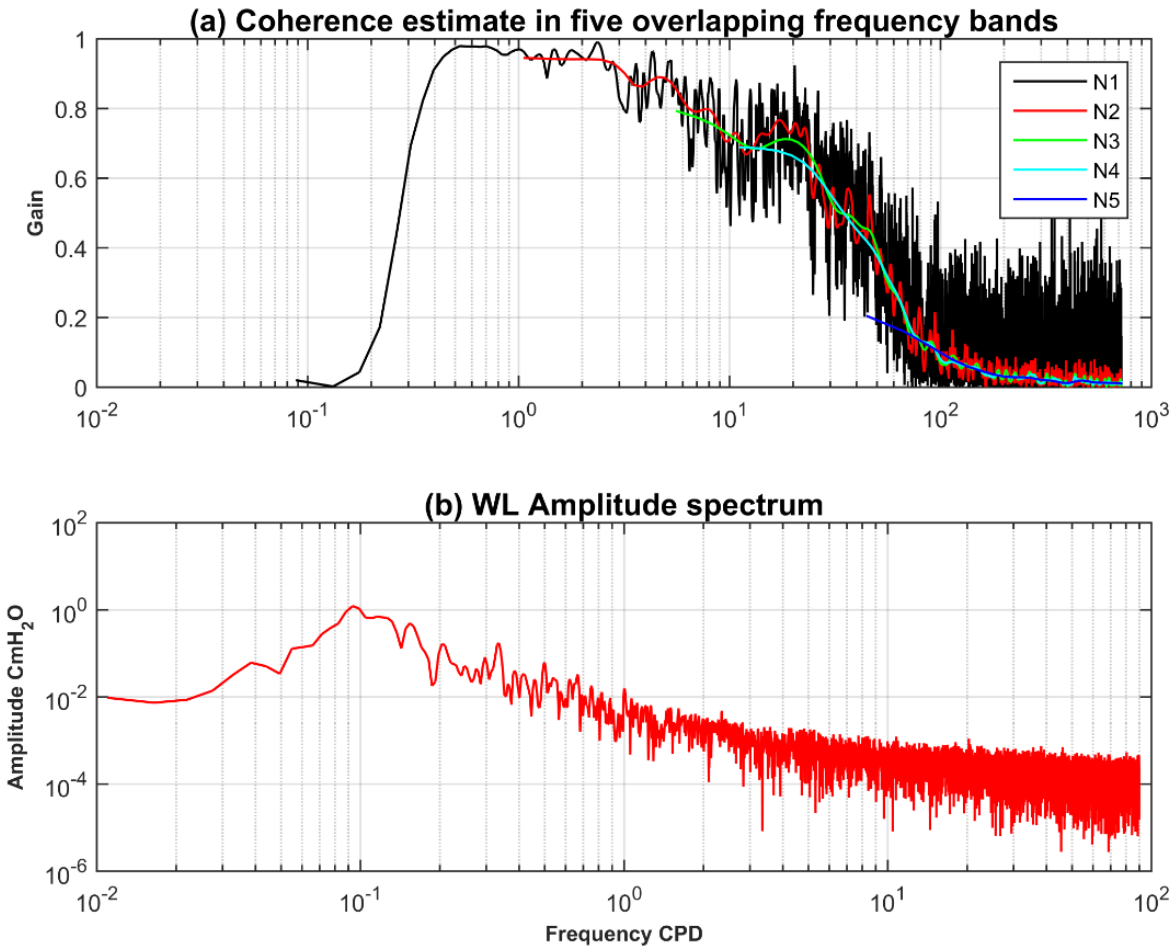

Figure 16: Coherence and water level amplitude spectrum for Scott County Index Well. Low coherence at values less than 0.2 CPD and greater than 12 CPD are attributable to the effects of recharge and low barometric pressure signal amplitude at higher frequencies.

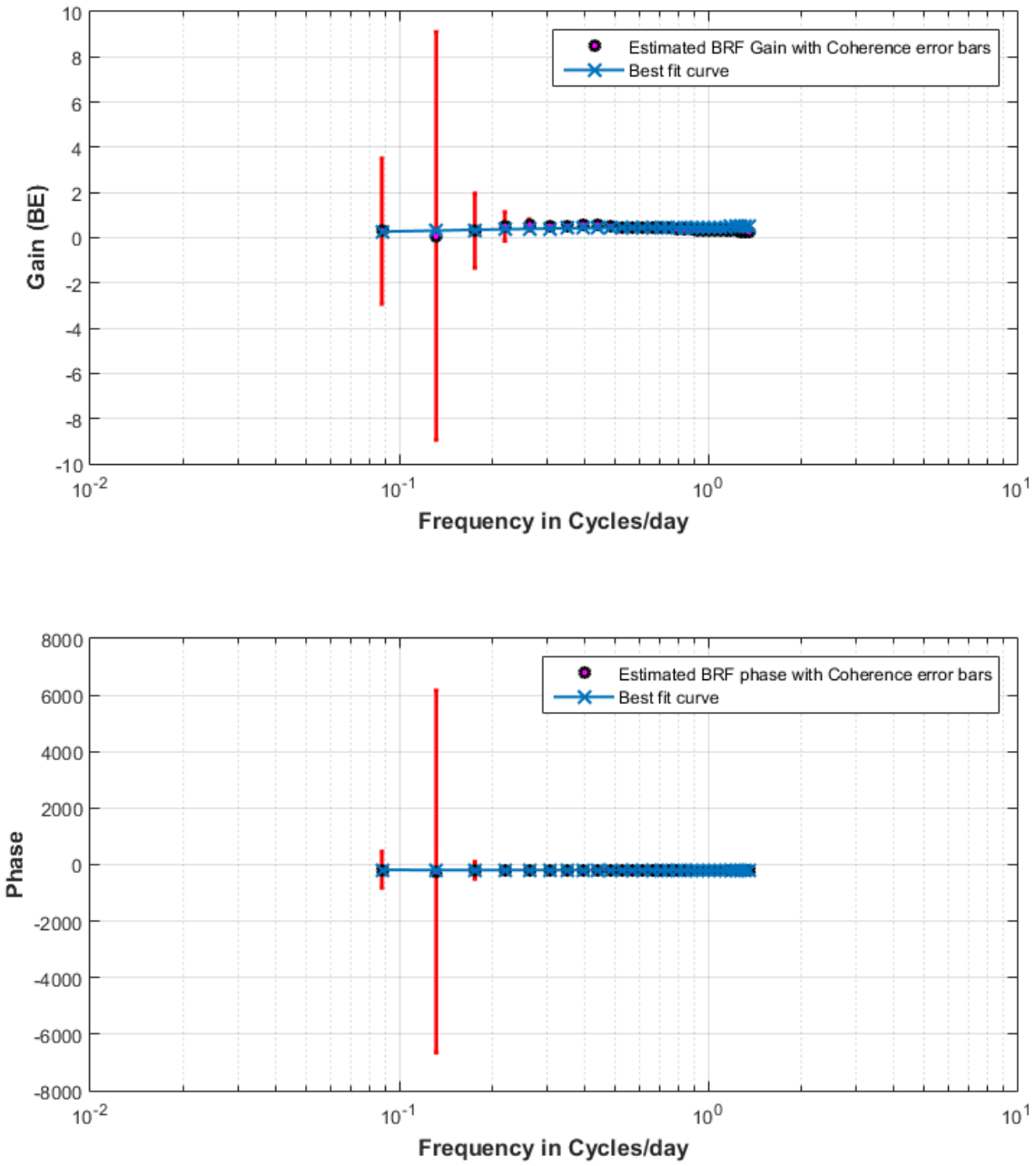

Figure 17: Estimated BRF (phase and gain) and best fit curves for Scott County Index Well. Larger margin of error at ~0.01 CPD may be due to recharge effects.

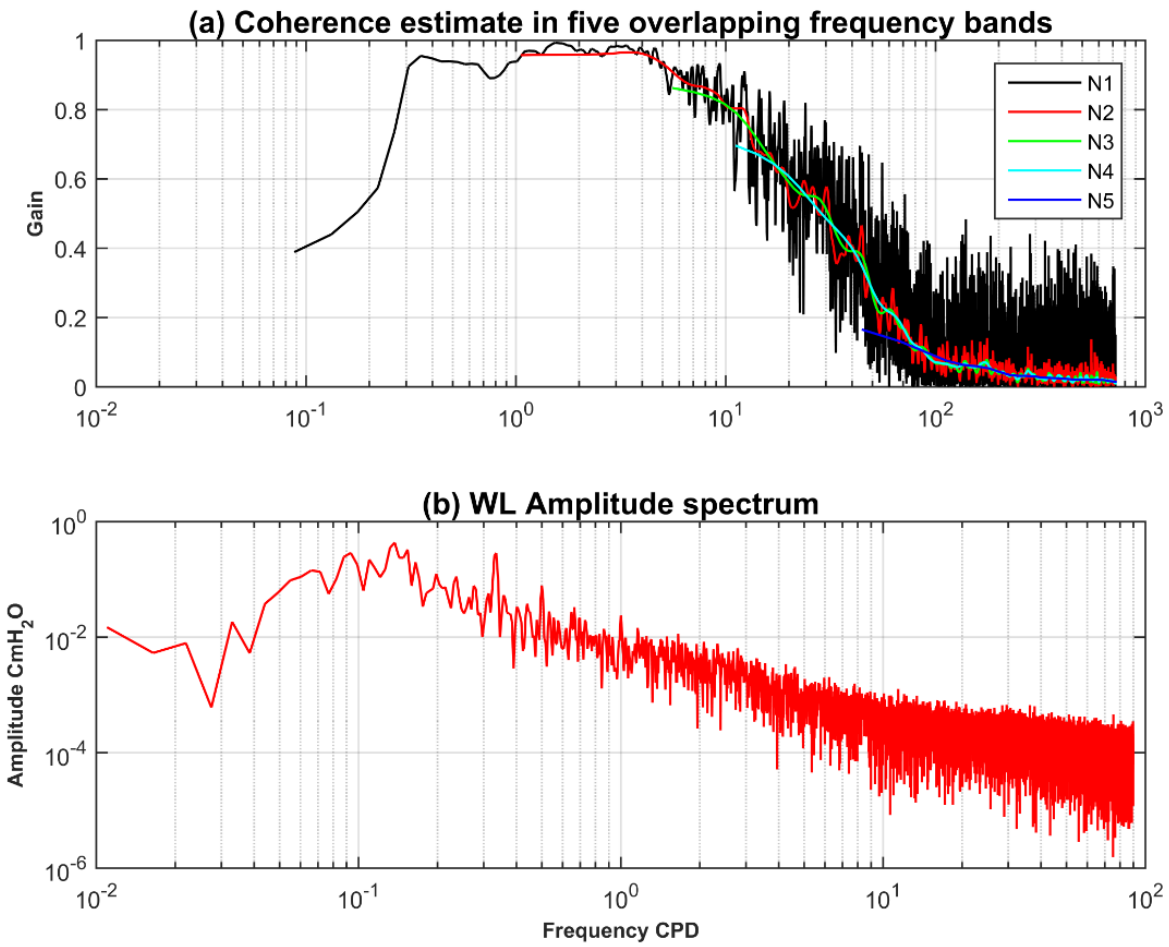

Figure 18: Coherence and water level amplitude spectrum for Thomas County Index Well. Low coherence at values less than 0.2 CPD and greater than 12 CPD are attributable to the effects of recharge and low barometric pressure signal amplitude at higher frequencies.

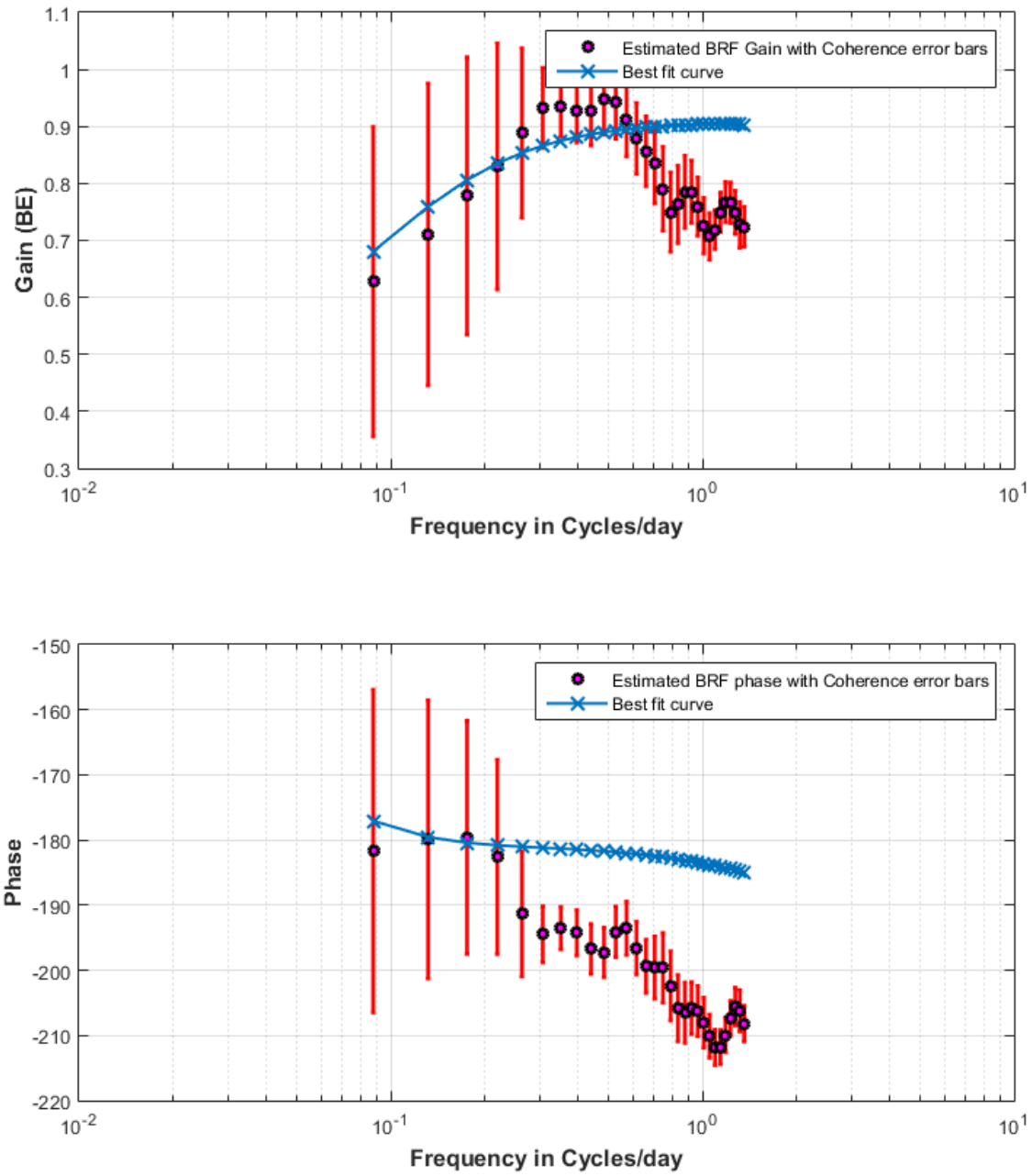

Figure 19: Estimated BRF (phase and gain) and best fit curves for Thomas County Index Well.

5.5 Sources of Error

Several potential sources of error should be considered when interpreting the results of this study. Possible sources of error are aquifer geometry, earth tides, recharge, and groundwater pumping. These potential sources of error are detailed in the paragraphs below.

One possible, but likely minor, source of error arises from the aquifer geometry at the SC and TH sites compared with that assumed for the frequency domain BRF analytical solution developed by Rojstaczer (1988) and later modified and coded in MATLAB by Hussein et al. (2013). In Rojstaczer's (1988) solution, the aquifer is assumed to be semiconfined; however, both the SC and TH sites feature predominately unconfined conditions. Rojstaczer's (1988) solution was modified to incorporate a dimensionless aquifer term representing the movement of the water table within an unconfined aquifer (Rojstaczer and Riley, 1990). Although both of these models use an identical mathematical representation of vertical air flow within the vadose zone, the model developed by Rojstaczer and Riley (1990) uses a different set of governing equations and boundary conditions to express vertical groundwater flow within an unconfined aquifer. In this modified solution, the response of water in wells screened in an unconfined aquifer with a thick (>20 m) vadose zone is given by the vertically averaged pressure change within the aquifer over the screened interval of the well. Vertical averaging minimizes the influence of the water table on unconfined aquifer response by reducing the magnitude of vertical hydraulic diffusivity, effectively isolating the aquifer at depth. Therefore, wells located within unconfined aquifers with thick vadose zones can experience water level responses in the screened interval qualitatively similar to wells within a semiconfined aquifer since the influence of the water table on aquifer response is minimal (Rojstaczer and Riley, 1990). Based on this assessment of the similarities between the unconfined and the semiconfined versions of the

frequency domain analytical models, the use of the MATLAB code developed by Hussein et al. (2013) seems justified.

An additional, although unlikely, potential source of error is from earth tides, which occur as a result of lunar and solar gravitational influences on the earth (e.g. Van Camp, 2005; Gonthier, 2007). Earth tides induce slight changes in the shape of the geoid due to compression or tension within earth's crust, which can in turn cause slight fluctuations of the water table within aquifers (Jacob, 1940; Rojstaczer and Riley, 1990). There are five primary diurnal and semidiurnal components of earth tides that influence water level response at lower frequencies (< 2 CPD) and can lead to low coherence between water level and barometric pressure signals (Ritzi et al., 1991; Gonthier 2007; Hussein et al., 2013). Although minor, earth tides can induce finite water level fluctuations on the order of a few centimeters (Hussein et al., 2013). For the purposes of this study, the influence of earth tides is assumed to be negligible in comparison to fluctuations induced by changes in barometric pressure, as was quantitatively demonstrated by previous researchers at the two sites (Buddemeier et al., 2010).

Groundwater recharge could also present a source of error in estimating the hydraulic parameters in this study, but this seems unlikely. Barometric pressure and water level data were detrended prior to analysis to minimize the potential effect of recharge (Hussein et al., 2013). Additionally, recharge tends to interfere with the coherence of barometric pressure and water level signals at low frequencies (~0.015 CPD), below the frequency band analyzed in this study (0.1 – 50 CPD). For semiarid climates like those found at the SC and TH sites, low recharge rates further minimize any signal distortion that may occur due to groundwater recharge (Butler et al., 2011).

Finally, groundwater pumping has the potential to cause a small distortion of the water level response. Given that the study area is located within the HPA, a prominent source of groundwater for agriculture, groundwater pumping must be considered, as nearby groundwater irrigation wells pump several thousand liters of water per minute. However, barometric pressure and water level data were collected during the recovery period of the agricultural water use season when irrigation pumps were mostly inactive. Data collection was done during this period to ensure minimal influence of pumping on the water level signal, following the methods of Butler et al. (2011).

6. Conclusions

The results of this study indicate estimates of hydraulic properties derived from both time and frequency domain BRFs are functional only as lower boundary estimates of the true T or K_x value for a given portion of an aquifer. Other studies utilizing both time and frequency domain BRF approaches have cited the time delay in water flow between the borehole and the aquifer due to wellbore storage as well as incomplete connection between the borehole and the aquifer due to skin effects as possible reasons for the underestimation of K_x values (Furbish, 1991; Spane, 2002; Hussein et al., 2013). Although it is possible that skin effects play a role in the underestimation of K_x values, the most likely explanation for the discrepancy is that the frequency and time domain BRF analytical models are not accounting for an additional hydrogeological process, such as a vertical component of flow within the aquifer above the screened interval of a well. As a result, the true K_x values are likely higher than those estimated through BRF analyses.

This study demonstrates that both time and frequency domain BRFs are capable of providing similar estimates of BE for a given well. At both the SC and TH sites, the estimated BE was within 10% for both BRF methods.

K_z values calculated through the estimation of vertical hydraulic diffusivity in the HPA are within the same order of magnitude as those in other aquifers with similar hydrogeological settings featuring thick vadose zones (Rojstaczer and Riley, 1990; Evans et al., 1991). However, these results are likely inaccurate given the implausibly low estimates of α values, low estimates of K_x values, and apparent systematic deviations in the frequency domain fitting curves.

The most significant result from this work is the change in the time domain BRFs at both the SC and TH sites from 2013 to 2015. Estimated K_x values decreased at both sites and α decreased at the TH site. The observed changes in the BRFs at these sites provides further evidence that BRFs are transient in nature and can potentially indicate changes in local hydrogeological conditions with time (Butler et al., 2011; Butler et al., 2014).

7. Future Work

A possibility for future work would be to implement the frequency domain analytical BRF model in MATLAB to account for the dimensionless water table frequency parameter used by Rojstaczer and Riley (1990). This would more accurately represent the fluctuation of the water table within unconfined aquifers with thick vadose zones. Similarly, it may be useful to derive the analytical solution for the frequency domain BRF to account for partial penetration. It is expected that both of these efforts would result in larger estimated values for the vertical component of groundwater flow (both K_z and hydraulic diffusivity) at the SC and TH sites.

Incorporating wellbore storage and skin effects into the analytical solution would also likely be useful in improving estimates of K_x.

The recording period for simultaneous collection of barometric pressure and water level data could also be increased from less than three weeks to more than one year. Increasing the recording period of these data would extend the frequency domain BRF model to lower frequencies, which would improve estimates of vertical hydraulic diffusivity since this is the most sensitive parameter at frequencies less than 1 CPD (Hussein et al., 2013; Odling et al., 2015).

References

Acworth, R.I. and T. Brain. 2008. Calculation of barometric efficiency in shallow piezometers using water levels, atmospheric and earth tide data. *Hydrogeology Journal* 16, no. 8, DOI: 10.1007/s10040-008-0333-y.

Alsumait, J.S., J.K. Sykulski, and A.K. Al-Othman. 2010. A hybrid GAPS-SQP method to solve power system valve-point economic dispatch problems, *Appl. Energy* 87, DOI: 10.1016/j.apenergy.2009.10.007.

Anochikwa, C.I., G. van der Kamp, and S.L. Barbour. 2012. Interpreting pore-water pressure changes induced by water table fluctuations and mechanical loading due to soil moisture changes. *Canadian Geotechnical Journal* 49, no. 3, DOI: 10.1139/T11-106.

Batu, V. 1998. *Aquifer Hydraulics*. New York: John Wiley and Sons.

Bendat, J.S. and A.G. Piersol. 2000. *Random Data Analysis and Measurement Procedures*. New York, N.Y.: John Wiley & Sons.

Bohling, G.C., Jin, W., and J.J. Butler, Jr. 2011. Kansas Geological Survey Barometric Response Function Software User's Guide. *Kansas Geological Survey, Open-File Report* 2011-10.

Buddemeier, R.W., R. Stotler, J.J. Butler, Jr., W. Jin, K. Beeler, E. Reboulet, P.A. Macfarlane, S. Kreitzer, D.O. Whittemore, G. Bohling, and B.B Wilson. 2010. High Plains Aquifer calibration monitoring well program: Third year progress report. *Kansas Geological Survey open file report* 2010-3.

Butler, J.J. Jr., 1998, *The Design, Performance, and Analysis of Slug Tests.* Florida: CRC Press.

Butler, J.J. Jr., W. Jin, G.A. Mohammed, and E.C. Reboulet. 2011. New insights from well responses to fluctuations in barometric pressure. *Ground Water* 49, no. 4, DOI: 10.1111/j.1745-6584.2010.00768.x.

Butler, J.J. Jr., R.L. Stotler, D.O. Whittemore, and E.C. Reboulet. 2013a. Interpretation of water level changes in the High Plains Aquifer in Western Kansas. *Ground Water* 51, no. 2, DOI: 10.1111/j.1745-6584.2012.00988.x.

Butler, J.J. Jr., D.O. Whittemore, G.C. Bohling, E.C. Reboulet, R.L. Stotler, and B.B. Wilson. 2013b. High Plains Aquifer index well program: 2012 annual report. *Kansas Geological Survey open file report* 2013-1.

Butler, J.J. Jr., G.C. Bohling, E.C. Reboulet, and J. Olson. 2013c. Signal not noise: Getting more from water-level responses to barometric-pressure fluctuations: Abstract 9198, 2013 Ground Water Summit, National Ground Water Association, San Antonio, TX, May 1.

Butler, J.J. Jr., D.O. Whittemore, E.C. Reboulet, R.L. Stotler, G.C. Bohling, J.C. Olson, and B.B. Wilson. 2014. High Plains Aquifer index well program: 2013 annual report. *Kansas*

Geological Survey Open-File Report 2014-1.Carslaw, H.S., and J.C. Jaeger. 1959. *Conduction of Heat in Solids*. New York: Oxford University Press.

Chapman, S. and R.S. Lindzen. 1970. *Atmospheric Tides, Thermal and Gravitational*, D. Reidel, Dordrecht, Netherlands.

Cooper, H.H. Jr., J.D. Bredehoeft, I.S. Papadopulos, and R.R. Bennett. 1965. The response of well-aquifer systems to seismic waves. *Journal of Geophysical Research* 70, 3915-3926.

Cooper, H.H. Jr., J.D. Bredehoeft, and I.S. Papadopulos. 1967. Response of a finite-diameter well to an instantaneous charge of water. *Water Resources Research* v. 3, no. 1: 263-269.

Davis, D.R., and T.C. Rasmussen. 1993, A comparison of linear regression with Clark's method for estimating barometric efficiency of confined aquifers. *Water Resources Research* 29, no. 6: 1849-1854.

Evans, K., J. Beavan, D. Simpson, and S. Mousa. 1991. Estimating aquifer parameters from analysis of forced fluctuations in well level: An example from the Nubian formation near Aswan, Egypt 3. Diffusivity estimates for saturated and vadose zones. *Journal of Geophysical Research* 96, no. B7: 12,161-12,191.

Ferris, J.G., D.B. Knowles, R.H. Brown, and R.W. Stallman. 1962. Theory of aquifer tests. U.S. Geological Survey water-Supply Paper 1536E. http://pubs.usgs.gov/wsp/wsp1536-E/pdf/wsp 1536-Ea.pdf (accessed June 8, 2014).

Freeze, R.A., and J.A. Cherry. 1979. Groundwater. New Jersey: Prentice-Hall.

Frye, J.C. 1945. Geology and ground-water resources of Thomas County, Kansas. *Kansas Geological Survey Bulletin 59*.

Furbish, D.J. 1991. The response of water level in a well to a time series of atmospheric loading under confined conditions. *Water Resources Research* 27, no. 4: 557-568.

Geldon, A. L., J.D. Earle, and A.M.A. Umari. 1997. Determination of barometric efficiency and effective porosity, boreholes UE-25 c#1, UE-25 c#2, and UE-25 c#3, Yucca Mountain, Nye County, Nevada. U.S. Geological Survey Water-Resources Investigations report 97-4098.

Gonthier, G.J. 2007. A graphical method for estimation of barometric efficiency from continuous data—Concepts and application to a site in the piedmont, Air Force Plant 6, Marietta, Georgia. U.S. Geological Survey Scientific Investigation Report 2007-5111.

Gubbins, D. 2004. Time series analysis and inverse theory for geophysicists. New York: Cambridge University Press.

Gutentag, E.D. and L.E. Stullken. 1976. Ground-water resources of Land and Scott Counties, Western Kansas. *Kansas Geological Survey Irrigation Series* no. 1.

Halford, K.J., C.A. Garcia, J. Fenelon, and B. Mirus. 2012. Advanced methods for modeling water-levels and estimating drawdowns with SeriesSEE, and Excel Add-in. U.S. Geological Survey Techniques and Methods 4-F4. U.S. Geological Survey Scientific Investigations Report 2006-5024.

Hare, P.W., and R.E. Morse. 1997. Water-level fluctuations due to barometric pressure changes in an isolated portion of an unconfined aquifer. *Ground Water* 35, no. 4: 667-671.

Harrington, G., and P. Cook. 2011. Mechanical loading and unloading of confined aquifers: Implications for the assessment of long-term trends in potentiometric levels. Australian Government National Water Commission. *Waterlines Report Series* no. 51.

Healy, R.W., and P.G. Cook. 2002. Using groundwater levels to estimate recharge. *Hydrogeology Journal* 10, no. 1, DOI: 10.1007/s10040-001-0178-0.

Hussein, M.E.A., N.E. Odling, and R.A. Clark. 2013. Borehole water level response to barometric pressure as an indicator of aquifer vulnerability. *Water Resources Research* 49, DOI: 10.1002/2013WR014134, 2013.

Hvorslev, M.J. 1951. Time lag and soil permeability in ground-water observations. *Waterways Experiment Station. Corps of Engineers, U.S. Army*, Bulletin no. 36.

Jacob, C.E. 1940. On the flow of water in an elastic artesian aquifer. *Transactions AGU* 21: 574-586.

Liuni, M.P., M. Loddo, and D. Schiavone. 2010. Non-linear inversion using a hybrid global search algorithm: Applications in gravimetry, extended abstract, presented at *International Workshop on Adding New Value to Electromagnetic, Gravity and Magnetic Methods for Exploration*, EGM 2010, Capri, Italy, 11-14 Apr.

Lu, N. 1999. Time-series analysis for determining vertical air permeability in vadose zones. *Journal of Geotechnical and Geoenvironmental Engineering* 125: 69-77.

Maupin, M.A. and N.L. Barber. 2005. Estimated withdrawals from principal aquifers in the United States, 2000. *U.S. Geological Survey Circular 1279.*

Meinzer, O.E. 1928. Compressibility and elasticity of artesian aquifers. *Economic Geology* v. 23: 263-291

Meyer, W.R., E.D. Gutentag, and D.H. Lobmeyer. 1970. Geohydrology of Finney County, Southwestern Kansas. United States Geological Survey Water-Supply Paper 1891.

Midwest Geosciences Group. 2007. Field Guide for Slug Testing and Data Analysis.

Odling, N.E., R.P. Serrano, M.E.A. Hussein, M. Riva, and A. Guadagnini. 2015. *Journal of Hydrology* 520: 143-156.

Olsthoorn, T.N. 2008. Do a bit more with convolution. *Ground Water* 46, no. 1: 13-22.

Pascal, B. 1973. *The Physical Treatises of Pascal.* New York: Octagon Books.

Price, M. 2009. Barometric water-level fluctuations and their measurement using vented and pressure transducers. *Quarterly Journal of Engineering Geology and Hydrogeology* 42, no. 2: 245-250.

Quilty, E.G., and E.A. Roeloffs. 1991. Removal of barometric pressure response from water level data. *Journal of Geophysical Research* 96, no B6:10,209-10,218.

Rasmussen, T.C., and L.A. Crawford. 1997. Identifying and removing barometric pressure effects in confined and unconfined aquifers. *Ground Water* 35, no. 3: 502-511.

Ritizi, R.W., S. Sorooshian, and P.A. Hsieh. 1991. The estimation of fluid flow properties from the response of water levels in wells to the combined atmospheric and earth tide forces. *Water Resources Research* 27, no. 5: 883-893.

Rojstaczer, S. 1988. Determination of fluid flow properties from the response of water levels in wells to atmospheric loading. *Water Resources Research* 24, no. 11: 1927-1938.

Rojstaczer, S., and F.S. Riley. 1990. Response of the water level in a well to earth tides and atmospheric loading under unconfined conditions. *Water Resources Research* 26, no. 8: 1803-1817.

Spane, F.A. 2002. Considering barometric pressure in ground-water flow investigations. *Water Resources Research* 38, no. 6, DOI: 10.1029/2001WR000701.

Terzaghi, K. 1925. *Erdbaummechanic auf Bodenphysikalishe Grundlage*. Leipzig, Germany: Franz Deticke.

Toll, N.J. and T.C. Rasmussen. 2007. Removal of barometric pressure effects and earth tides from observed water levels. *Ground Water* 45, no 1: 101-105.

Van Camp, M., and P. Vauterin. 2005. Tsoft: graphical and interactive software for the analysis of time series and Earth Tides. *Computers & Geosciences* 31, no 5: 631-460.

Van der Kamp, G., and J.E. Gale. 1983. Theory of earth tide and barometric effects in porous formations with compressible grains. *Water Resources Research* 19, no. 2: 538-544.

Young, D.P, R.W. Buddemeier, D.O. Whittemore, and E.C. Reboulet. 2007. High Plains Aquifer calibration monitoring well program: Year 1 progress report on well installation and aquifer response. *Kansas Geological Survey Open-file Report* 2007-30.

Waite, H.A. 1947. Geology and ground-water resources of Scott County, Kansas. *Kansas Geological Survey Bulletin 66*.

Weeks, E.P. 1979. Barometric fluctuations in wells tapping deep unconfined aquifers. *Water Resources Research* 15, no. 5: 1167-1176.

Appendix A: Analytical Time Domain BRF Model - Excel Spreadsheet Code

The Excel spreadsheet used to estimate pneumatic diffusivity (α) and horizontal hydraulic conductivity (K_x) is outlined below. This spreadsheet was originally developed by Butler et al. (2013) and adapted for the purposes of this study. The spreadsheet can be broken down into four essential individual components: 1. Pneumatic transmission model of Weeks (1979); 2. Hvorslev slug test model (Hvorslev 1951); 3. BRF with well-formation effects; and 4. Empirical BRF calculated via the Kansas Geological Survey Barometric Response Function Software (Bohling et al., 2011) (Figures A1-A4). The four components of this spreadsheet and their respective cell codes are presented below:

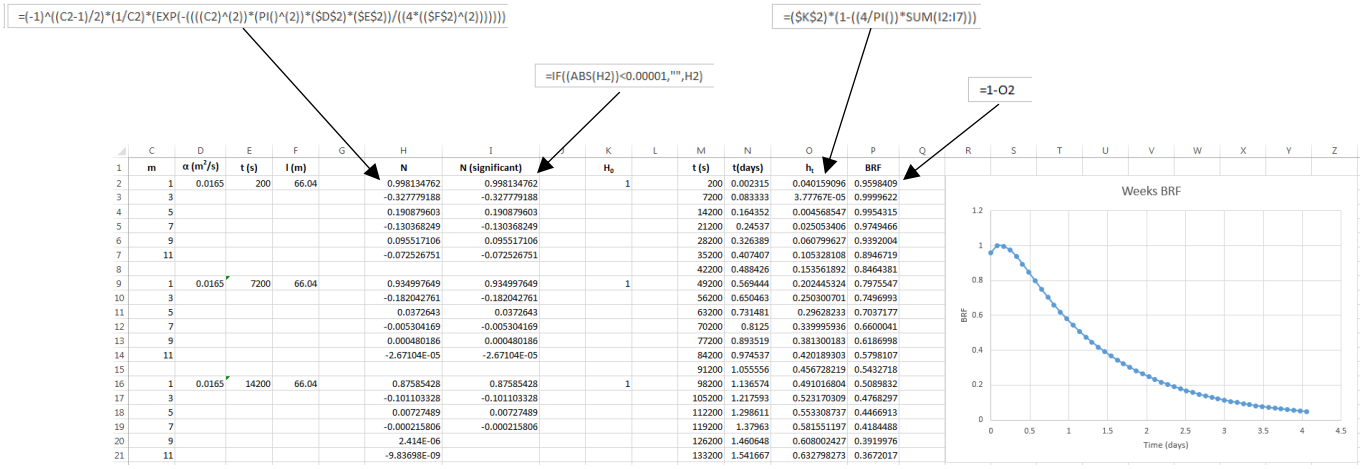

	C	D	E	F	G	H	I	J	K	L	M	N	O	P	Q
1	m	α (m^2/s)	t (s)	l (m)		N	N (significant)		H_0		t (s)	t(days)	h_t	BRF	
2	1	0.0165	200	66.04		0.998134762	0.998134762		1		200	0.002315	0.040159096	0.9598409	
3	3					-0.327779188	-0.327779188				7200	0.083333	3.77767E-05	0.9999622	
4	5					0.190879603	0.190879603				14200	0.164352	0.004568547	0.9954315	
5	7					-0.130368249	-0.130368249				21200	0.24537	0.025053406	0.9749466	
6	9					0.095517106	0.095517106				28200	0.326389	0.060799627	0.9392004	
7	11					-0.072526751	-0.072526751				35200	0.407407	0.105328108	0.8946719	
8											42200	0.488426	0.153561892	0.8464381	
9	1	0.0165	7200	66.04		0.934997649	0.934997649		1		49200	0.569444	0.202445324	0.7975547	
10	3					-0.182042761	-0.182042761				56200	0.650463	0.250300701	0.7496993	
11	5					0.0372643	0.0372643				63200	0.731481	0.29628233	0.7037177	
12	7					-0.005304169	-0.005304169				70200	0.8125	0.339995936	0.6600041	
13	9					0.000480186	0.000480186				77200	0.893519	0.381300183	0.6186998	
14	11					-2.67104E-05	-2.67104E-05				84200	0.974537	0.420189303	0.5798107	
15											91200	1.055556	0.456728219	0.5432718	
16	1	0.0165	14200	66.04		0.87585428	0.87585428		1		98200	1.136574	0.491016804	0.5089832	
17	3					-0.101103328	-0.101103328				105200	1.217593	0.523170309	0.4768297	
18	5					0.00727489	0.00727489				112200	1.298611	0.553308737	0.4466913	
19	7					-0.000215806	-0.000215806				119200	1.37963	0.581551197	0.4184488	
20	9					2.414E-06					126200	1.460648	0.608002427	0.3919976	
21	11					-9.83698E-09					133200	1.541667	0.632798273	0.3672017	

Figure A1: Weeks (1979) Pneumatic Transmission Model.

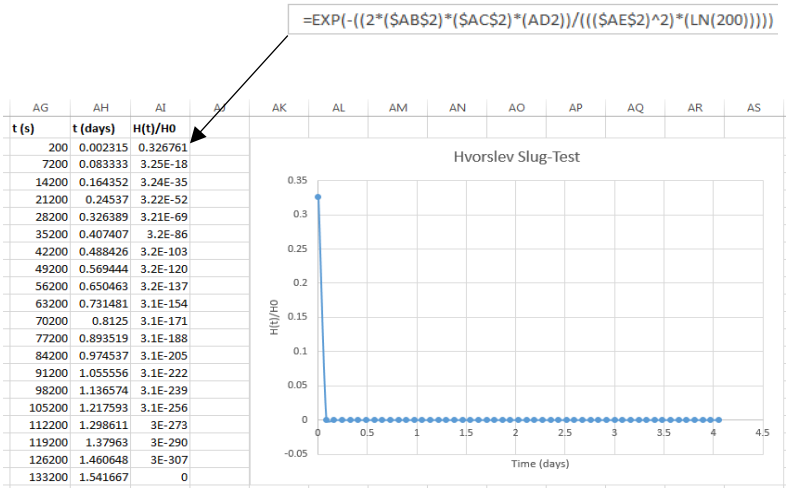

t (s)	t (days)	H(t)/H0
200	0.002315	0.326761
7200	0.083333	3.25E-18
14200	0.164352	3.24E-35
21200	0.24537	3.22E-52
28200	0.326389	3.21E-69
35200	0.407407	3.2E-86
42200	0.488426	3.2E-103
49200	0.569444	3.2E-120
56200	0.650463	3.2E-137
63200	0.731481	3.1E-154
70200	0.8125	3.1E-171
77200	0.893519	3.1E-188
84200	0.974537	3.1E-205
91200	1.055556	3.1E-222
98200	1.136574	3.1E-239
105200	1.217593	3.1E-256
112200	1.298611	3E-273
119200	1.37963	3E-290
126200	1.460648	3E-307
133200	1.541667	0

Figure A2: Hvorslev (1951) Slug Test Model.

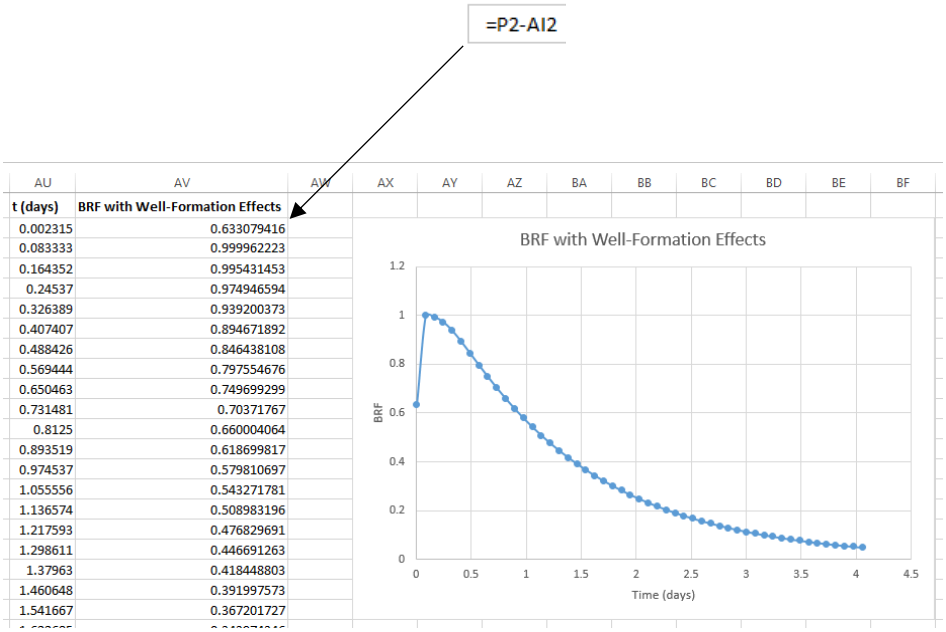

t (days)	BRF with Well-Formation Effects
0.002315	0.633079416
0.083333	0.999962223
0.164352	0.995431453
0.24537	0.974946594
0.326389	0.939200373
0.407407	0.894671892
0.488426	0.846438108
0.569444	0.797554676
0.650463	0.749699299
0.731481	0.70371767
0.8125	0.660004064
0.893519	0.618699817
0.974537	0.579810697
1.055556	0.543271781
1.136574	0.508983196
1.217593	0.476829691
1.298611	0.446691263
1.37963	0.418448803
1.460648	0.391997573
1.541667	0.367201727

Figure A3: Analytical BRF with Well-Formation Effects.

BI	BJ	BK	BL	BM	BN	BO	BP	BQ	BR	BS	BT
t (days)	**Empirical BRF**		**dates: 1/4/2013-3/9/2013**								
0	0.60396011										
0.041667	0.899030745										
0.083333	0.942400761										
0.125	0.999505159										
0.166667	0.959596053										
0.208333	0.936575126										
0.25	0.926006188										
0.291667	0.902085185										
0.333333	0.855596849										
0.375	0.838610787										
0.416667	0.824675073										
0.458333	0.79138896										
0.5	0.771612287										
0.541667	0.757066316										
0.583333	0.735109718										
0.625	0.738042259										
0.666667	0.703364882										
0.708333	0.674381082										
0.75	0.643644615										
0.791667	0.6211914										

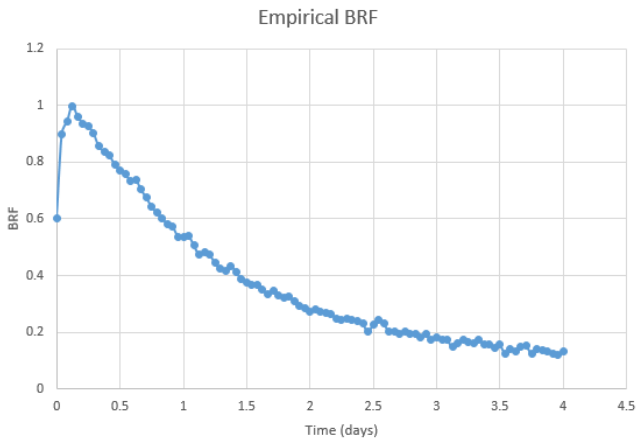

Figure A4: Empirical BRF.

These four individual components are superimposed to create an analytical solution for estimating α and K_x by adjusting these values until a visual match is achieved between the analytical solution and the empirical time domain BRF. An example of the visual curve fitting is shown in Figure A5.

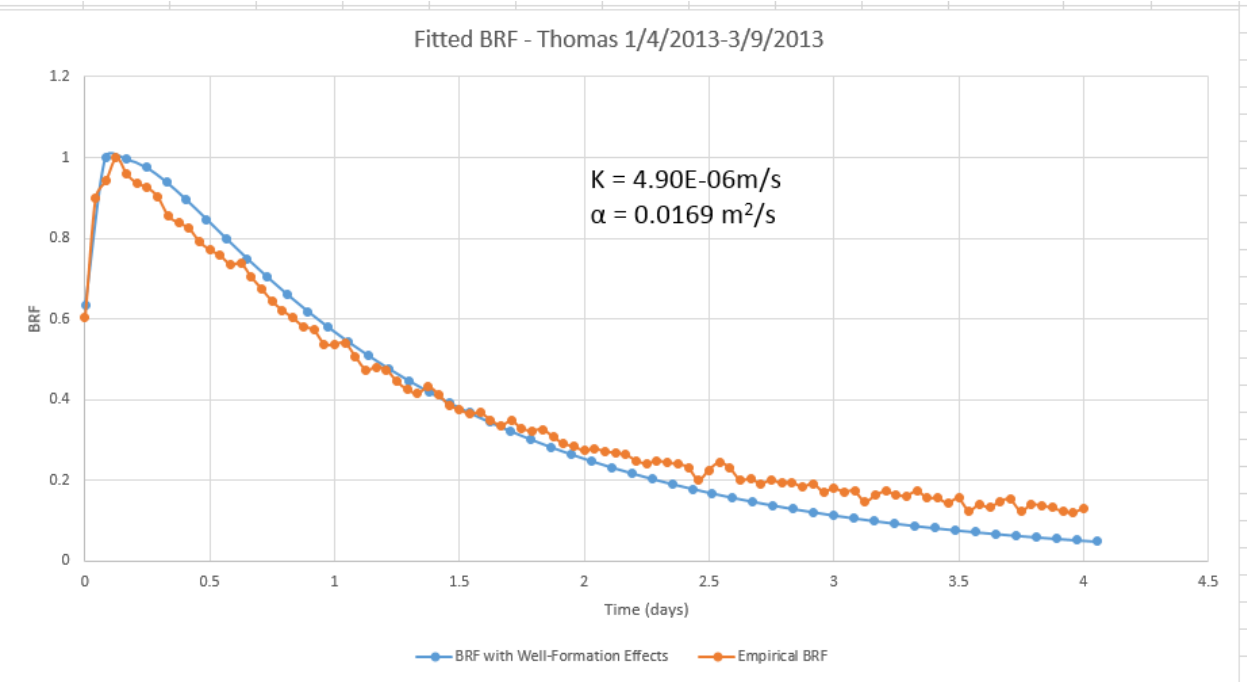

Figure A5: Parameter estimation through visual curve matching of time domain BRF analytical model to empirical time domain BRF.

Appendix B: Analytical Frequency Domain BRF Model – MATLAB code

```
% BRF CODE
%
% This code estimates a barometric response function (BRF) with one standard deviation error bars
% from time series data of borehole water levels and barometric pressure, using the cross-spectral
% deconvolution-averaging method of Welch P.D. [1967], The Use of Fast Fourier Transform for the
%Estimation of Power Spectra: A Method Based on Time Averaging Over Short, Modified Periodograms.
%IEEE Trans. Audio Electroacoustics, AU-15, 70-73.
%
% AUTHOR:
% Mahmoud E.A. Hussein, School of Earth and Environment, University of Leeds, UK
% This code was created as part of the PhD study:
% Hussein MEA. 2012. Borehole water level response to barometric pressure as an indicator of
% groundwater vulnerability. PhD thesis, School of Earth and Environment, University of Leeds, UK.
%
% REQUIREMENTS:
% This program requires the Matlab Signal Processing Toolbox.
% External routine required:
% errorbarlogx.m : function to control errorbar cap width in log scale
% (Frederic Moisy, Copyright (c) 2006)
%
%*******************************************************************************
% INSTRUCTIONS
%
% For best results, time series of borehole water level and barometric pressure data should have all
% influences other than barometric pressure (such as Earth tides, ocean tides, recharge) removed from
% the water level record.
%
% To use the BRF code follow the instructions below:
%
% 1.  Input data files for borehole water level and barometric pressure records must be stored as an
% ascii files, in column vector format and named 'A_WL_output.txt' and 'A_Bp_output.txt' respectively.
%
% 2.  Open the BRF.m file and input the following data:
% a) Input values for parameters K1, K2, K3, K4 and K5 (lines number 35-39, section D.3). These control
% the number of points used in the calculation of the Fast Fourier Transform (FFT) by padding the input
% signals with zeros which increases resolution of the barometric response function and minimises
% artefacts of undesired periodicity. Default number is the next power of 2 to the total number of
% samples in each segment (K=0).
% b) Input lower cut-off frequency for each overlapping frequency band, parameters:
%          COFh1, COFh2, COFh21, COFh22, COFh3 (lines number 44-48).
% Save the BRF.m file.
%
% 3.  Run code by typing 'BRF' in Matlab command window, and press ENTER.
%
% 4.  Four figures are displayed:
```

```
% Figure (1a): Frequency versus coherence between water level and barometric pressure signals for the
%                   five frequency bands.
% Figure (1b): Plot of the amplitude spectrum of water level signal.
% Figure (2a): Plots of frequency versus gain for the BRF from the five frequency bands.
% Figure (2b): Plots of frequency versus phase for the BRF from the five frequency bands.
%
% 5.  Use coherence (Figure 1a) and estimated response functions for five overlapping frequency bands
% (Figure 2a and 2b) to identify frequencies where switches will be made from one frequency
% band to the next. Look for the lowest frequency point where each pair of curves coincide.
% In response to prompts, input selected intersections (in cycles/day).
%
% 6.  Two figures are displayed:
% Figure (2c): Frequency versus barometric response function gain
% Figure (2d): Frequency versus barometric response function phase
% Use this to check the results of the intersection points you have chosen.
%
% 7.  The frequency range over which the barometric response function is determined is made up of a
% continuous frequency band, with additional (optional) points at 1 and 2 cycles/day. At the prompt,
% input upper frequency limit (in cycles/day) for the continuous frequency band.
%
% 8.  Additional points to be included in final response function:
%         - at prompt, enter (1) to include data point at 1 cycle/day or (2) to exclude it.
%         - at prompt, enter (1) to include data point at 2 cycles/day or (2) to exclude it.
%
% 9.  Figure 3, the final barometric response function with error bars is displayed.
%
% 10.  The number of segments and length of each in days for each frequency band is displayed on the
% Matlab command window.
%
% 11.  A file named 'output_to_fit.txt' is saved. This file contains a column vector composed of seven
% concatenated vectors of equal length; gain , phase , frequency , error in gain , error in phase ,
% barometric response function expressed as a complex number (real and imaginary parts).
% The 'output_to_fit.txt' file is used as input to the BRF_Fitting.m code which fits the
% barometric response function to the theoretical BRF model of Rojstazcer (1988).
%
%*************************************************************************
%*************************************************************************
%
% Clearing MATLAB
clear all
close all
clc
%
%*************************************************************************
% Loading the input data files
%
load -ascii A_Bp_output.txt
```

```
load -ascii A_WL_output.txt
% Reading input data files
%
Bpcorr1=A_Bp_output;
WL2D=A_WL_output;
%*************************************************************************
%
tl=length(Bpcorr1);
t_int=input('Input the signal sampling interval [minutes]: ');
FS=1/(t_int/(24*60));
%
%*************************************************************************
% USER DEFINED INPUT
%*************************************************************************
% K factor and the minimum frequency for each frequency band
%
% K factor controlls number of points used for in computation of the FFT at each frequency band.
% The default number for FFT is the next power of 2 of the total number of
% samples in each segment (at K=0). K=1 will increase the power of 2 by one.
%
k1=1;    % frequency band No.1
k2=1;    % frequency band No.2
k3=1;    % frequency band No.3
k4=1;    % frequency band No.4
k5=1;    % frequency band No.5
%*************************************************************************
% Minimum frequency for each frequency band
COFh1=0.003;    % frequency band No.1
COFh2=0.01;     % frequency band No.2
COFh21=0.05;    % frequency band No.3
COFh22=0.35;    % frequency band No.4
COFh3=0.7;      % frequency band No.5
%*************************************************************************
% P1 is the 1st point recorded in the final concatenated BRF output file,
% if you would like to ignore some initial points, just change P1
P1=1;
%
%*************************************************************************
% FREQUENCY BAND NO.(1):
%*************************************************************************
%
segment_1 =ceil((24*60)/(t_int*COFh1));          % Number of points in frequency band No.1
segment_1_days=(segment_1*t_int)/(24*60);
N_Seg_1=floor(tl/(segment_1/2))-1;               % Number of segments based on 50% overlap
%
NFFT1= 2^(nextpow2(segment_1)+k1);
%
```

```
% Apply high pass Butterworth filter with cut-off defined by the minimum frequency of band 1
%
    COFNh=COFh1/(FS/2);                 % cutoff frequency normalized by the Nyquist freq
    [b,a]=butter(4,COFNh,'high');
    WLAfterFilter1=detrend(filtfilt(b,a,WL2D));
    Bpafterfilter1=detrend(filtfilt(b,a,Bpcorr1));
%
% Calculate the coherence between the Water level and Barometric Pressure signals
[Cohfinal1,ffinal1]=mscohere(WLAfterFilter1,Bpafterfilter1,hann(segment_1,'periodic'),[],NFFT1,FS/8640
0);
[Txy1,FFF1] = tfestimate(Bpafterfilter1,WLAfterFilter1,hann(segment_1,'periodic'),[],NFFT1,FS/86400);
FFF_CPD1=FFF1*24*60*60;
FLIM_a = dsearchn(FFF_CPD1,COFh1);
GG1=abs(Txy1);
PP1=((atan(imag(Txy1)./real(Txy1)))*180/pi)-180;
%
% Calculate error bars for barometric response function gain and phase from coherence
Frac_Overlap=0.5;                                   % 50% overlap as default
DOF1=N_Seg_1-(N_Seg_1-1)*Frac_Overlap;              % Degrees of freedom
%
xxxx1=length(ffinal1);
SegmarA1=zeros(xxxx1,1);
SegmarP1=zeros(xxxx1,1);
%
for loop1=1:xxxx1;
   Segma1=(0.5*(1/DOF1)*((1/(Cohfinal1(loop1,1))^2)-1))^0.5;
   SegmarA1(loop1,1)=Segma1*GG1(loop1,1);
   SegmarP1(loop1,1)=Segma1*(180/pi);
end
%
%*************************************************************************
% FREQUENCY BAND NO.(2):
%*************************************************************************
%
segment_2 =ceil((24*60)/(t_int*COFh2));          % Number of points in frequency band No.2
segment_2_days=(segment_2*t_int)/(24*60);
N_Seg_2=floor(tl/(segment_2/2))-1;
%
NFFT2= 2^(nextpow2(segment_2)+k2);
% Apply high pass Butterworth filter with cut-off defined by the minimum frequency of band 2
%
    COFNh=COFh2/(FS/2);                 % cutoff frequency normalized by Nyquist freq
    [b,a]=butter(4,COFNh,'high');
    WLAfterFilter2=detrend(filtfilt(b,a,WL2D));
    Bpafterfilter2=detrend(filtfilt(b,a,Bpcorr1));
%
```

```
[Cohfinal2,ffinal2]=mscohere(WLAfterFilter2,Bpafterfilter2,hann(segment_2,'periodic'),[],NFFT2,FS/8640
0);
%
% Coherence between the Water level and Barometric Pressure signals
[Txy2,FFF2] = tfestimate(Bpafterfilter2,WLAfterFilter2,hann(segment_2,'periodic'),[],NFFT2,FS/86400);
FFF_CPD2=FFF2*24*60*60;
FLIM_b = dsearchn(FFF_CPD2,COFh2);
GG2=abs(Txy2);
PP2=((atan(imag(Txy2)./real(Txy2)))*180/pi)-180;
%
% Calculating  error bars for gain and phase from coherence
Frac_Overlap=0.5;                                % 50% overlap as default
DOF2=N_Seg_2-(N_Seg_2-1)*Frac_Overlap;       % Degrees of freedom
%
xxxx2=length(ffinal2);
SegmarA2=zeros(xxxx2,1);
SegmarP2=zeros(xxxx2,1);
%
for loop2=1:xxxx2;
   Segma2=(0.5*(1/DOF2)*((1/(Cohfinal2(loop2,1))^2)-1))^0.5;
   SegmarA2(loop2,1)=Segma2*GG2(loop2,1);
   SegmarP2(loop2,1)=Segma2*(180/pi);
end
%
%*************************************************************************
% FREQUENCY BAND NO.(3):
%*************************************************************************
%
segment_21 =ceil((24*60)/(t_int*COFh21)); % Number of points in frequency band No.3
segment_21_days=(segment_21*t_int)/(24*60);
N_Seg_21=floor(tl/(segment_21/2))-1;
%
NFFT21= 2^(nextpow2(segment_21)+k3);
% Apply high pass Butterworth filter with cut-off defined by the minimum frequency of band 3
%
    COFNh=COFh21/(FS/2);                         % cutoff frequency normalized to Nyquist freq
    [b,a]=butter(4,COFNh,'high');
    WLAfterFilter21=detrend(filtfilt(b,a,WL2D));
    Bpafterfilter21=detrend(filtfilt(b,a,Bpcorr1));
%
% Coherence between the Water Level and Barometric Pressure signals
[Cohfinal21,ffinal21]=mscohere(WLAfterFilter21,Bpafterfilter21,hann(segment_21,'periodic'),[],NFFT21,
FS/86400);
[Txy21,FFF21] =
tfestimate(Bpafterfilter21,WLAfterFilter21,hann(segment_21,'periodic'),[],NFFT21,FS/86400);
FFF_CPD21=FFF21*24*60*60;
FLIM_b21= dsearchn(FFF_CPD21,COFh21);
```

```
GG21=abs(Txy21);
PP21=((atan(imag(Txy21)./real(Txy21)))*180/pi)-180;
%
% Calculate  error bars for gain and phase based on the coherence
Frac_Overlap=0.5;                                   % 50% overlap as default
DOF21=N_Seg_21-(N_Seg_21-1)*Frac_Overlap;           % Degrees of freedom
%
xxxx21=length(ffinal21);
SegmarA21=zeros(xxxx21,1);
SegmarP21=zeros(xxxx21,1);
%
for loop21=1:xxxx21;
   Segma21=(0.5*(1/DOF21)*((1/(Cohfinal21(loop21,1))^2)-1))^0.5;
   SegmarA21(loop21,1)=Segma21*GG21(loop21,1);
   SegmarP21(loop21,1)=Segma21*(180/pi);
end
%
%*************************************************************************
% FREQUENCY BAND NO.(4):
%*************************************************************************
%
segment_22 =ceil((24*60)/(t_int*COFh22)); % Number of points in frequency band No.4
segment_22_days=(segment_22*t_int)/(24*60);
%
N_Seg_22=floor(tl/(segment_22/2))-1;
%
NFFT22= 2^(nextpow2(segment_22)+k4);
% Apply high pass Butterworth filter with cut-off defined by the minimum frequency of band 4
%
    COFNh=COFh22/(FS/2);                %the Cutoff frequency normalized to the nyquist freq
    [b,a]=butter(4,COFNh,'high');
    WLAfterFilter22=detrend(filtfilt(b,a,WL2D));
    Bpafterfilter22=detrend(filtfilt(b,a,Bpcorr1));
%
%Coherence between the Water level and Barometric Pressure signals
[Cohfinal22,ffinal22]=mscohere(WLAfterFilter22,Bpafterfilter22,hann(segment_22,'periodic'),[],NFFT22,
FS/86400);
[Txy22,FFF22] =
tfestimate(Bpafterfilter22,WLAfterFilter22,hann(segment_22,'periodic'),[],NFFT22,FS/86400);
FFF_CPD22=FFF22*24*60*60;
FLIM_b22= dsearchn(FFF_CPD22,COFh22);
GG22=abs(Txy22);
PP22=((atan(imag(Txy22)./real(Txy22)))*180/pi)-180;
%
% Calculating the error bars for gain and phase from coherence
Frac_Overlap=0.5;                                   % 50% overlap as default
DOF22=N_Seg_22-(N_Seg_22-1)*Frac_Overlap;           % Degrees of freedom
```

```
%
xxxx22=length(ffinal22);
SegmarA22=zeros(xxxx22,1);
SegmarP22=zeros(xxxx22,1);
%
for loop22=1:xxxx22;
   Segma22=(0.5*(1/DOF22)*((1/(Cohfinal22(loop22,1))^2)-1))^0.5;
   SegmarA22(loop22,1)=Segma22*GG22(loop22,1);
   SegmarP22(loop22,1)=Segma22*(180/pi);
end
%
%*************************************************************************
% FREQUENCY BAND NO.(5):
%*************************************************************************
%
segment_3 =ceil((24*60)/(t_int*COFh3)); % Number of points in frequency band No.5
segment_3_days=(segment_3*t_int)/(24*60);
N_Seg_3=floor(tl/(segment_3/2))-1;
%
NFFT3= 2^(nextpow2(segment_3)+k5);
% Apply high pass Butterworth filter with cut-off defined by the minimum frequency of band 5
%
    COFNh=COFh3/(FS/2);                  %the Cutoff frequency normalized to the nyquist freq
    [b,a]=butter(4,COFNh,'high');
    WLAfterFilter3=detrend(filtfilt(b,a,WL2D));
    Bpafterfilter3=detrend(filtfilt(b,a,Bpcorr1));
%
%Coherence between the Water levels and Barometric Pressure signals
[Cohfinal3,ffinal3]=mscohere(WLAfterFilter3,Bpafterfilter3,hann(segment_3,'periodic'),[],NFFT3,FS/8640
0);
%
[Txy3,FFF3] = tfestimate(Bpafterfilter3,WLAfterFilter3,hann(segment_3,'periodic'),[],NFFT3,FS/86400);
%
FFF_CPD3=FFF3*24*60*60;
FLIM_c = dsearchn(FFF_CPD3,COFh3);
GG3=abs(Txy3);
PP3=((atan(imag(Txy3)./real(Txy3)))*180/pi)-180;
%
% Calculating the error bars for gain and phase from coherence
Frac_Overlap=0.5;                              % 50% overlap as default
DOF3=N_Seg_3-(N_Seg_3-1)*Frac_Overlap;       % Degrees of freedom
%
xxxx3=length(ffinal3);
SegmarA3=zeros(xxxx3,1);
SegmarP3=zeros(xxxx3,1);
%
for loop3=1:xxxx3;
```

```
   Segma3=(0.5*(1/DOF3)*((1/(Cohfinal3(loop3,1))^2)-1))^0.5;
   SegmarA3(loop3,1)=Segma3*GG3(loop3,1);
   SegmarP3(loop3,1)=Segma3*(180/pi);
end
%
%*************************************************************************
%
% calculate water level amplitude spectrum
%
NFFTtl= 2^(nextpow2(tl));
Winnew=hamming(tl,'periodic');
WLAFDETh=detrend(WLAfterFilter1).*Winnew;
WLAF=fft(WLAFDETh,NFFTtl)/tl;
WLAFRAA=2*abs(WLAF);
Fc=(0:(NFFTtl-1))*FS/NFFTtl;
%
%*************************************************************************
% PLOT OF COHERENCE FOR ALL FREQUENCY BANDS
%*************************************************************************
fh1 = figure(1);                        % returns the handle to the figure object
set(fh1, 'color', 'white');             % sets the color to white
subplot(2,1,1)
semilogx(FFF_CPD1(FLIM_a:end),Cohfinal1(FLIM_a:end),'k',FFF_CPD2(FLIM_b:end),Cohfinal2(FLIM_b:en
d),'r',FFF_CPD21(FLIM_b21:end),Cohfinal21(FLIM_b21:end),'g',FFF_CPD22(FLIM_b22:end),Cohfinal22(FL
IM_b22:end),'c',FFF_CPD3(FLIM_c:end),Cohfinal3(FLIM_c:end),'b','LineWidth',1)
legend('N1','N2','N3','N4','N5')
ylabel('Gain','FontWeight','bold','FontSize',9)
title('(a) Coherence estimate in five overlapping frequency bands','FontWeight','bold','FontSize',13)
grid on
%
%*************************************************************************
% PLOT WATER LEVEL AMPLITUDE SPECTRUM
%*************************************************************************
%
subplot(2,1,2)
loglog(Fc(FLIM_a:(NFFT1/2)),WLAFRAA(FLIM_a:(NFFT1/2)),'r','LineWidth',1)
xlabel('Frequency CPD','FontWeight','bold','FontSize',9)
ylabel('Amplitude CmH_2O','FontWeight','bold','FontSize',9)
title('(b) WL Amplitude spectrum','FontWeight','bold','FontSize',13)
grid on
%
print '-dpng' '-r600' coherence_RF_cutoff_0.003.png
close all
%
%*************************************************************************
% PLOTS OF BAROMETRIC RESPONSE FUNCTIONS (GAIN AND PHASE)
%*************************************************************************
```

```
%
fh2 = figure(2);                                        % returns the handle to the figure object
set(fh2, 'color', 'white');                             % sets the color to white
subplot(2,2,1)
semilogx(FFF_CPD1(FLIM_a:end),GG1(FLIM_a:end),'ko-',FFF_CPD2(FLIM_b:end),GG2(FLIM_b:end),'ro-
',FFF_CPD21(FLIM_b21:end),GG21(FLIM_b21:end),'go-
',FFF_CPD22(FLIM_b22:end),GG22(FLIM_b22:end),'co-',FFF_CPD3(FLIM_c:end),GG3(FLIM_c:end),'bo-
','LineWidth',1,'MarkerSize',4)
hleg1 = legend('N1','N2','N3','N4','N5');
set(hleg1,'Location','SouthEast')
ylabel('Gain','FontWeight','bold','FontSize',9)
title('(a) Estimated response function GAIN in five overlapping frequency
bands','FontWeight','bold','FontSize',8)
grid on
subplot(2,2,3)
semilogx(FFF_CPD1(FLIM_a:end),PP1(FLIM_a:end),'ko-',FFF_CPD2(FLIM_b:end),PP2(FLIM_b:end),'ro-
',FFF_CPD21(FLIM_b21:end),PP21(FLIM_b21:end),'go-
',FFF_CPD22(FLIM_b22:end),PP22(FLIM_b22:end),'co-',FFF_CPD3(FLIM_c:end),PP3(FLIM_c:end),'bo-
','LineWidth',1,'MarkerSize',4)
legend('N1','N2','N3','N4','N5')
xlabel('Frequency in CPD','FontWeight','bold','FontSize',12)
ylabel('Phase','FontWeight','bold','FontSize',9)
title('(b) Estimated response function PHASE in five overlapping frequency
bands','FontWeight','bold','FontSize',8)
grid on
%
%*************************************************************************
%   Reading user input on frequency band intersections, determined from figure 2
%*************************************************************************
%
z1=input('input the chosen intersection frequency between bands 1,2:    ');
x1 = dsearchn(FFF_CPD1,z1);    % end of freq band   (1)
x2 = dsearchn(FFF_CPD2,z1);    % start of freq band (2)
%
z2=input('input the chosen intersection frequency between bands 2,3:    ');
x22 = dsearchn(FFF_CPD2,z2);   % end of freq band   (2)
x3 = dsearchn(FFF_CPD21,z2);   % start of freq band (3)
%
z3=input('input the chosen intersection frequency between bands 3,4:    ');
x33 = dsearchn(FFF_CPD21,z3);  % end of freq band   (3)
x4 = dsearchn(FFF_CPD22,z3);   % start of freq band (4)
%
z4=input('input the chosen intersection frequency between bands 4,5:    ');
x44 = dsearchn(FFF_CPD22,z4);  % end of freq band   (4)
x5 = dsearchn(FFF_CPD3,z4);    % start of freq band (5)
%
%*************************************************************************
```

```
% Concatenate response function vectors
Ft1=[FFF_CPD1(FLIM_a:x1)
;FFF_CPD2(x2+1:x22);FFF_CPD21(x3+1:x33);FFF_CPD22(x4+1:x44);FFF_CPD3(x5+1:end)];
%
%*************************************************************************
%
Gt=[GG1(FLIM_a:x1)    ;GG2(x2+1:x22)    ;GG21(x3+1:x33)    ;GG22(x4+1:x44);  GG3(x5+1:end)];
Pt=[PP1(FLIM_a:x1)    ;PP2(x2+1:x22)    ;PP21(x3+1:x33)    ;PP22(x4+1:x44)  ;PP3(x5+1:end)];
SAt=[SegmarA1(FLIM_a:x1);SegmarA2(x2+1:x22);SegmarA21(x3+1:x33);SegmarA22(x4+1:x44)
;SegmarA3(x5+1:end)];
SPt=[SegmarP1(FLIM_a:x1);SegmarP2(x2+1:x22);SegmarP21(x3+1:x33);SegmarP22(x4+1:x44)
;SegmarP3(x5+1:end)];
Txyt=[Txy1(FLIM_a:x1)  ;Txy2(x2+1:x22)   ;Txy21(x3+1:x33)   ;Txy22(x4+1:x44) ;Txy3(x5+1:end)];
Ft=[FFF_CPD1(FLIM_a:x1) ;FFF_CPD2(x2+1:x22);FFF_CPD21(x3+1:x33);FFF_CPD22(x4+1:x44)
;FFF_CPD3(x5+1:end)];
%
%*************************************************************************
% PLOT FINAL RESPONSE FUNCTION
%*************************************************************************
%
subplot(2,2,2)
semilogx(FFF_CPD1(FLIM_a:x1),GG1(FLIM_a:x1),'k.',FFF_CPD2(x2+1:x22),GG2(x2+1:x22),'r.',FFF_CPD21(
x3+1:x33),GG21(x3+1:x33),'g.',FFF_CPD22(x4+1:x44),GG22(x4+1:x44),'c.',FFF_CPD3(x5+1:end),GG3(x5+1
:end),'b.','MarkerSize',10)
hleg1 = legend('N1','N2','N3','N4','N5');
set(hleg1,'Location','SouthEast')
ylabel('Gain','FontWeight','bold','FontSize',9)
title('(b)Selected response function','FontWeight','bold','FontSize',8)
grid on
subplot(2,2,4)
semilogx(FFF_CPD1(FLIM_a:x1),PP1(FLIM_a:x1),'k.',FFF_CPD2(x2+1:x22),PP2(x2+1:x22),'r.',FFF_CPD21(x
3+1:x33),PP21(x3+1:x33),'g.',FFF_CPD22(x4+1:x44),PP22(x4+1:x44),'c.',FFF_CPD3(x5+1:end),PP3(x5+1:en
d),'b.','MarkerSize',10)
legend('N1','N2','N3','N4','N5')
xlabel('Frequency in CPD','FontWeight','bold','FontSize',12)
ylabel('Phase','FontWeight','bold','FontSize',9)
grid on
%
%*************************************************************************
% SELECT FREQUENCY RANGE FOR THE FINAL BAROMATRIC RESPONSE FUNCTION
%*************************************************************************
%
P22=input('Input upper frequency limit for continous frequency band:    ');
     P2= dsearchn(Ft,P22);

% user seleacted point at 1 cpd
zzz1=input('Include point at 1 CPD? if yes input(1); if no input(2):   ','s');
```

```
%
switch zzz1
  case '1'
     P1cpd= dsearchn(Ft,1);
  case '2'
     P1cpd=[];
end
%
% user selected point at 2 cpd
zzz2=input('Include point at 2 CPD? if yes input(1), if no input(2):   ','s');
switch zzz2
  case '1'
     P2cpd=dsearchn(Ft,2);
  case '2'
     P2cpd=[];
end
%
GG_S=[Gt(P1:P2);Gt(P1cpd);Gt(P2cpd)];
PP_S=[Pt(P1:P2);Pt(P1cpd);Pt(P2cpd)];
FF_S=[Ft(P1:P2);Ft(P1cpd);Ft(P2cpd)];
SA_S=[SAt(P1:P2);SAt(P1cpd);SAt(P2cpd)];
SP_S=[SPt(P1:P2);SPt(P1cpd);SPt(P2cpd)];
Txy_S=[Txyt(P1:P2);Txyt(P1cpd);Txyt(P2cpd)];
%*************************************************************************************
% PLOT THE FINAL BAROMETRIC RESPONSE FUNCTION WITH ERROR BARS
%*************************************************************************************
fh3 = figure(3);                              % returns the handle to the figure object
set(fh3, 'color', 'white');            % sets the color to white
%
% GAIN PLOT
%
subplot(2,2,2)
errorbar(FF_S,GG_S,SA_S,'ko','MarkerEdgeColor','k','MarkerFaceColor','g','MarkerSize',4,'LineWidth',1);
% function to control and homogenize the errorbar cap width in log scale, Copyright (c) 2006, Frederic
Moisy
errorbarlogx(0.003)
xlabel('Frequency CPD','FontWeight','bold','FontSize',12)
ylabel('Gain','FontWeight','bold','FontSize',9)
title('SELECTED BRF','FontWeight','bold','FontSize',13)
grid on
axis tight
subplot(2,2,4)
%
% PHASE PLOT
%
errorbar(FF_S,PP_S,SP_S,'ko','MarkerEdgeColor','k','MarkerFaceColor','g','MarkerSize',4,'LineWidth',1);
```

```
% function to control and homogenize the errorbar cap width in log scale, Copyright (c) 2006, Frederic
Moisy
errorbarlogx(0.003)
xlabel('Frequency CPD','FontWeight','bold','FontSize',12)
ylabel('Phase','FontWeight','bold','FontSize',9)
grid on
axis tight
%
Real=real(Txy_S);
Imag=imag(Txy_S);
%
% Save selected BRF and errorbars components in file 'output_to_fit.txt' as a single vector
%
output_to_fit=[GG_S; PP_S; FF_S; SA_S; SP_S;Real;Imag];
save -ascii output_to_fit.txt output_to_fit
```

```
%ERRORBARLOGX Homogenize the error bars for X-axis in log scale.
%   ERRORBARLOGX turns the X-axis of the current error bar plot to log
%   scale, and homogonizes the length of the horizontal segements which
%   terminate the vertical error bars.
%
%   By default, Matlab's ERRORBAR draws vertical error bars which are
%   terminated by small horizontal segments of uniform length for the X-
%   axis in linear scale. But when turning the X-axis to log scale, these
%   segments become uneven. Using ERRORBARLOGX makes them uniform again.
%
%   ERRORBARLOGX(N) specifies the relative length of the horizontal
%   segments, normalized with the total range of the data. By default,
%   N=0.01 is used.
%
%   Limitations: ERRORBARLOGX acts only on the last drawn curve. If this
%   curve is not an error bar plot, it won't work.
%
%   Example:
%     x=logspace(1,3,20);
%     y=5*(1 + 0.5*(rand(1,20)-0.5)).*x.^(-2);
%     errorbar(x,y,y/2,'o-');
%     errorbarlogx(0.03);
%
%   F. Moisy
%   Revision: 1.00,  Date: 2006/01/20
%
%   See also ERRORBAR.


% History:
% 2006/01/20: v1.00, first version.

if nargin==0, epsilon=0.01; end; % default normalized segment length

set(gca,'XScale','log'); % set the X axis in log scale.

ca = get(gca); % current axe properties
cd = get(ca.Children(1)); % current data properties
heb = cd.Children(2); % handle to current error bars
ceb = get(heb); % current error bars properties

% ceb.XData is an array of length 9*length(data).
% for each data point, ceb.XData contains 3 blocks of 3 numbers:
% X0 X0 NaN X0-DX X0+DX Nan XO-DX X0+DX Nan
% So it is necessary to change the 4th, 5th, 7th and 8th values.

% logarithmic length of the horizontal segments:
```

```
dx = 10^(log10(ceb.XData(length(ceb.XData)-8)/ceb.XData(1))*epsilon);

% computes the new horizontal segments for each data point:
for i=1:(length(ceb.XData)/9),
   ii=(i-1)*9+1; % index of the first error bar data for the point #i
   ceb.XData(ii+3) = ceb.XData(ii)/dx;
   ceb.XData(ii+4) = ceb.XData(ii)*dx;
   ceb.XData(ii+6) = ceb.XData(ii)/dx;
   ceb.XData(ii+7) = ceb.XData(ii)*dx;
end;

set(heb,'XData',ceb.XData); % sets the changes in the error bar properties
```

```
% BRF_Fitting.m
%
% This code optimizes the fit of the model for barometric response functions in semi-confined aquifers
% by Rojstazcer (1988) to observed barometric response function data, using a Hybird PS-GA
% algorithm. The model of Rojstazcer (1988) is modified to include the capillary fringe attenuation factor
% (Evans et al., 1991).
%
% AUTHOR:
% Mahmoud E.A. Hussein, School of Earth and Environment, University of Leeds, UK.
% This code was created as part of the PhD study:
% Hussein MEA. 2012. Borehole water level response to barometric pressure as an indicator of
% groundwater vulnerability. PhD thesis, School of Earth and Environment, University of Leeds, UK.
%
%*************************************************************************
%
% The code determines the following best fit parameters:
% BE - static barometric efficiency (-)
% Lunsat - thickness of the vadose zone in the confining layer (m)
% Dcon - hydraulic diffusivity of the saturated zone in the confining layer (m^2/d)
% Dunsat - pneumatic diffusivity of the vadose zone in the confining layer (m^2/d)
% Taqu - transmissivity of the aquifer (m^2/d)
% Tcf - attenuation factor (-)
%
% Parameters held constant that are provided by the user are:
% Scon - storage coefficient of the confining layer (m^-1)
% Saqu - storage coefficient of the aquifer (m^-1)
% bcon - thickness of saturated confining layer (m)
% Drift - total thickness of the confining layer (m)
% rw - borehole radius (m)
%
%*************************************************************************
% REFERENCES:
% 1) Rojstaczer, S. (1988), Determination of fluid-flow properties from the response of water levels in
% wells to atmospheric loading, Water Resources Research, 24(11), 1927-1938.
% 2) Evans, K., J. Beavan, D. Simpson and S. Mousa (1991), Estimating aquifer parameters from analysis
% of forced fluctuations in well level: An example from the Nubian formation near Aswan, Egypt.
% 3. Diffusivity estimates for saturated and vadose zones, Journal of Geophysical Research-Solid
% Earth and Planets, 96(B7): 12161-12191.
%
%*************************************************************************
% REQUIREMENTS:
% This program requires the Matlab Global Optimaization and Parallel Computing Toolboxes.
% External routines required:
```

```
%       AF_Function.m: function to compute model curves (Rojstaczer, 1988)
%       errorbarlogx.m : function to control errorbar cap width in log scale
%       (Frederic Moisy, Copyright (c) 2006)
%
%*************************************************************************
% INSTRUCTIONS:
%
% 1. Open the program code in Matlab.
%
%2. Open the BRF_Fitting.m AND in the AF_Function.m codes in the Matlab editor.
% Enter input constants Scon, Saqu, bcon, Drift, rw in BOTH files.
%               BRF_Fitting.m:  lines 128-131
%               AF_Function.m: lines 23, 24, 30, 31
% Save both files.
%
% 3. In the BRF_Fitting.m file, input lower bounds (lb) and upper bounds
% (ub) for each fitting parameter to constrain the optimization:  lines 140-141
%
% 4. Check that the population size parameter is greater than the number of data points in the
% water level record (line number 71). This is set to the default of 10000.
%
% 5. Store input barometric response function data as a text file called 'output_to_fit.txt'. This is the
output file from the BRF code.
% The data are stored in a concatonated list in the order: gain, phase, frequency, gain error bars,
% phase error bars, real part of BRF as a complex number, imaginary part of BRF as a complex number.
%
% 6. To run the BRF_Fitting code, write BRF_Fitting' in the Matlab command window and press enter.
%
% 7. Figure 1 will be displayed showing:
%   (a) steps of the Genetic algorithm (GA) with generation number on the horizontal axis versus the
% objective function best value.
%   (b) Values of the best fit solution of each fitting parameter plotted as a bar chart.
% In the lower left corner of Figure 1 there is an interactive button labelled ‘stop’. If you feel satisfied
% with the GA results so far and want to switch to the Pattern search algorithm (PS), click the 'stop'
% button. Otherwise it will switch automatically when the difference between two consecutive solutions
% is less than the threshold (default 10.0E-6).
%
% 8. When the fitting process is complete, Figure 2 shows the best fit model curve together with the
% input barometric response function and its one standard deviation error bars.
%
% 9. Finally, the Matlab command window shows step by step details of the optimization process for
% GA and PS algorithms, best fit parameters values, the minimum objective function value and the time
% elapsed during the optimization process.
%
```

```
%*************************************************************************************
%*************************************************************************************
%
set(0,'DefaultFigureWindowStyle','docked')
format short
format compact
close all
%
%*********************************************************************
% LOAD BAROMETRIC RESPONSE FUNCTION (BRF) DATA TO BE FITTED
% Data are stored in the file 'output_to_fit.txt'
%-------------------------------------------------------------------------------------------------------
%
load output_to_fit.txt
outl=length(output_to_fit);
div=outl/7;
G1=output_to_fit(1:div);              % BRF Gain
P1=output_to_fit((div+1):(2*div));          % BRF Phase
F1=output_to_fit((2*div+1):(3*div));       % Frequency
AE1=output_to_fit((3*div+1):(4*div));    % BRF Gain Error bars
PE1=output_to_fit((4*div+1):(5*div));    % BRF Phase Error bars
Real1=output_to_fit((5*div+1):(6*div)); % BRF as complex number - real part
Imag1=output_to_fit((6*div+1):end);     % BRF as complex number - imaginary
%
Po1=1;
limit=30;
G=G1(Po1:limit);           % Gain
P=P1(Po1:limit);           % Phase
F=F1(Po1:limit);           % Frequency
AE=AE1(Po1:limit);         % Gain Error bars
PE=PE1(Po1:limit);         % Phase Error bars
Imag=Imag1(Po1:limit); % Imaginary part of BRF as a complex number
%
%*********************************************************************
% OPTIMIZING MODEL FIT TO INPUT BAROMETRIC RESPONSE FUNCTION
%
%*********************************************************************
%
% USER SUPPLIED FIXED INPUT PARAMETERS
%-------------------------------------------------------------------------------------------------------
rw=0.0985;       % borehole radius
Drift=16.15;      % thickness of confining layer
Scon=1e-3;     % confining layer storage coefficient=Ss*b (Dimensionless)
Saqu=1e-5;       % aquifer layer storage coefficient=Ss*b (Dimensionless)
```

```
C=86400;


% USER SUPPLIED UPPER AND LOWER BOUND FOR PARAMETERS
%-------------------------------------------------------------------------------------------------------
%  BE       Taqu          Dcon       Dunsat      Lunsat    Tc
lb=[0.0      (0.001/C)     0.001/C      0.001/C      1.0     0   ];
ub=[1        (1000/C)      1000/C        1000/C      1.75     1   ];
nvars=6;
%*************************************************************************
%*************************************************************************
%
% Pattern search options
%
psoptions= psoptimset('TolMesh',1e-6,...
                'TolFun', 1e-6,...
                'MaxIter', Inf,...
                'MaxFunEvals', 100000000,...
                'PollMethod', 'MADSPositiveBasisNp1',...
                'CompletePoll','on',...
                'SearchMethod', @searchlhs,...
                'CompleteSearch','on',...
                'Display','iter',...
                'Cache','off',...
                'ScaleMesh','on');
%
% Genetic Algorithm default option settings
options = gaoptimset;
options = gaoptimset(options,'HybridFcn', {@patternsearch ,psoptions},...
                    'MigrationDirection', 'Both',...
                    'Display', 'iter',...
                    'PlotFcns', {  @gaplotbestf @gaplotbestindiv },...
                    'PopulationSize',10000,...
                    'PopInitRange',[lb;ub],...
                    'Generations',Inf,...
                    'MutationFcn',@mutationadaptfeasible,...
                    'FitnessLimit',0.0001,...
                    'TolFun',1e-12,...
% The following line can be disabled if the Parallel Computing toolbox is not available
                    'UseParallel','always');

tic;
% HYDIRD Optimization equation
```

```
[New_Parameters,fval,exitflag,output,population,score] = ...
ga(@AF_Function,nvars,[],[],[],[],lb,ub,[],options);
toc;
%
% updating parameter values
%
Static_BE=New_Parameters(1);
Taquifer_m2_day=New_Parameters(2)*24*60*60;
Dcon=New_Parameters(3)*24*60*60;
Dunsat=New_Parameters(4)*24*60*60;
Lunsat=New_Parameters(5);
Tc=New_Parameters(6);
% Calculate confining layer hydraulic parameters
K_con_m_day=Dcon*(Scon);              % K of saturated zone in confining layer
%
Kuns=Scon*Dunsat;                     % K of vadose zone in confining layer
bcon=Drift-Lunsat;                    % thickness between the water table and the top of aquifer
%
% calculating best fit curves for the gain and phase
%
W=((2*pi*(rw^2)*(F/(24*60*60)))/(New_Parameters(2)))'; % Calculating the horizontal axis of
dimensionless frequency
WL=length(W);
omega=(2*pi*(F/(24*60*60)));
%
QW=((New_Parameters(2))*(bcon^2))/(2*(New_Parameters(3))*(rw^2));
RQ=((Lunsat^2)*New_Parameters(3))/(New_Parameters(4)*(bcon^2));
%
% Pre_allocation for all parameters
Q=zeros(WL,1);
M=zeros(WL,1);
N=zeros(WL,1);
q=zeros(WL,1);
Po=zeros(WL,1);
X=zeros(WL,1);
X1=zeros(WL,1);
Gain=zeros(WL,1);
Phase=zeros(WL,1);
%
for m=1:WL;
%
%Calculate Q values each value of W
Q(m,1)=double(QW*W(1,m));
%
```

```
%Calculating R value for each value of Q
R=RQ*Q;
%
% Calculate M and N (Rojstaczer (1988), equations 4a and 4b)
M(m,1)=Tc*double((2*cosh(R(m,1)^0.5)*cos(R(m,1)^0.5))/(cosh(2*(R(m,1)^0.5))+cos(2*(R(m,1)^0.5))));
N(m,1)=Tc*double((2*sinh(R(m,1)^0.5)*sin(R(m,1)^0.5))/(cosh(2*(R(m,1)^0.5))+cos(2*(R(m,1)^0.5))));
%
% Calculate far field pore pressure of the aquifer Po (Rojstazcer (1988), equations 8,17a)
Po(m,1)=double(((M(m,1)+1i*N(m,1))-(1-(New_Parameters(1))))*exp(-(1i+1)*(Q(m,1)^0.5))+(1-
(New_Parameters(1))));
%
% Calculate q=2Q/S' (Rojstazcer (1988), equation 10)
q(m,1)=double(2*Q(m,1)/Scon);
%
% Calculating the amplitude of well water level fluctuation X=(Xopg/A)
% (Rojstaczer (1988), equations 13,16,17b)
Ko=besselk(0,double((((W(1,m)^2)*(((Saqu)^2)+(1/(q(m,1)^2))))^0.25)*exp(1i*0.5*(atan(q(m,1)*(Saqu))
)));
X1(m,1)=(-1+Po(m,1))/(1+((1i*0.5*(W(1,m))*Ko)));
%
% Calculate the modulus (BE) and Argument (Phase) from X (Rojstaczer (1988), equations 18a, 18b)
Gain(m,1)=abs(X1(m,1));
Phase(m,1)=((atan(imag(X1(m,1))/real(X1(m,1))))*(180/pi))-180; % to convert the phase from radian to
degree
%
end
%%%%%%%%%%%%%%%%%%%%%%%%%%%%%%%%%%%%%%%%%%%%%%%%%%%%%%%%%%%%%%%%%%%%%%%%%%%%%%%%%%%%%%%%%%%%%%%%
% Extending the frequency range of the determined best fit curves for gain and phase
%
Ext_f=0.0001:0.002:10;
W=((2*pi*(rw^2)*(F/(24*60*60)))/(New_Parameters(2)))'; % Calculating the horizontal axis of
dimensionless frequency
W_ext=((2*pi*(rw^2)*(Ext_f'/(24*60*60)))/(New_Parameters(2)))'; % Calculating the horizontal axis of
dimensionless frequency
WL1=length(W_ext);
%
Gain_ext=zeros(WL1,1);
Phase_ext=zeros(WL1,1);
%
for m=1:WL1;
%
% Calculate Q value for each value of W
Q(m,1)=double(QW*W_ext(1,m));
```

```
%
% Calculate R value for each value of Q
R=RQ*Q;
%
% Calculate M and N (Rojstaczer (1988), equations 4a and 4b)
M(m,1)=Tc*double((2*cosh(R(m,1)^0.5)*cos(R(m,1)^0.5))/(cosh(2*(R(m,1)^0.5))+cos(2*(R(m,1)^0.5))));
N(m,1)=Tc*double((2*sinh(R(m,1)^0.5)*sin(R(m,1)^0.5))/(cosh(2*(R(m,1)^0.5))+cos(2*(R(m,1)^0.5))));
%
% Calculate far field pore pressure of the aquifer Po (Rojstaczer (1988), eq 8, 17a)
Po(m,1)=double(((M(m,1)+1i*N(m,1))-(1-(New_Parameters(1))))*exp(-(1i+1)*(Q(m,1)^0.5))+(1-
(New_Parameters(1))));
%
% Calculate q=2Q/S' (Rojstaczer (1988), eq 10)
q(m,1)=double(2*Q(m,1)/Scon);
%
% Calculate the amplitude of well water level fluctuation X=(Xopg/A) (Rojstaczer (1988), eq 13, 16, 17b)
Ko=besselk(0,double((((W_ext(1,m)^2)*(((Saqu)^2)+(1/(q(m,1)^2))))^0.25)*exp(1i*0.5*(atan(q(m,1)*(Sa
qu))))));
X(m,1)=(-1+Po(m,1))/(1+((1i*0.5*(W_ext(1,m))*Ko)));
%
% Calculate the modulus (BE) and Argument (Phase) from X (Rojstaczer (1988), eq 18a, 18b) and convert
% phase from radians to degrees
Gain_ext(m,1)=abs(X(m,1));
Phase_ext(m,1)=((atan(imag(X(m,1))/real(X(m,1))))*(180/pi))-180;
%
end
%
%%%%%%%%%%%%%%%%%%%%%%%%%%%%%%%%%%%%%%%%%%%%%%%%%
% PLOTTING BAROMETRIC RESPONSE FUNCTION DATA WITH ERROR BARS AND BEST FIT CURVES
%%%%%%%%%%%%%%%%%%%%%%%%%%%%%%%%%%%%%%%%%%%%%%%%%
%
display('****************** Table of outputs ******************')
FITTING_PARAMETERS={'SBE',Static_BE,'Taqu(m2/d)=',Taquifer_m2_day...
   ,'Dcon(m2/d)=',Dcon,'Dunsat(m2/d)=',Dunsat,'Q/W=',QW,'R/Q_ratio=',RQ,'Lunsat=',Lunsat,'Tc=',Tc}
%#ok<NOPTS>
%
ESTIMATED_PARAMETERS={'kcon(m/d) = ',K_con_m_day,'kunsat(m/d)=',Kuns, 'Time(min)=',toc/60}
%#ok<NOPTS>
display('********************************************************')
%
%***********************************************************************************
% PLOTTING BRF DATA AND BEST FIT MODEL CURVES
%***********************************************************************************
%
```

```
% 1) GAIN PLOT
figure
fh1 = figure(1); % returns the handle to the figure object
set(fh1, 'color', 'white'); % sets the color to white
subplot(2,2,1)
errorbar(F,G,AE,'ro','MarkerEdgeColor','k','MarkerFaceColor','m','MarkerSize',5,'LineWidth',2);
% external function code homogenize the error bar cap width in log (Frederic Moisy 2006)
errorbarlogx(0.003)
hold on
plot(F,Gain,'-x','LineWidth',1.5,'MarkerSize',8)
set(gca,'XScale','log')
xlabel('Frequency in Cycles/day','FontWeight','bold','FontSize',12)
ylabel('Gain (BE)','FontWeight','bold','FontSize',12)
grid on
legend('Estimated BRF Gain with Coherence error bars','Best fit curve')
%
% 2) PHASE PLOT
subplot(2,2,3)
errorbar(F,P,PE,'ro','MarkerEdgeColor','k','MarkerFaceColor','m','MarkerSize',5,'LineWidth',2)
% external function code homogenize the error bar cap width in log (Frederic Moisy 2006)
errorbarlogx(0.003)
hold on
plot(F,Phase,'-x','LineWidth',1.5,'MarkerSize',8)
set(gca,'XScale','log')
xlabel('Frequency in Cycles/day','FontWeight','bold','FontSize',12)
ylabel('Phase','FontWeight','bold','FontSize',12)
grid on
legend('Estimated BRF phase with Coherence error bars','Best fit curve')
%
%*************************************************************************************
% Plotting extensions of best fit curves to higher and lower frequencies
%
% gain extension
subplot(2,2,2)
errorbar(F,G,AE,'ro','MarkerEdgeColor','k','MarkerFaceColor','m','MarkerSize',5,'LineWidth',2);
% external function code homogenize the error bar cap width in log (Frederic Moisy 2006)
errorbarlogx(0.003)
hold on
plot(Ext_f,Gain_ext,'-','LineWidth',1.5)
set(gca,'XScale','log')
xlabel('Frequency in Cycles/day','FontWeight','bold','FontSize',12)
ylabel('Gain (BE)','FontWeight','bold','FontSize',12)
grid on
legend('Estimated BRF Gain with Coherence error bars','Best fit curve')
```

```
%
% phase extension
subplot(2,2,4)
errorbar(F,P,PE,'ro','MarkerEdgeColor','k','MarkerFaceColor','m','MarkerSize',5,'LineWidth',2)
% external function code homogenize the error bar cap width in log (Frederic Moisy 2006)
errorbarlogx(0.003)
hold on
plot(Ext_f,Phase_ext,'-','LineWidth',1.5)
set(gca,'XScale','log')
xlabel('Frequency in Cycles/day','FontWeight','bold','FontSize',12)
ylabel('Phase','FontWeight','bold','FontSize',12)
grid on
legend('Estimated BRF phase with Coherence error bars','Best fit curve')
%
clock
%
%*********************************************************************************
% FINAL BEST FIT PARAMETERS
%*********************************************************************************
%
Static_BEo=New_Parameters(1);
Taquifero=New_Parameters(2)*C;
Dcono=New_Parameters(3)*C;
Dunsato=New_Parameters(4)*C;
Lunsato=New_Parameters(5);
Tco=New_Parameters(6);
%
%*********************************************************************************
%   PLOTTING OUTPUT OF FITTING PROCESS
%*********************************************************************************
%
figure
fh2 = figure(2); % returns the handle to the figure object
set(fh2, 'color', 'white'); % sets the color to white
subplot(3,2,1)
plot(population(:,1), score,'o','MarkerSize',6)
xlabel('BE','FontWeight','bold','FontSize',12)
ylabel('Fvalue','FontWeight','bold','FontSize',12)
hold on
plot(Static_BEo,fval,'.r','MarkerSize',15)
hold off
%
subplot(3,2,2)
plot(population(:,2).*C, score,'o','MarkerSize',6)
```

```
xlabel('Taqu m^2/day','FontWeight','bold','FontSize',12)
ylabel('Fvalue','FontWeight','bold','FontSize',12)
hold on
plot(Taquifero,fval,'.r','MarkerSize',15)
hold off
%
subplot(3,2,3)
plot(population(:,3).*C, score,'o','MarkerSize',6)
xlabel('Dcon m^2/day','FontWeight','bold','FontSize',12)
ylabel('Fvalue','FontWeight','bold','FontSize',12)
hold on
plot(Dcono,fval,'.r','MarkerSize',15)
hold off
%
subplot(3,2,4)
plot(population(:,4).*C, score,'o','MarkerSize',6)
xlabel('Dunsat m^2/day','FontWeight','bold','FontSize',12)
ylabel('Fvalue','FontWeight','bold','FontSize',12)
hold on
plot(Dunsato,fval,'.r','MarkerSize',15)
hold off
%
subplot(3,2,5)
plot(population(:,5), score,'o','MarkerSize',6)
xlabel('Lunsat m','FontWeight','bold','FontSize',12)
ylabel('Fvalue','FontWeight','bold','FontSize',12)
hold on
plot(Lunsato,fval,'.r','MarkerSize',15)
hold off
%
subplot(3,2,6)
plot(population(:,6), score,'o','MarkerSize',6)
xlabel('Tcf','FontWeight','bold','FontSize',12)
ylabel('Fvalue','FontWeight','bold','FontSize',12)
hold on
plot(Tco,fval,'.r','MarkerSize',15)
hold off
%
%*************************************************************************
%                          END
%*************************************************************************
```

```
function [errmin] = AF_Function(param)
%*************************************************************************
% This function is called by program BRF_Fitting.m . This function:
% 1) Reads the barometric response function (BRF) data to be fitted is read from file 'output_to_fit.txt
% 2) Computes model barometric response curves (Rojstazcer, 1988) from best fit parameters to date
% 3) Computes the square of differences between model and observed barometric response function
%    (in the complex plane)
%*************************************************************************
%
SBE=param(1);
Taqu=param(2);   % m^2/s
Dcon=param(3);   % m^2/s
Dunsat=param(4); % m^2/s
Lunsat=param(5); % m
Tc=param(6);     % m
%
%*************************************************************************
% USER SUPPLIED INPUT PARAMETERS
%*************************************************************************
% FIXED INPUT PARAMETERS
rw=0.0985;
Drift=16.15;            % total thickness of the confining layer (m)
bcon=Drift-Lunsat;      % vertical distance between water table and the top aquifer (m)
Scon=1e-3;              % confining layer storage coefficient (Dimensionless)
Saqu=1e-5;              % aquifer storage coefficient (Dimensionless)
%
load output_to_fit.txt
%
Po1=1;
limit=30;
%
outl=length(output_to_fit);
div=outl/7;
F1=output_to_fit((2*div+1):(3*div));                    % Frequencies
Real1=output_to_fit((5*div+1):(6*div));                 % real part of BRF as a complex number
Imag1=output_to_fit((6*div+1):end); %#ok<COLND>         % imaginary part of BRF as a complex number
%
F=F1(Po1:limit);
Real=Real1(Po1:limit);
Imag=Imag1(Po1:limit);
%
%*************************************************************************
W=((2*pi*(rw^2)*(F/(24*60*60)))/(Taqu))'; % dimensionless frequency
WL=length(W);
QW=((Taqu)*(bcon^2))/(2*(Dcon)*(rw^2));
RQ=((Lunsat^2)*Dcon)/(Dunsat*(bcon^2));
%
```

```
%*****************************************************************************
% Pre_allocation for all parameters
Q=zeros(WL,1);
M=zeros(WL,1);
N=zeros(WL,1);
q=zeros(WL,1);
Po=zeros(WL,1);
Xm=zeros(WL,1);
%
MReal=zeros(WL,1);
MImag=zeros(WL,1);
for m=1:WL;
%
%Calculate Q values for for each value of W
Q(m,1)=double(QW*W(1,m));
%
%Calculating R value for each value of Q
R=RQ*Q;
%
%Calculate M and N (Rojstaczer 1988, equations 4a and 4b)
M(m,1)=Tc*double((2*cosh(R(m,1)^0.5)*cos(R(m,1)^0.5))/(cosh(2*(R(m,1)^0.5))+cos(2*(R(m,1)^0.5))));
N(m,1)=Tc*double((2*sinh(R(m,1)^0.5)*sin(R(m,1)^0.5))/(cosh(2*(R(m,1)^0.5))+cos(2*(R(m,1)^0.5))));
%
%Calculate far field pore pressure of the aquifer Po (Rojstazcer 1988, equations 8,17a)
Po(m,1)=double(((M(m,1)+1i*N(m,1))-(1-SBE))*exp(-(1i+1)*(Q(m,1)^0.5))+(1-SBE));
%
%Calculate q=2Q/S' (Rojstazcer 1988, equations 10)
q(m,1)=double(2*Q(m,1)/(Scon));
%
%Calculate amplitude of water level fluctuation (Rojstazcer 1988, equations 13,16,17b)
Ko=besselk(0,double((((W(1,m)^2)*(((Saqu)^2)+(1/(q(m,1)^2))))^0.25)*exp(1i*0.5*(atan(q(m,1)*(Saqu))
))));
Xm(m,1)=(-1+Po(m,1))/(1+((1i*0.5*(W(1,m))*Ko)));
%
MReal(m,1)=real(Xm(m,1));
MImag(m,1)=imag(Xm(m,1));
%
end
% Calculate square of differences between observed BRF and model
R=(MReal-Real).^2;
I=(MImag-Imag).^2;
errmin=sum(R)+sum(I);
%
end
%*****************************************************************************
```

```
%ERRORBARLOGX Homogenize the error bars for X-axis in log scale.
%   ERRORBARLOGX turns the X-axis of the current error bar plot to log
%   scale, and homogonizes the length of the horizontal segements which
%   terminate the vertical error bars.
%
%   By default, Matlab's ERRORBAR draws vertical error bars which are
%   terminated by small horizontal segments of uniform length for the X-
%   axis in linear scale. But when turning the X-axis to log scale, these
%   segments become uneven. Using ERRORBARLOGX makes them uniform again.
%
%   ERRORBARLOGX(N) specifies the relative length of the horizontal
%   segments, normalized with the total range of the data. By default,
%   N=0.01 is used.
%
%   Limitations: ERRORBARLOGX acts only on the last drawn curve. If this
%   curve is not an error bar plot, it won't work.
%
%   Example:
%     x=logspace(1,3,20);
%     y=5*(1 + 0.5*(rand(1,20)-0.5)).*x.^(-2);
%     errorbar(x,y,y/2,'o-');
%     errorbarlogx(0.03);
%
%   F. Moisy
%   Revision: 1.00,  Date: 2006/01/20
%
%   See also ERRORBAR.


% History:
% 2006/01/20: v1.00, first version.

if nargin==0, epsilon=0.01; end; % default normalized segment length

set(gca,'XScale','log'); % set the X axis in log scale.

ca = get(gca); % current axe properties
cd = get(ca.Children(1)); % current data properties
heb = cd.Children(2); % handle to current error bars
ceb = get(heb); % current error bars properties

% ceb.XData is an array of length 9*length(data).
% for each data point, ceb.XData contains 3 blocks of 3 numbers:
% X0 X0 NaN X0-DX X0+DX Nan XO-DX X0+DX Nan
% So it is necessary to change the 4th, 5th, 7th and 8th values.

% logarithmic length of the horizontal segments:
```

```
dx = 10^(log10(ceb.XData(length(ceb.XData)-8)/ceb.XData(1))*epsilon);

% computes the new horizontal segments for each data point:
for i=1:(length(ceb.XData)/9),
   ii=(i-1)*9+1; % index of the first error bar data for the point #i
   ceb.XData(ii+3) = ceb.XData(ii)/dx;
   ceb.XData(ii+4) = ceb.XData(ii)*dx;
   ceb.XData(ii+6) = ceb.XData(ii)/dx;
   ceb.XData(ii+7) = ceb.XData(ii)*dx;
end;

set(heb,'XData',ceb.XData); % sets the changes in the error bar properties
```

Appendix C: Slug Test Model Fitting Curves

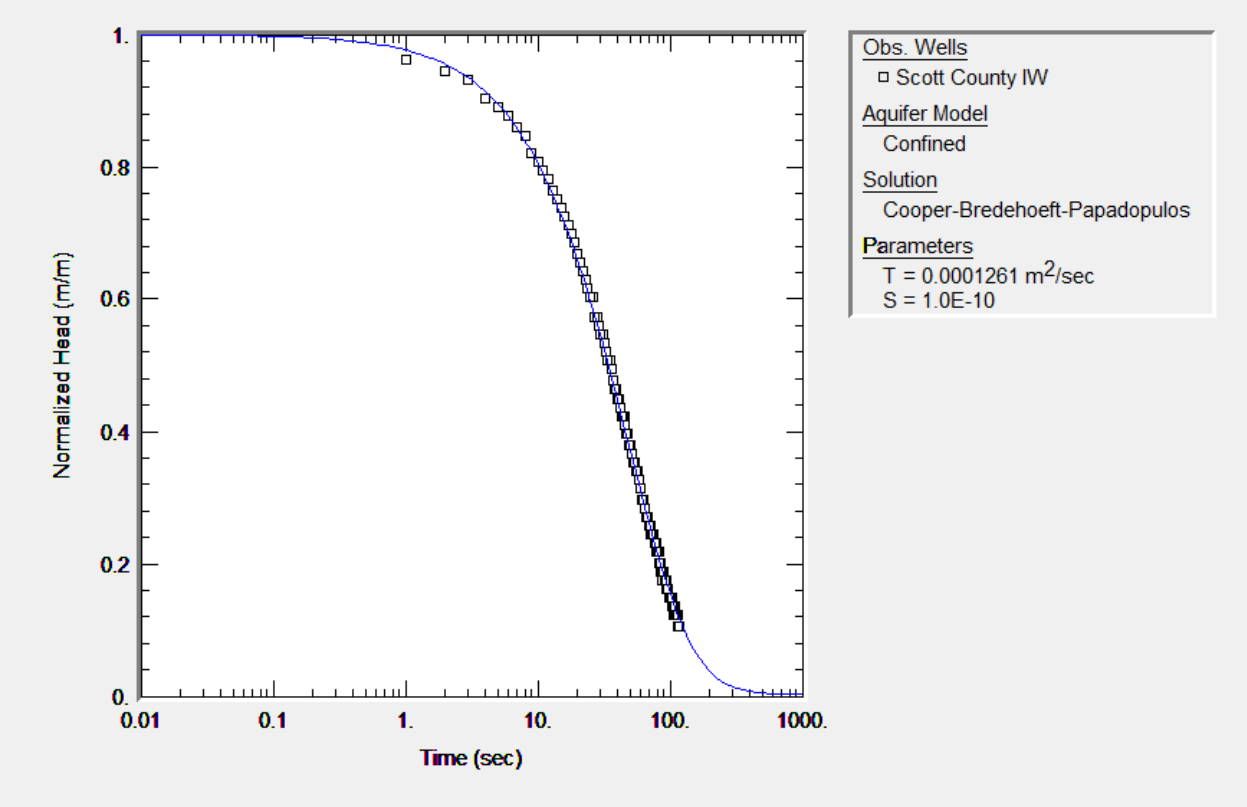

Figure C1: Cooper et al. (1967) slug test model fitting curve for Scott County Index Well.

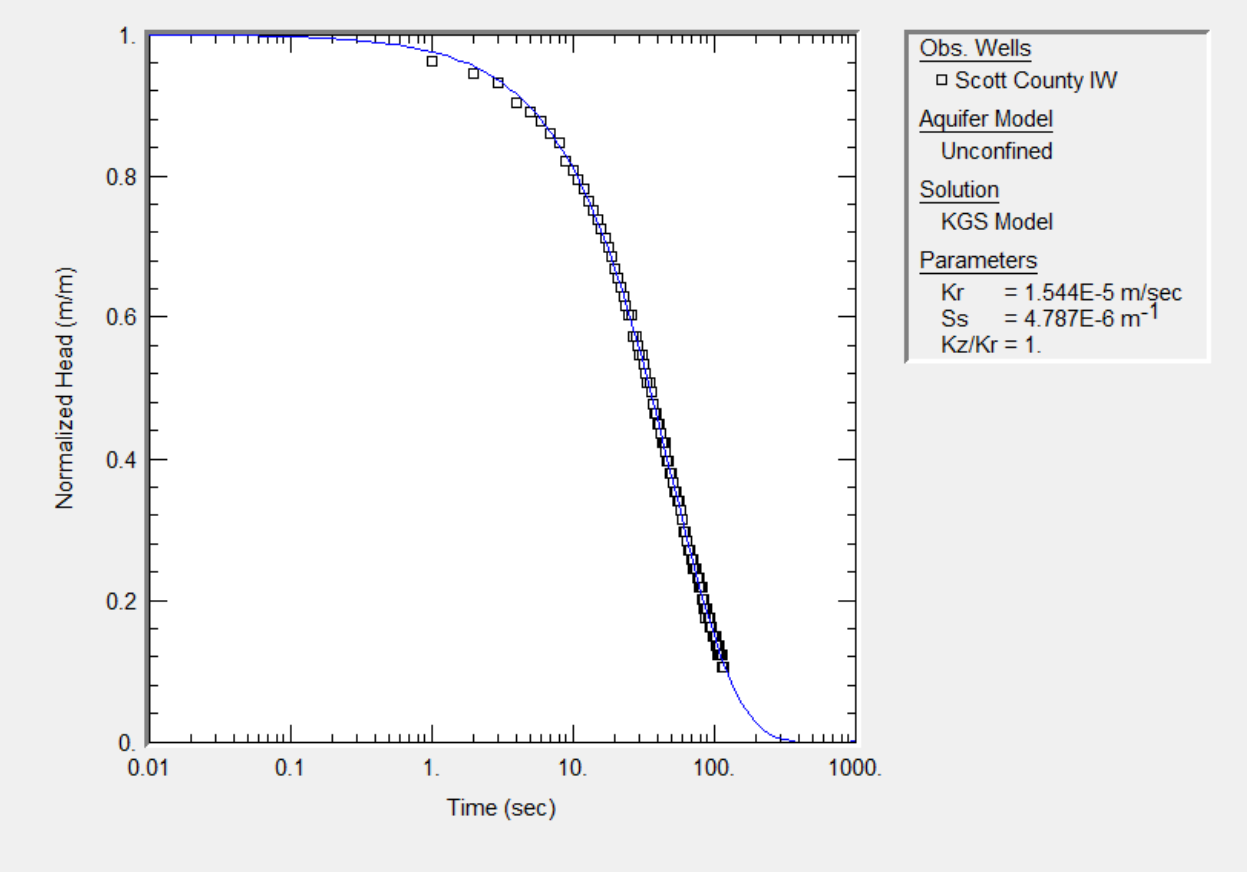

Figure C2: KGS (1994) slug test model fitting curve for Scott County Index Well.

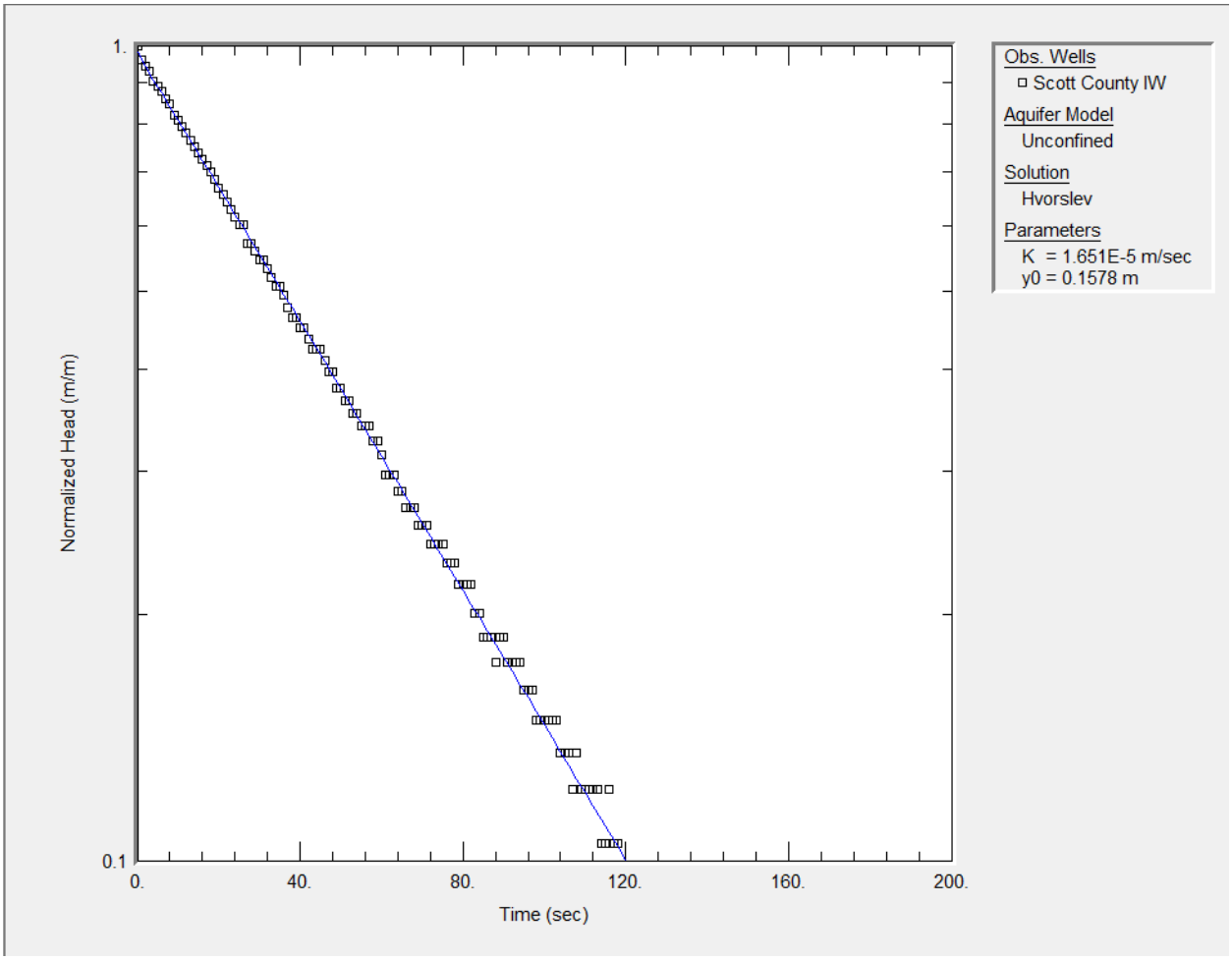

Figure C3: Hvorslev (1951) slug test model fitting curve for Scott County Index Well.

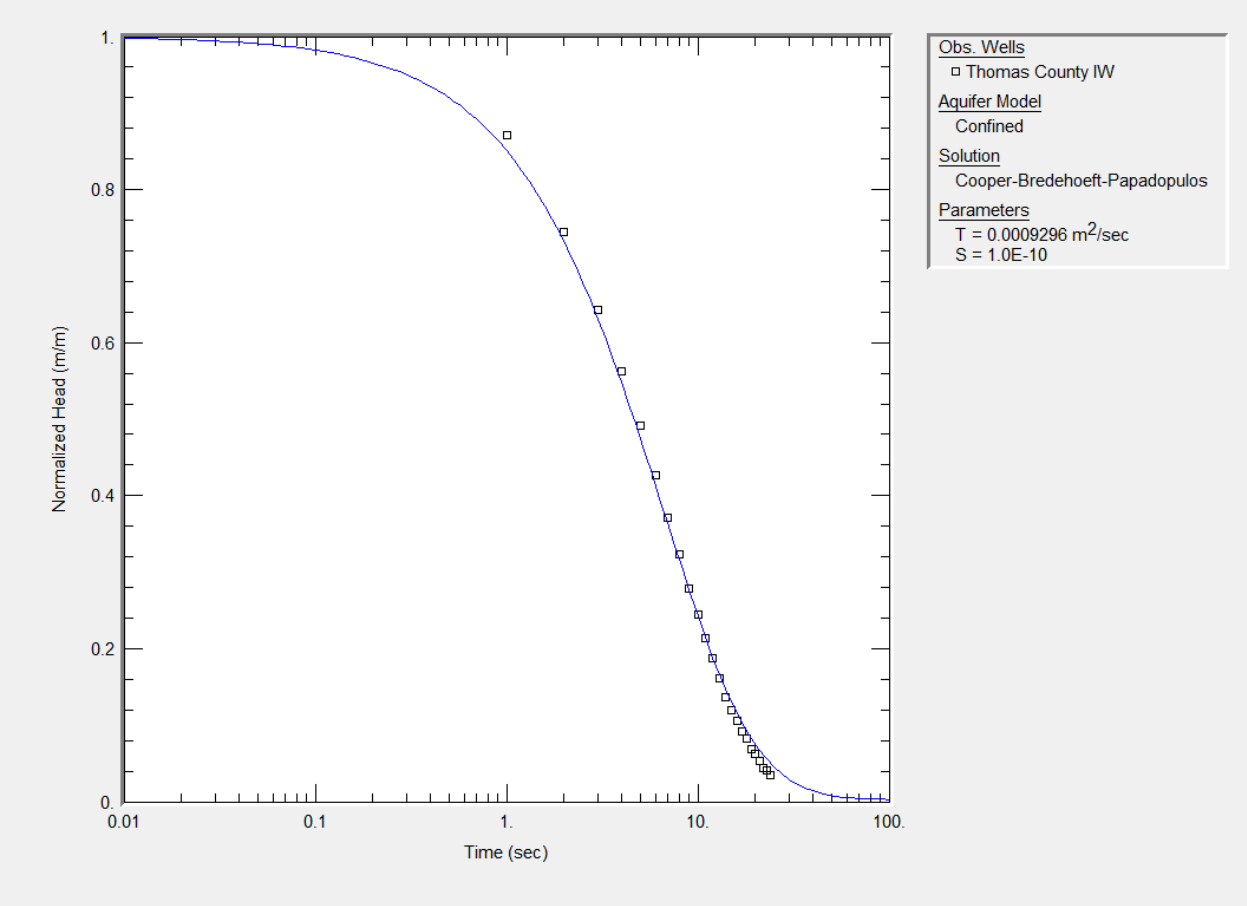

Figure C4: Cooper et al. (1967) slug test model fitting curve for Thomas County Index Well.

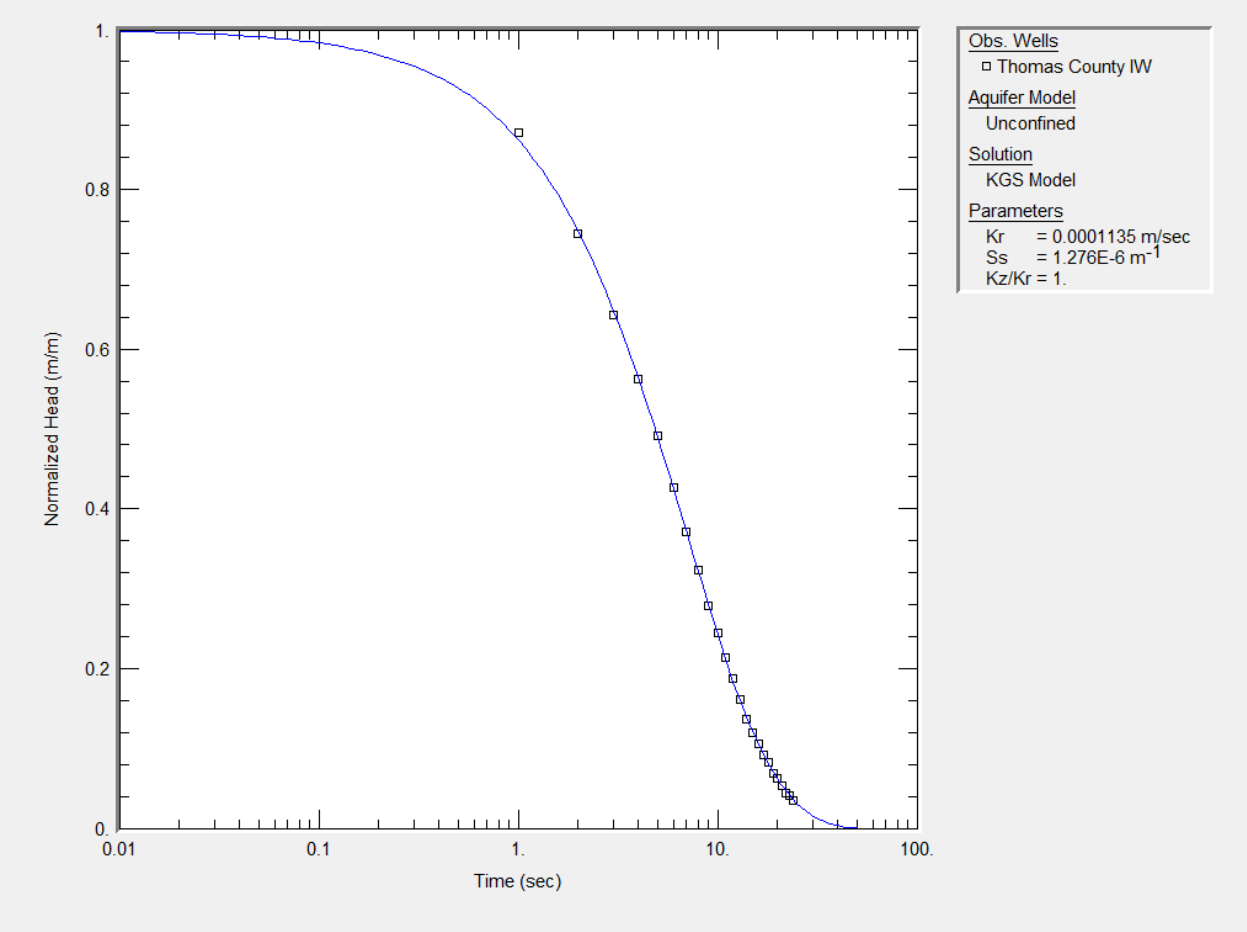

Figure C5: KGS (1994) slug test model fitting curve for Thomas County Index Well.

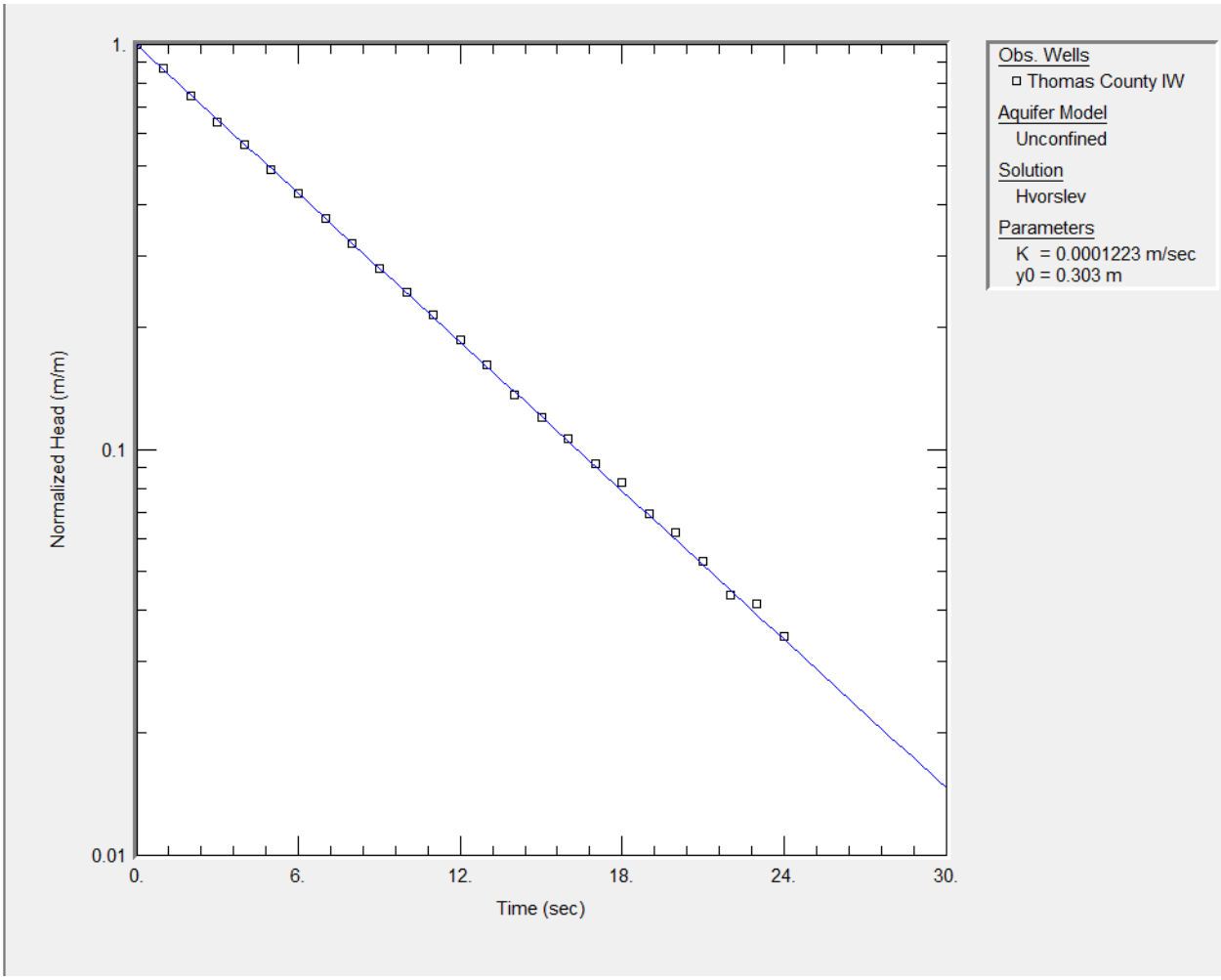

Figure C6: Hvorslev (1951) slug test model fitting curve for Thomas County Index Well.

Table C1: Scott County Index Well slug test data.

Time (sec)	Displacement (m)
0.00	0.161
1.00	0.155
2.00	0.152
3.00	0.150
4.00	0.146
5.00	0.144
6.00	0.141
7.00	0.139
8.00	0.137
9.00	0.132
10.00	0.130
11.00	0.128
12.00	0.126
13.00	0.123
14.00	0.121
15.00	0.119
16.00	0.117
17.00	0.115
18.00	0.113
19.00	0.110
20.00	0.108
21.00	0.106
22.00	0.103
23.00	0.101
24.00	0.099
25.00	0.097
26.00	0.097
27.00	0.092
28.00	0.092
29.00	0.090
30.00	0.088
31.00	0.088
32.00	0.086
33.00	0.084
34.00	0.082
35.00	0.082
36.00	0.080

37.00	0.077
38.00	0.075
39.00	0.075
40.00	0.072
41.00	0.072
42.00	0.070
43.00	0.068
44.00	0.068
45.00	0.068
46.00	0.066
47.00	0.064
48.00	0.064
49.00	0.061
50.00	0.061
51.00	0.059
52.00	0.059
53.00	0.057
54.00	0.057
55.00	0.055
56.00	0.055
57.00	0.055
58.00	0.053
59.00	0.053
60.00	0.051
61.00	0.048
62.00	0.048
63.00	0.048
64.00	0.046
65.00	0.046
66.00	0.044
67.00	0.044
68.00	0.044
69.00	0.042
70.00	0.042
71.00	0.042
72.00	0.039
73.00	0.039
74.00	0.039
75.00	0.039
76.00	0.037
77.00	0.037
78.00	0.037

79.00	0.035
80.00	0.035
81.00	0.035
82.00	0.035
83.00	0.032
84.00	0.032
85.00	0.030
86.00	0.030
87.00	0.030
88.00	0.028
89.00	0.030
90.00	0.030
91.00	0.028
92.00	0.028
93.00	0.028
94.00	0.028
95.00	0.026
96.00	0.026
97.00	0.026
98.00	0.024
99.00	0.024
100.00	0.024
101.00	0.024
102.00	0.024
103.00	0.024
104.00	0.022
105.00	0.022
106.00	0.022
107.00	0.020
108.00	0.022
109.00	0.020
110.00	0.020
111.00	0.020
112.00	0.020
113.00	0.020
114.00	0.017
115.00	0.017
116.00	0.020
117.00	0.017
118.00	0.017
119.00	0.017
120.00	0.015

121.00	0.015
122.00	0.015
123.00	0.015
124.00	0.015
125.00	0.015
126.00	0.015
127.00	0.015
128.00	0.015
129.00	0.013
130.00	0.013
131.00	0.015
132.00	0.013
133.00	0.013
134.00	0.013
135.00	0.013
136.00	0.013
137.00	0.013
138.00	0.013
139.00	0.011
140.00	0.011
141.00	0.011
142.00	0.011
143.00	0.011
144.00	0.011
145.00	0.011
146.00	0.011
147.00	0.011
148.00	0.011
149.00	0.011
150.00	0.011
151.00	0.008
152.00	0.008
153.00	0.008
154.00	0.008
155.00	0.008
156.00	0.008
157.00	0.008
158.00	0.008
159.00	0.008
160.00	0.006
161.00	0.008
162.00	0.006

163.00	0.008
164.00	0.008
165.00	0.006
166.00	0.006
167.00	0.008
168.00	0.008
169.00	0.006
170.00	0.006
171.00	0.006
172.00	0.008
173.00	0.006
174.00	0.006
175.00	0.006
176.00	0.006
177.00	0.006
178.00	0.006
179.00	0.006
180.00	0.006
181.00	0.006
182.00	0.006
183.00	0.004
184.00	0.006
185.00	0.006
186.00	0.004
187.00	0.006
188.00	0.006
189.00	0.006
190.00	0.006
191.00	0.004
192.00	0.004
193.00	0.004
194.00	0.004
195.00	0.004
196.00	0.004
197.00	0.004
198.00	0.004
199.00	0.004
200.00	0.004
201.00	0.004
202.00	0.004
203.00	0.004
204.00	0.004

205.00	0.004
206.00	0.004
207.00	0.004
208.00	0.004
209.00	0.001
210.00	0.001
211.00	0.001
212.00	0.001
213.00	0.001
214.00	0.001
215.00	0.001
216.00	0.004
217.00	0.001
218.00	0.001
219.00	0.001
220.00	0.001
221.00	0.001
222.00	0.001
223.00	0.001
224.00	0.001
225.00	0.001
226.00	0.001
227.00	0.001
228.00	0.001
229.00	0.001
230.00	0.001
231.00	0.001
232.00	0.001
233.00	0.001
234.00	0.001
235.00	0.001
236.00	0.001
237.00	0.001
238.00	0.001
239.00	0.001
240.00	0.001
241.00	0.001
242.00	-0.001
243.00	0.001
244.00	0.001
245.00	0.001
246.00	0.001

247.00	0.001
248.00	-0.001
249.00	-0.001
250.00	-0.001
251.00	0.001
252.00	0.001
253.00	0.001
254.00	-0.001
255.00	-0.001
256.00	0.001
257.00	-0.001
258.00	-0.001
259.00	-0.001
260.00	0.001
261.00	0.001
262.00	0.001
263.00	0.001
264.00	-0.001
265.00	-0.001
266.00	-0.001
267.00	-0.001
268.00	0.001
269.00	-0.001
270.00	-0.001
271.00	-0.001
272.00	-0.001
273.00	0.001
274.00	-0.001
275.00	-0.001
276.00	-0.001
277.00	-0.001
278.00	-0.001
279.00	-0.001
280.00	-0.001
281.00	-0.001
282.00	-0.001
283.00	-0.001
284.00	-0.001
285.00	0.001
286.00	-0.001
287.00	-0.001
288.00	-0.001

289.00	-0.001
290.00	-0.001
291.00	-0.001
292.00	-0.001
293.00	-0.001
294.00	-0.001
295.00	-0.001
296.00	-0.001
297.00	-0.001
298.00	-0.001
299.00	0.001
300.00	-0.001
301.00	-0.001
302.00	-0.001
303.00	-0.001
304.00	-0.001
305.00	-0.001
306.00	0.001
307.00	-0.001
308.00	-0.001
309.00	-0.001
310.00	-0.001
311.00	-0.001
312.00	-0.001
313.00	-0.001
314.00	0.001
315.00	-0.001
316.00	-0.001
317.00	-0.001
318.00	0.001
319.00	-0.001
320.00	-0.001
321.00	-0.001
322.00	-0.001
323.00	-0.001
324.00	-0.001
325.00	-0.001
326.00	-0.001
327.00	0.001
328.00	-0.001
329.00	-0.001
330.00	-0.001

331.00	-0.001
332.00	-0.001
333.00	-0.001
334.00	-0.001
335.00	-0.001
336.00	-0.001
337.00	-0.001
338.00	-0.001
339.00	-0.001
340.00	-0.001
341.00	-0.001
342.00	-0.001
343.00	-0.001
344.00	-0.001
345.00	-0.003
346.00	-0.001
347.00	-0.001
348.00	-0.001
349.00	-0.001
350.00	-0.001
351.00	-0.001
352.00	-0.001
353.00	-0.001
354.00	-0.001
355.00	-0.001
356.00	-0.001
357.00	-0.001
358.00	-0.003
359.00	-0.001
360.00	-0.003
361.00	-0.001
362.00	-0.001
363.00	-0.001
364.00	-0.001
365.00	-0.001
366.00	-0.001
367.00	-0.001
368.00	-0.001
369.00	-0.001
370.00	-0.001
371.00	-0.001
372.00	-0.001

373.00	-0.001
374.00	-0.001
375.00	-0.001
376.00	-0.001
377.00	-0.001
378.00	-0.001
379.00	-0.001
380.00	-0.001
381.00	-0.001
382.00	-0.001
383.00	-0.003
384.00	-0.001
385.00	-0.001
386.00	-0.001
387.00	-0.001
388.00	-0.001
389.00	-0.001
390.00	-0.001
391.00	-0.001
392.00	-0.003
393.00	-0.001
394.00	-0.001
395.00	-0.001
396.00	-0.003
397.00	-0.003
398.00	-0.002
399.00	-0.001
400.00	-0.001
401.00	-0.001
402.00	-0.001
403.00	-0.001
404.00	-0.001
405.00	-0.003
406.00	-0.001
407.00	-0.001
408.00	-0.001
409.00	0.000

Table C2: Thomas County Index Well slug test data.

Time (sec)	Displacement (m)
0.00	0.304
1.00	0.266
2.00	0.227
3.00	0.196
4.00	0.172
5.00	0.150
6.00	0.130
7.00	0.113
8.00	0.098
9.00	0.085
10.00	0.075
11.00	0.065
12.00	0.057
13.00	0.049
14.00	0.041
15.00	0.037
16.00	0.032
17.00	0.028
18.00	0.025
19.00	0.021
20.00	0.019
21.00	0.016
22.00	0.013
23.00	0.013
24.00	0.011
25.00	0.009
26.00	0.008
27.00	0.007
28.00	0.006
29.00	0.006
30.00	0.004
31.00	0.004
32.00	0.004
33.00	0.004
34.00	0.003
35.00	0.003
36.00	0.002

37.00	0.001
38.00	0.001
39.00	0.001
40.00	0.001
41.00	0.001
42.00	0.001
43.00	0.001
44.00	0.001
45.00	0.000

Appendix D: Sensor Testing and Sampling Interval Analyses

The inherent difficulty in the data collection methodology for this study was simultaneously recording barometric pressure and water level data from two separate pressure sensors. The primary problem in attempting to record two different variables with two separate sensors was ensuring that both sensors remained synchronized over the duration of the recording period. Previous researchers (Quilty and Roeloffs, 1991) attempted to resolve this problem, also known as sensor drift, by averaging hourly sensor records to compensate for drift over the recording period. Since the present study relies on precise, simultaneous measurement of water level and barometric pressure data, alternative methodology was needed to ensure data quality for the process of hydrogeological parameter estimation through BRF analyses. Extensive lab testing of two INW PT2X Smart Sensors was conducted over the summer of 2015 prior to installing the sensors in the wells at the SC and TH sites to solve this problem.

The general methodology for testing these sensors involved alternatively submerging and removing the sensors at set time intervals from a graduated cylinder filled with water to simulate a step change in pressure. The data records from both sensors were then compared to examine how the sensors detected the artificially induced step changes in pressure at the set time intervals. Two different data recording techniques were used for these analyses. The first technique involved obtaining data records from each sensor via their respective integrated data loggers. The second technique was to utilize a Campbell Scientific CR1000 Measurement and Control System Datalogger as the recording device for the two pressure sensors by writing a program in Short Cut, the proprietary Windows-based program generator for Campbell Scientific dataloggers. Both of these methods involved synchronizing the internal clock of each sensor with a personal computer that was itself synchronized with the time-a.nist.gov server in Colorado, USA prior to

the initiation of the test. The internal clocks of each sensor were then cross referenced with one another as well as with the clock of the personal computer at the end of the recording period. More than twenty tests were conducted over a period of approximately one month during the summer of 2015 in an effort to eliminate sensor drift. The main variables changed during each of these tests were the sensor sampling interval and the induced pressure step change interval, with the former ranging from one second to one hour and the latter ranging from one second to two weeks.

The results of these tests demonstrated that records from the integrated dataloggers of each of the sensors consistently lagged behind those of the CR1000 by as much as twelve seconds. Additionally, the drift between each of the data records from the integrated dataloggers differed by as much as three seconds. Comparatively, data logged by the CR1000 for each sensor were more consistently synchronized with one another. The highest possible sampling interval, while maintaining synchronization between the sensors, was ten seconds. Ultimately, the best methodology for simultaneously recording water levels and barometric pressure for the purposes of this study was to utilize the CR1000 as the data logger for the two pressure sensors programmed with a sampling interval of ten seconds.

After establishing the sensor deployment methodology, additional experiments were conducted to assess the balance between signal resolution and data volume. Once the ten second water level and barometric pressure data were collected from the SC and TH sites, these data were condensed to larger sampling interval times of one minute, ten minutes, and one hour to establish the minimum sampling interval required to capture the water level response without sacrificing signal resolution. Qualitative analyses of these data indicate that ten minutes is the optimal sampling interval for capturing the fluctuations of the sampling interval. At this

sampling interval, a recording period of at least one year is necessary for sufficient data resolution for frequency domain BRF analyses (Hussein et al., 2013). A portion of the data collected from the TH site is presented below as an example (Figure D1). The one-hour data fails to capture the entire water level and barometric pressure signals, effectively averaging the individual data records made at more frequent sampling intervals of ten seconds, one minute, and ten minutes. There is a significant difference in the number of data records required for ten second and ten-minute data records. The ten-minute data consists of 3,616 records over the approximately 25 day recording period, which is nearly 99% less than the 216,986 data records of the ten second data. When coupled with the minimal loss in signal resolution, the relatively low data usage seems to indicate that ten minutes is the optimal sampling interval for medium to long term (days to months) water level and barometric pressure data analyses.

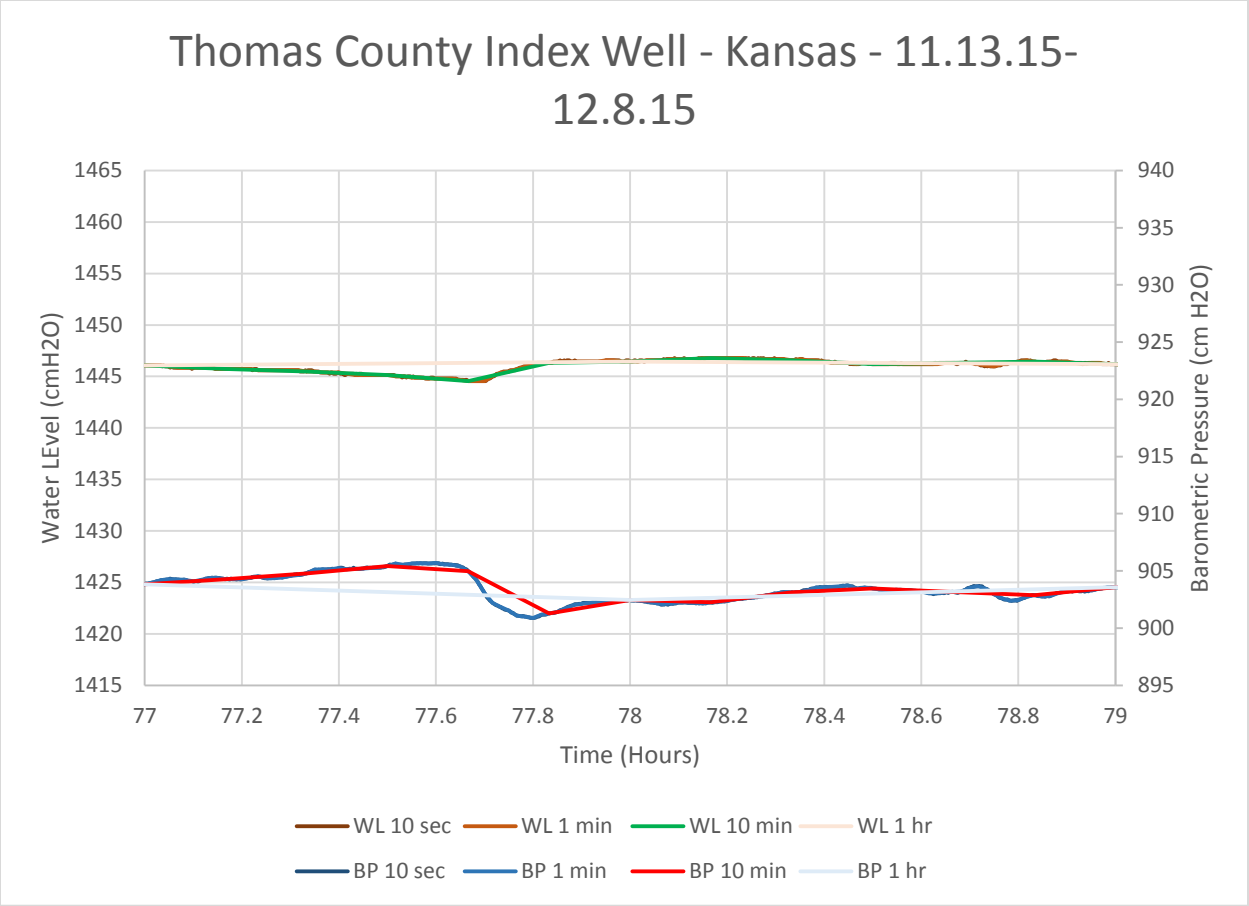

Figure D1: Sampling intervals of ten seconds, one minute, ten minutes, and one hour at Thomas County Index Well. Qualitative analyses indicate that the ten-minute sampling interval best optimizes signal to data storage ratio.